Fritz Laboratory Reports   Civil and Environmental Engineering

1980

Ultimate strength of ship hull girders under moment, shear and torque, July 1980 (Vaucher's M.S. Thesis) 453.6T
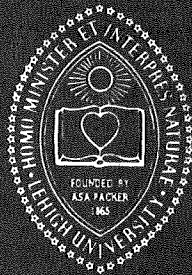
A. Vaucher

A. Ostapenko

Recommended Citation

Vaucher, A. and Ostapenko, A., "Ultimate strength of ship hull girders under moment, shear and torque, July 1980 (Vaucher's M.S. Thesis) 453.6T" (1980). *Fritz Laboratory Reports.* Paper 513.
http://preserve.lehigh.edu/engr-civil-environmental-fritz-lab-reports/513

Lehigh University

Maximum Strength of Ship Hulls

ULTIMATE STRENGTH OF SHIP HULL GIRDERS UNDER MOMENT, SHEAR AND TORQUE

by

Alexis Ostapenko

André Vaucher

July 1980

Report No. 453.6

Fritz Engineering Laboratory

Maritime Administration University Research Program

Report No. MA-RD-940-80077

ULTIMATE STRENGTH OF SHIP HULL GIRDERS

UNDER MOMENT, SHEAR AND TORQUE

FRITZ ENGINEERING
LABORATORY LIBRARY

Prepared by:

Alexis Ostapenko
Andre Vaucher

LEHIGH UNIVERSITY
Fritz Engineering Laboratory

F.E.L. Report No.453.6

JULY, 1980

U. S. DEPARTMENT OF COMMERCE, Maritime Administration
Office of Commercial Development

LEGAL NOTICE

50272-101

REPORT DOCUMENTATION PAGE	1. REPORT NO. MA-RD-940-80077	2.	3. Recipient's Accession No.
4. Title and Subtitle ULTIMATE STRENGTH OF SHIP HULL GIRDERS UNDER MOMENT, SHEAR AND TORQUE			**5. Report Date** July, 1980
			6.
7. Author(s) Alexis Ostapenko and Andre Vaucher			**8. Performing Organization Rept. No.** F.E.L. Rept. 453.6
9. Performing Organization Name and Address Lehigh University Dept. of Civil Engineering Fritz Engineering Laboratory #13 Bethlehem, Pa. 18015			**10. Project/Task/Work Unit No.** 453
			11. Contract(C) or Grant(G) No. (C) MA-79-SAC-B0019 (G)
12. Sponsoring Organization Name and Address Maritime Administration U. S. Department of Commerce Washington, D.C. 20230			**13. Type of Report & Period Covered** Final
			14.

15. Supplementary Notes

16. Abstract (Limit: 200 words)

A method was developed to analyze the behavior and ultimate strength of longitudinally stiffened ship hull girder segments of rectangular single-cell cross section, subjected to bending, shear and torsion. Principal features: (1) Enforcement of compatibility between individual nonlinear components of hull cross section; (2) Compression flange is treated as if formed from beam-columns each consisting of plate-stiffener (longitudinal) combination, pre- and postbuckling, large deformations and plastification are taken into account; (3) Webs (sides) are analyzed by a multiple tension-field approach considering redistribution of normal and shearing stresses between plate subpanels. Comparison of the method with the results of two tests on a small hull girder specimen showed that the method is acceptably accurate for the loading case of moment and shear but should be modified for the general loading case of moment, shear and torque to include the effect of warping deformations (deplanation) of the cross section.

17. Document Analysis a. Descriptors

Hulls (Structures)   Research
Ship Hulls   Model Tests
Ship Structural Components   Metals

b. Identifiers/Open-Ended Terms

Ultimate Strength Method   Stability Methods
Plates   Longitudinal Stability
Plate Girders   Buckling
Compatibility Methods   Torsion
                             Destructive Tests

c. COSATI Field/Group 13/10, 13/13, 14/02, 14/06

18. Availability Statement Approved for Release National Technical Information Springfield, Virginia 22151	**19. Security Class (This Report)** UNCLASSIFIED	**21. No. of Pages** 142
	20. Security Class (This Page) UNCLASSIFIED	**22. Price**

(See ANSI-Z39.18)   See Instructions on Reverse   OPTIONAL FORM 272 (4-77)
(Formerly NTIS-35)
Department of Commerce

TABLE OF CONTENTS

TABLE OF CONTENTS (CONT'D.)

ULTIMATE STRENGTH OF SHIP HULL GIRDERS
UNDER MOMENT, SHEAR AND TORQUE

by

Alexis Ostapenko[1]
Andre Vaucher[2]

ABSTRACT

A method is described for the determination of the behavior and
ultimate strength of longitudinally stiffened ship hull girder seg-
ments of rectangular single-cell cross section, subjected to bending,
shear and torque. The basic requirement of the method is to maintain
the compatibility of deformations between the individual nonlinear
components of the cross section. The compression flange is assumed
to be formed from identical beam-columns each consisting of a plate-
stiffener combination; residual stresses and pre- and post-buckling
behavior of the plate, as well as, large deformations and plastifi-
cation of the stiffener, are all taken into account. The tension
flange is assumed to be elastic-plastic. The webs (sides) are
analyzed by a multiple tension-field approach which considers redis-
tribution of normal and shearing stresses between the plate subpanels.
It is assumed in the method that a section plane before deformations
remains plane after deformations (Navier-Bernoulli) and that shearing
stresses in flanges have no effect on deformations or conditions of
buckling or yielding.

A comparison of the method with the results of two tests on a
small hull girder specimen showed that the method is acceptably
accurate for the loading case of moment and shear (symmetrical loads)
but should be modified for the general loading case of moment, shear
and torque (unsymmetrical loads) to include the effect of warping
deformations (deplanation) of the cross section.

---
[1] Prof., Dept. of Civ. Engrg., Lehigh University, Bethlehem, Pa.
[2] Res. Asst., Dept. of Civ. Engrg., Lehigh University, Bethlehem, Pa.

1. INTRODUCTION

1.1 Background and Related Research

A need for developing a reliable method of evaluating the
maximum strength of ship hulls has been becoming more and more
important with the growing knowledge of ship loads. Although the
traditional methods of ship-design as evolved through the years of
practical experience give adequately safe ship structures, it has
been shown by full scale tests that the mechanism of failure is
often very different from the mechanism predicted by these methods (1).
The major contributing factor to the discrepancy has been the non-
linear behavior of the individual components and of the whole hull
system. Also the rapid introduction of novel ship types (large
tankers, container, LNG, special navy ships) required a more rational
approach to ship design than the semi-empirical traditional methods.

The accuracy of linear analysis has been improved through the
use of computers, and a considerable amount of research has been
conducted on the ultimate strength behavior of individual ship hull
components: individual plates (2,3,4), stiffened plates and grillages
(5,6,7,8,10,11,12) and plate girders under shear and bending (13,14,
15,16,17,18,19,20,21,23,24). However, knowledge of the behavior of
individual components is not sufficient for accurately predicting
the ultimate strength of a ship hull girder since the components
reach their ultimate strength at different levels of deformation.
Some segments may be already in the postultimate range of reduced
capacity when others just attain their maximum strength. Thus, a

2

summation of the individual strengths may lead to a higher apparent capacity than the true strength which involves geometric interaction between the components.

The general concern of structural engineers with rational maximum strength methods is probably best underscored by the intensive work on the development of design specifications based on ultimate strength for box girder bridges presently taking place in West Germany, Great Britain and the United States (25,26).

1.2 Purpose and Scope

The main purpose of this research was to develop an analytical method for determining the ultimate strength of longitudinally and transversely stiffened box girders of the scantlings typical for ship hulls and subjected to the combined effects of bending, shear and torque. The effect of normal loading would be added at a later phase of this research.

The basic individual components of a hull girder's cross section are subjected primarily to uniform axial compression or tension with or without lateral pressure (bottom or deck plating), or to variable normal and shear forces (side plating). A typical cross section is shown in Fig. 1.

The usual procedure for estimating the ultimate strength of a cross section is based on the determination of the ultimate carrying capacities of individual components and summing them up. However,

3

this procedure often does not account for the compatibility of deformations between the components of the cross section and thus may lead to an overestimation of the ultimate strength.

In the development of the new analytical model, the principal problem was in evolving a methodology for determining the relationship between the loads (moment, shear and thrust) on the cross section and the axial deformation of the flanges. This relationship was needed for establishing compatibility between the flanges and the webs. As none of the available theories gives a direct relationship, it was necessary to undertake a new study.

Full advantage was taken of the research previously done on the strength of individual components. Of particular importance were the methods and computer programs developed at Lehigh University and elsewhere for the analysis of the ultimate strength of ship bottom plating (6,8,9,10) and of plate girders (17,18,26).

In addition to the development of the theoretical method, two tests were conducted on a model hull girder. These tests served to verify the soundness of some simplifying assumptions which had to be made in developing the theory and to point out the areas and considerations which should be included to make the theory more accurate.

1.3 General Outline

This report describes a method of ultimate strength analysis of longitudinally and transversely stiffened box girders of the

scantlings typical for ship hulls, the results of two tests and a comparison between the theoretical and test results. Also, recommendations are made for the improvement of the method and for further experimental work.

2. THEORETICAL ANALYSIS

2.1 Introduction

The thin-walled beam theory can be used for analyzing box girders as long as they behave linearly. However, this theory is no longer valid after the plate components buckle or behave non-linearly under combined loads. To overcome these difficulties, a new theory was developed to take into account the nonlinear behavior up to the ultimate carrying capacity and into the post-ultimate range.

Caldwell proposed a direct solution for obtaining the ultimate bending strength of a hull girder section by assuming a fully plastified cross section. The postbuckling response of the plate components was proposed to be incorporated by means of the effective width at the maximum plate capacity and the longitudinals were assumed not to buckle (27).

Nonlinear behavior of stiffened plating was studied by several researchers, for example, by means of large-deflection orthotropic plate analysis (28), finite elements (29), or beam-column idealization (6, 8, 9,10).

The method proposed here considers the overall nonlinear behavior of a box section by taking into account the compatibility of deformations between the individual nonlinear components. The main effort in developing this method was on the establishment of computerized procedures for defining the nonlinear behavior of the

6

flange and web components and then enforcing compatibility for a given combination of forces by an iterative process. Some of the novel features of the method are the consideration of strain reversal in the compression flange and the use of different materials for the plates of webs and flanges and the stiffeners.

The compression flange is treated as a beam-column analyzed by considering the pre- and postbuckling behavior of the plate and large deformations of the plate-stiffener combination. The effect of initial imperfections and residual stresses can be taken into account.

The tension flange is assumed to be linearly elastic-perfectly plastic.

The web is analyzed by considering the redistribution of shearing and axial forces between the plate subpanels and the ultimate strength is obtained as the sum of individual contributions.

Analysis is performed on a hull girder segment which is defined as the longitudinal portion of the girder between two adjacent transverse stiffener rings or bulkheads. For the purpose of analysis, the hull girder is idealized as shown in Fig. 2. The overall dimensions of a segment are the length a, width b and depth d. The spacing of the longitudinals in the compression and tension flanges is usually constant, b_c and b_t, respectively, and in the webs, it may be variable (d_i).

Forces on a segment, moment M, shear V and torque T, are defined in terms of a load parameter W which is equivalent to a concentrated transverse load acting on a simply supported beam as shown in Fig. 2. The forces are specified at mid-length of the segment as indicated in Fig. 3, and they are assumed to be valid for the full length of the segment.

2.2 Assumptions

The following general assumptions were made to simplify the problem to a manageable configuration:

1. Girder is straight and prismatic.

2. Cross section has a single cell rectangular shape and is symmetrical about its vertical centroidal axis.

3. A section plane before deformation remains plane after deformation (Navier-Bernoulli hypothesis).

4. Transverse in-plane loads on the flanges and webs are negligible.

5. Stresses due to the deformation of the shape of the cross section are negligible.

6. Material has bilinear elastic-plastic stress-strain relationship. However, nonlinear materials can be also considered by defining the stress-strain relationship with a series of points.

7. Transverses are rigid enough to provide unyielding support to the flange and web plating. Rotationally, this support can be pinned or fixed.

Some additional specialized assumptions are stated in the discussion of particular components.

2.3 Basic Stresses in a Box Girder Section

2.3.1 Effects of Moment and Shear

Prior to plate buckling and, if the effect of shear lag is neglected, stresses in a box girder section due to moment and shear can be computed by using the ordinary beam theory. Then, the normal stresses will be constant across the width of the flanges and will vary linearly in the webs. The shearing stresses, on the other hand, will be linear in the flanges and almost constant in the webs.

After one or more plate components buckle under such a stress distribution, the stresses cannot be directly superposed, and the analysis is performed after making the following assumptions for the postbuckling range:

- The effect of shearing stresses in the flanges is neglected in computing the ultimate capacity.

- After buckling, the web subpanels cannot carry any additional normal stresses.

- Shearing stresses are uniform in a particular web subpanel.

2.3.2 Effect of Torque

Most of the torque in a girder with a closed cross section is carried by pure (St. Venant) torsion even in the cases for cross sections restrained from warping. It is thus practical to neglect the shearing and normal stresses due to warping (32). Then the shear forces in the webs and flanges due to torque are, respectively,

9

$$\text{Web:} \quad V_{WT} = q_t d \tag{1}$$

$$\text{Flange:} \quad V_{FT} = q_t b \tag{2}$$

where the shear flow q_t is given by

$$q_t = \frac{T}{2A_o} \tag{3}$$

with A_o being the enclosed area

$$A_o = bd \tag{4}$$

However, this situation changes when one of the components, usually a web, is significantly weakened in the postbuckling range. Then, a closed section is transformed into an open "channel" section, with the weak component not participating in carrying additional torque, the shear center shifts and the additional torque must be mostly carried by warping stresses. The present version of the method does not consider this transformation.

2.4 Behavior of Webs

Webs of box girders have the same basic geometry and are subjected to similar types of loading, bending and shear, as the webs of plate girders. Thus, it is prudent to take advantage of the research conducted on plate girders in arriving at a method for analyzing box girder webs (13,14,15,16,17,26,31,32). The only significant difference is in the relative size of the flanges and their ability to influence the postbuckling strength of the web plate since the thin

10

flange plate of a box girder provides very little in-plane support to the web plate in comparison with the large flanges of an ordinary plate girder (26).

Of the several methods developed for analyzing longitudinally stiffened plate girders a simpler one was selected and then modified to incorporate some of the more advanced features (17,31).

Up to the load causing buckling in one of the subpanels, the web is assumed to behave linearly with the shearing and normal stresses in a constant proportion. Once buckling occurs in a sub-panel, the postbuckling strength of this subpanel is assumed to develop independently from the behavior of other subpanels.

The ultimate shear capacity of the whole web is given by a sum of the ultimate shear strengths of the subpanels.

$$V_{wu} = \sum_{i=1}^{n} (V_{bi} + V_{tfi}) \tag{5}$$

where

$$V_{bi} = \tau_{cri} \, d_i \, t_w = \text{buckling strength of the i-th subpanel} \tag{6}$$

$$V_{tfi} = \tau_{tfi} \, d_i \, t_w = \text{tension-field strength of the i-th} \tag{7}$$
subpanel

Unlike some other analytical models, this model neglects the direct contribution of the flanges and longitudinal stiffeners to the shear carrying capacity V_{wu}.

The critical shearing stress, τ_{cri}, of Eq. 6 for each subpanel is computed from the buckling interaction equation, Eq. 8, in which the bending, σ_{bcri}, and normal, σ_{ccri}, stresses are in known proportion to the shearing stress.

$$\left(\frac{\tau_{cri}}{F_{vcri}}\right)^2 + \left(\frac{\sigma_{bcri}}{F_{bcri}}\right)^2 + \frac{\sigma_{ccri}}{F_{ccri}} \leqq 1.0 \tag{8}$$

The reference buckling stresses F_{vcri}, F_{bcri} and F_{ccri} are computed using the formulas of Table 1. These formulas are based on the assumption that the plate subpanels are simply supported at all four edges and are valid for the respective stresses acting alone [26].

The equivalent shearing stress τ_{tfi} in Eq. 7 is due to the postbuckling formation of the tension field and is given by

$$\tau_{tfi} = \frac{\sigma_{ti}}{2\sqrt{1.6 + \alpha_{min}^2}} \tag{9}$$

where

$$\sigma_{ti} = F_y - \sqrt{0.25(\sigma_{ccri} - \sigma_{bcri})^2 + 3\,\tau_{cri}} \tag{10}$$

is the tension field stress at the ultimate condition for the i-th subpanel and

$$\alpha_{min} = a/d_{i\,max} \tag{11}$$

is the aspect ratio of the widest subpanel. Thus, α_{min} is the same for all the subpanels [26,31].

Since the individual subpanels of the web in general have different widths d_i and are subjected to different combinations of bending and normal stresses, their buckling and the attainment of the ultimate condition do not occur simultaneously and are staggered in the course of the overall deformation and loading of the web. The lower plot of Fig. 4 shows the shearing deformations τ vs. γ of three subpanels of a sample web shown in the upper sketch of the figure. The conditions of buckling and ultimate strength are labeled for subpanel 3, and they are seen to be at different levels of the overall shearing deformation γ than for the other subpanels (17).

Deformation of each subpanel up to the point of buckling is linear and is readily defined by

$$\gamma_{cri} = \tau_{cri}/G \qquad (12)$$

On the other hand, the postbuckling deformation cannot be accurately established. In Figure 4, it is approximated by a straight line connecting the buckling deformation with the ultimate deformation (γ_{cr3} to γ_{u3} for subpanel 3). The ultimate deformation of a subpanel is assumed to be reached when a diagonal fiber in the subpanel yields due to the racking deformation of the edge lines assumed to retain their original lengths (17). Thus,

$$\gamma_{ui} = \frac{F_y}{E}\left(\alpha_i + \frac{1}{\alpha_i}\right) \qquad (13)$$

where
$$\alpha_i = a/d_i \qquad (14)$$

The application of Eqs. 5, 6 and 7 at each of the kink points
of the τ_i-γ_i diagrams of Fig. 4 results in a relationship between
V_w and γ for the whole web. In the process of computing this
relationship it is important to keep in mind that, whereas the shear
on a subpanel can increase after buckling, the normal stresses are
assumed to remain constant and, thus, the additional moment corres-
ponding to the increase in the total web shear must be redistributed
to the flanges, the longitudinal web stiffeners and to the yet
unbuckled web subpanels. With the assumption of "the plane section
remaining plane", this redistribution process gives a corresponding
relationship between the total shear V_w and moment M_w acting on the
web and the normal strains at the top and bottom edges where the
compatibility of strains is enforced between the webs and flanges.

In the present formulation, it is assumed that longitudinal
stiffeners are linearly elastic up to yielding, but this assumption
can be modified in the future once the criteria for their premature
failure or nonlinear behavior are established.

2.5 Behavior of Longitudinally Stiffened Compression Flange

2.5.1 Introduction

The compression flange of a hull girder section (the deck for
the sagging and the bottom for the hogging moment) is assumed to be
adequately supported at the transverses and, thus, consists of a
longitudinally stiffened plate subjected to axial compression and,
for the bottom, lateral loading. In the present method, the effect

14

of lateral loading is neglected* and the flange plating is assumed to be either simply supported or fixed at the transverses. The side edges (junctions to the webs) are assumed to be free to rotate or displace in the plane of the plate (11).

The nonlinearity of the axial behavior of such a plating arises from the unsymmetry of the cross section (longitudinals are on one side), welding residual stresses, possibility of buckling of the plate components, initial imperfections and lateral loading. The method which was previously developed to overcome these difficulties was to replace the analysis of a longitudinally stiffened plate panel with a large-deflection analysis of a beam-column (8,9). This method was adapted for the present research, particularly, the computer program of Reference 9.

The simplifying assumptions of the method are the following:

- The plate is very flexible in comparison with the relatively large longitudinals and therefore the interaction between the longitudinals through the plate may be neglected. Then, each longitudinal with its tributary portion of the plate may be considered as an independent substitute beam-column subjected to axial and lateral loads.

---

*Lateral loading can be considered with only minor modifications of the computer program.

- The response of the plate component of the beam-column cross section
  is assumed to correspond to the behavior of a very long plate with
  the width equal to the spacing of the longitudinals. The side
  edges are assumed to be simply supported, but they must remain
  straight although they may have in-plane motion.
- The effect of lateral loading on the plate behavior is neglected
  since it has been found to have little effect on the buckling and
  postbuckling behavior (8) and the bending stresses (in the plate
  spanning between longitudinals) may be treated as a tertiary
  condition, i.e., checked separately. Then, the distributed
  lateral loading q' is applied as a line load q on the beam-column
  as shown in Fig. 5.

Since the basic program computes only the length of a pin- or
fixed-ended beam column subjected to the given axial and lateral
loads and having an assumed mid-span curvature, several supplementary
operations had to be developed to obtain a complete relationship
between the axial load and axial deformation for a zero lateral
loading and a specified length. These operations are described in
the subsequent articles.

2.5.2 Behavior of Plate under Compression

In this study, the axial behavior of a plate under compression
is described by a relationship between the average stress and the
overall strain which also is the strain at the edges. Such a
relationship can be supplied to the program by a series of points

16

obtained, for example, from a test, or by a computational procedure. In the following a computational procedure which is a part of the program is described.

The basic assumptions about the geometry, boundary conditions and the type of loading are stated in Article 2.5.1. Additionally, the plate is assumed to be perfectly flat and the effect of shearing stresses produced by shear V and torque T on the axial buckling stress and the postbuckling behavior is neglected as has been justified by some previous studies (33)

For smaller values of b_c/t there is no buckling and the plate responds according to the stress-strain diagram of the material.

The three ranges of the plate response for larger values of b_c/t are indicated in Fig. 6 by the patterns of the pertinent stress distributions and in Fig. 7 by the average stress vs. strain curve.

1) The linearly (or nonlinearly) elastic prebuckling and buckling range. The stress is uniform and at the end of the range the buckling stress is

$$\sigma_{cr} = \frac{\pi^2 E_t}{12(1-\nu^2)(b_c/t)^2} k \tag{15}$$

where the buckling coefficient is conservatively taken to be k = 4.0.

2) Elastic postbuckling range. The elastic postbuckling relationship is described by Koiter's equation which gives the average stress in terms of the overall (edge) strain (2)

17

$$\frac{\sigma_{ave}}{\sigma_{cr}} = 1.2\left(\frac{\epsilon}{\epsilon_{cr}}\right)^{0.6} - 0.65\left(\frac{\epsilon}{\epsilon_{cr}}\right)^{0.2} + 0.45\left(\frac{\epsilon}{\epsilon_{cr}}\right)^{-0.2} \tag{16}$$

The stress pattern in Fig. 6 is nonuniform and the average stress vs. strain relationship in Fig. 7 is noticeably flatter than the material stress-strain curve.

3) <u>Ultimate stress condition</u> is assumed to be developed when the maximum (edge) stress of the nonuniform pattern reaches yield stress level. This assumption has been confirmed by numerous tests and some theoretical analyses (4,5,8). Shortening of the plate beyond this point generally shows a reduction of the average stress as indicated in Fig. 7 by the curve portion labeled "True" (4,5). However, numerous sample computations have demonstrated that in stiffened plating of the proportions typical for ship structures, ultimate strength of the plating is reached at the plate strains which do not exceed by much the ultimate strain and, when they do, the effect is insignificant. It is thus safe to assume that, as shown in Fig. 7, the average stress remains constant for larger deformations (8).

Welding residual stresses typical for longitudinally stiffened plates are shown in Fig. 8. Their effect on the buckling and post-buckling ranges of σ_{avg} vs. ϵ is included in the method (8).

2.5.3 <u>Beam-Column Analysis</u>

The beam-column to be analyzed is shown in Fig. 5. It is subjected to an axial load P, end moments M and a line loading q.

The cross section consists of the plate with the stress-strain
characteristics established above in Art. 2.5.2 and the longitudinal
stiffener of depth d_s with a stress-strain response given by the mater-
ial, usually, the linearly elastic-perfectly plastic diagram of steel.

The analysis is performed for an axial load P and a line loading
q which are kept constant. The principal operations are described
below.

Moment-Axial Force-Curvature

A distribution of strains and corresponding stresses in a
cross section subjected to an axial load and a moment is shown in
Fig. 9. Compressive stresses are positive and tensile negative. The
strains vary linearly through the depth. Stresses in the stiffener
correspond to the stress-strain diagram of the material (a nonlinear
material is assumed for this illustration). The average stress in
the plate is according to the stress-strain relationship defined in
Art. 2.5.2; it is seen to be lower than the stress in the stiffener
at the junction. Axial force P, moment M and curvature φ are
readily computed for a given strain-stress pattern.

$$P = \int_A \sigma \, dA \tag{17}$$

$$M = -\int_A \sigma \, z \, dA \tag{18}$$

$$\varphi = \frac{\varepsilon_{pl} - \varepsilon_{fl}}{d_s} \tag{19}$$

19

where A = total area of the cross section

σ = axial stress, a function of z

z = distance from the geometric centroid of the cross section

d_s = stiffener depth

ϵ_{pl} = edge strain in the plate

ϵ_{fl} = strain in stiffener flange

A pair of ϵ_{pl} and ϵ_{fl} results in a set of P, M and φ. By varying ϵ_{pl} and ϵ_{fl}, a sufficient number of sets of P, M and φ are obtained to generate M-φ (moment-curvature) relationships for some specified values of P. A sample of corresponding plots is shown in Fig. 10 for three values of P in an ascending order of magnitude $(P_1 > P_2 > P_3)$. The direction of bending and curvature is indicated by small sketches. The following observations are noteworthy: (1) Curvature is not zero for zero moment; (2) For bending with the plate on the concave side (right side of the plot) the moment capacity may be greater for a higher axial force, e.g., for P_2 vs. P_1; (3) For bending with the plate on the convex side (left side of the plot) the moment capacities are inversely related to the magnitudes of axial forces, i.e., greater M for smaller P, and all of them are noticeably smaller than for concave bending. An M-P-φ diagram for a symmetrical section would have passed through the origin and would have been the same for both directions of bending.

Integration Procedure

A stepwise integration procedure is used to compute the length of the beam-column subjected to given values of the axial force P

20

and lateral loading q and having a prescribed curvature φ_o at mid-span. The ends may be simply supported (M = 0) or fixed (slope $\theta = 0$).

Since the structure is symmetrical, only half of the length is integrated, starting at mid-span as shown in Fig. 11. The equilibrium equations for each differential segment of length ds, formulated considering large deformations are the following:

$$\frac{dM}{ds} = \left(1 - \frac{d_p}{d_s} \varphi \right) q \sin \theta \qquad (20)$$

$$\frac{dV}{ds} = \left(1 - \frac{d_p}{d_s} \varphi \right) q \cos \theta \qquad (21)$$

$$\frac{dM}{ds} = -M \sin \theta - V \cos \theta \qquad (22)$$

where
$$\sin \theta = dy/ds \qquad (23)$$

$$\cos \theta = dx/ds \qquad (24)$$

$$\varphi = d\theta/ds \qquad (25)$$

All other notation is shown in Fig. 11.

In performing numerical integration the differential element is changed to a finite element of Δs length and the equilibrium equations are transformed as follows in nondimensionalized form:

$$\underline{H}_{i+1} = \underline{H}_i + k_6 [\underline{\Delta y} + k_7 (\cos \theta_{i+1} - \cos \theta_i)] \qquad (26)$$

$$\underline{V}_{i+1} = \underline{V}_i + k_6 [\underline{\Delta x} - k_7 (\sin \theta_{i+1} - \sin \theta_i)] \qquad (27)$$

21

$$\underline{M}_{i+1} = \underline{M}_i + k_8\{(\underline{H}_i - k_6 k_7 \cos\theta_i)\underline{\Delta y} + (\underline{V}_i + k_6 k_7 \cos\theta_i)\underline{\Delta x}$$

$$+ \frac{1}{2} k_6 (\underline{\Delta y}^2 + \underline{\Delta x}^2)\} \tag{28}$$

$$\underline{\Delta y} = \underline{\Delta s} \sin\theta_i + k_5\left(\frac{\overline{\varphi}_i}{3} + \frac{\overline{\varphi}_{i+1}}{6}\right)\cos\theta_i (\underline{\Delta s})^2 \tag{29}$$

$$\underline{\Delta x} = \underline{\Delta s} \cos\theta_i - k_5\left(\frac{\overline{\varphi}_i}{3} + \frac{\overline{\varphi}_{i+1}}{6}\right)\sin\theta_i (\underline{\Delta s})^2 \tag{30}$$

$$\theta_{i+1} = \theta_i + k_5\left(\frac{\overline{\varphi}_i + \overline{\varphi}_{i+1}}{2}\right)\underline{\Delta s} \tag{31}$$

where

$$k_5 = \frac{r}{d_s} \epsilon_o \tag{32}$$

$$k_6 = \frac{qr}{\sigma_o A} \tag{33}$$

$$k_7 = \frac{d_p}{r} \tag{34}$$

$$k_8 = -\frac{r}{d_s} \tag{35}$$

$$\underline{H} = \frac{H}{\sigma_o A} \tag{36}$$

$$\underline{P} = \frac{P}{\sigma_o A} \tag{37}$$

$$\underline{V} = \frac{V}{\sigma_o A} \tag{38}$$

$$\underline{M} = \frac{M}{\sigma_o A d_s} \tag{39}$$

22

$$\underline{\Delta y} = \frac{\Delta y}{r} \tag{40}$$

$$\underline{\Delta x} = \frac{\Delta x}{r} \tag{41}$$

$$\underline{\Delta s} = \frac{\Delta s}{r} \tag{42}$$

$$\overline{\omega} = \varphi \frac{d_s}{\epsilon_o} \tag{43}$$

r = radius of gyration = $\sqrt{I/A}$

ϵ_o = buckling or yield strain, depending on whether buckling occurs or not

σ_o = buckling or yield stress, depending on whether buckling occurs or not

The details of the mathematical development can be found in References 6 and 8.

The integration process starts at mid-span with the following initial values:

$$\underline{H} = \underline{P}$$

$$\underline{x} = \underline{y} = \underline{s} = 0$$

$$\theta = 0$$

$$\underline{V} = 0 \quad (\text{by symmetry})$$

and the assumed mid-span curvature equal to $\overline{\varphi}_o$.

Then, $\underline{P}$ and $\overline{\varphi}_o$ give the mid-span moment $\underline{M}_o$ from the M-P-φ relationship of Fig. 10.

With the segment length $\underline{\Delta s}$ specified and the curvature at the end of the segment set to equal $\bar{\varphi}_o$, the forces and deformations at the segment end are computed from Eqs. 26 to 31. Then, the new moment is used in the M-P-φ relationship to find a corrected value of $\bar{\varphi}$ at the end of the segment. This $\bar{\varphi}$ will in general differ from the previously assumed value $(\bar{\varphi}_o)$. The process is repeated until the successive values of $\bar{\varphi}$ at the segment end satisfy the desired tolerance.

The final values of $\underline{H}$, $\underline{V}$, $\underline{M}$, θ, $\underline{x}$, $\underline{y}$, $\underline{s}$, and $\bar{\varphi}$ are then used as initial values for the next $\underline{\Delta s}$ increment and the iterative process is repeated.

The integration is continued in this manner until the desired end conditions are met ($\underline{M} = 0$ for simple support or $\theta = 0$ for fixed support). The value of s at this point gives then the length of the beam-column which is in equilibrium under the given P and q and has the mid-span curvature of $\bar{\varphi}_o$.

$$\underline{L} = 2s_{end} \tag{44}$$

This procedure is shown in the flow chart of Fig. 12.

Ultimate Strength

By assigning a series of values to the initial mid-span curvature $\bar{\varphi}_o$ and performing the integration procedure described above, the corresponding lengths $\underline{L}$ are obtained for the same values of P and q. The resultant relationship between L and $\bar{\varphi}_o$ is shown in

24

Fig. 13. In it the maximum length L_{max} is the length of the beam-column with the given cross section and end conditions for which the specified P and q are ultimate loads P_u and q_u.

If the actual length a of the beam-column is less than L_{max}, the curve in Fig. 13 gives two deformation geometries of equilibrium, i.e., two points for a load-deformation analysis of the beam-column. This is shown in Fig. 14a for $P = P_1$.

Axial Load vs. Axial Shortening

Figure 14 shows how the L vs. φ_o curves are used to obtain the P vs. axial shortening relationship (P vs. Δ) for a beam-column under the same lateral loading q.

1) By varying the value of P a set of L vs. φ_o curves are obtained as shown in Fig. 14a.

2) Since the axial load P and curvature φ are known along the beam-column during the integration process, the axial shortening Δ is readily computed and a set of L vs. Δ curves are obtained. A corresponding plot is given in Fig. 14b. In this, the total axial shortening Δ is defined by

$$\Delta = \Delta_p + \Delta_c \tag{45}$$

where Δ_p = axial shortening due to axial strain (effect of P)

Δ_c = axial shortening due to curvature

3) By entering the L vs. Δ graph (Fig. 14b) with the value of the given length L = a, the Δ values corresponding to each value of P are found. The results are then combined into a P

25

vs. Δ curve valid for a specified lateral loading q and length L = a as shown in Fig. 14c. The peak of the curve gives the ultimate axial strength of the beam-column.

2.5.4 Effect of Strain Reversal

A special correction for the effect of strain reversal had to be made in the post-ultimate range of the P-Δ relationship. The need for this arose from the fact that the procedure described above for obtaining the L vs. φ_o and P vs. Δ curves is based on formulating an equilibrium condition on a member deformed to the configuration considered. This is equivalent to obtaining each point of the P-Δ curve as if the path of deformation followed a straight line from the origin as indicated by the dashed line in Fig. 15. Whereas the pre-ultimate range of the P-Δ curve which is for an increasing value of P is not affected by this procedure, the post-ultimate range becomes very distorted. This is shown in Fig. 15 by the dotted z-shaped curve defined by crosses. In this case the nonlinear and plastic deformations which had taken place under the higher past load and subsequent elastic relaxation are not taken into account.

In order to correct the anomaly of the reduction of the deformation indicated by the dashed curve, the true deformation path including the strain reversal resulting from the drop in the axial load in the post-ultimate range was approximated by modifying Eq. 45 to

$$\Delta = \Delta_{pu} + \Delta_c \qquad (46)$$

26

where Δ_{pu} is the axial shortening which existed under the ultimate

load P_u (at the peak). It replaces Δ_c computed for the

given P and is assumed to remain constant throughout the

post-ultimate range.

Δ_c is the curvature shortening computed for P.

The result of this adjustment is shown in Fig. 15.

2.5.5 Axial Behavior

The computerized procedure described above requires that the

lateral loading q be non-zero* and thus the procedure is not directly

applicable to the analysis of ship deck plating. To obtain the

pure axial load vs. shortening behavior, a set of P vs. Δ curves are

computed for decreasing values of q and the P-values for q = 0 are

extrapolated.

Two examples of such extrapolation are shown in Fig. 16 for

the ultimate capacity of the compression flange of the test specimen.

The top plot is for the original design dimensions and the nominal

yield stress. The bottom plot is for the dimensions and the yield

stress as they were measured in the fabricated specimen. Another

example is given in Fig. 17 where the complete P vs. Δ curve with

a number of initial curves for various values of q are shown. Usual-

ly three values of q between 0.03 and 0.10 were sufficient.

---

*An alternate method would have been to introduce initial geometric
 imperfections, see Art. 2.5.7.

2.5.6 Axial Behavior of Compression Flange

P vs. Δ behavior of a beam-column adjusted for strain reversal and extrapolated to zero lateral loading (q = 0) is assumed to represent the P vs. Δ response of the whole compression flange. An example is given in Fig. 17 where the top curve is the extrapolation to q = 0 from P-Δ curves for non-zero q's and is thus the desired P vs. Δ relationship.

For comparison, the response of a tension flange, corresponding to the material stress-strain diagram is also shown in Fig. 17.

For greater convenience of parametric studies, the axial load is nondimensionalized to $P/P_y = P/AF_y$ and the axial shortening to $\Delta/a\varepsilon_y$.

2.5.7 Consideration of Initial Imperfections

Initial deflections due to fabrication were not considered in the procedure described above. However, a modification can be readily made by transforming the initial deflection patterns into a curvature diagram and then adding the corresponding curvature values at each segment in the integration process. Since the integration length L may be longer than the actual length of the beam-column a, the initial curvature diagram should be extended, by, for example, making it constant and equal to the end value of curvature or to zero.

28

2.6 Behavior and Ultimate Strength of Hull Girder Segment

Once the load-deformation behavior of the individual components is defined, the analysis of the behavior of the entire hull girder segment proceeds by enforcing the compatibility between these components as the load parameter is incremented. In summary, the following load-deformation relationships of the components are involved:

- τ vs. γ relationships for the subpanels of the webs (Fig. 4). Redistribution of the stresses over the web depth is taken into account.

- P/P_y vs. $(\Delta/a)/\epsilon_y$ relationship for the longitudinally stiffened compression flange (Fig. 17).

- σ vs. ϵ relationship (material curve) for the tension flange, the stiffeners and the unbuckled subpanels of the webs.

The internal forces acting on the mid-segment section--moment, shear and torque--are related to the applied load W as shown in Fig. 3. Using load W as the loading parameter, the functional dependence can be expressed by the following equations:

$$V = C \; W \tag{47}$$

$$M = C_1 \; d \; V = C \; C_1 \; d \; W \tag{48}$$

$$T = C_2 \; d \; V = C \; C_2 \; d \; W \tag{49}$$

C = proportionality factor between the cross-sectional shear and the applied load W (load parameter)

C_1 = moment-shear ratio $\left(= \dfrac{M}{Vd} \right)$

C_2 = torque-shear ratio $\left(= \dfrac{T}{Vd} \right)$

d = depth of the cross section

For this study, the average strain in the junction line of the web under the higher shear and the compression flange was chosen to be the deformation parameter. This strain corresponded to the average shortening of the compression flange, Δ/a.

Two examples of the resultant curves for load-deformation relationships are shown in Figs. 18 and 19. These are respectively for Tests 1 and 3, but using the design dimensions and a somewhat different test arrangement than used in the actual tests.

The procedure for obtaining the W vs. $(\Delta/a)/\varepsilon_y$ relationship is conveniently explained in conjunction with the flow chart given in Fig. 20.

1) $\Delta/a = \varepsilon_c$ is the average axial strain of the stiffened flange under compression. An initial value of ε_{ci} is assumed.

2) A value of the strain in the tension flange ε_{tj} is assumed and, since the section remains plane after deformation (Assumption 3 in Sect. 2.2), the linear strain distribution in the cross section is used to compute the stress distribution from the response relationships of the individual components. In the process, it is assumed that, whereas the shear on a web subpanel can increase after buckling, the normal stresses remain at the level of buckling.

30

3) The total axial force on the cross section (Eq. 50) is computed
from the stresses and compared with the given value N_o ($N_o = 0$
in this case). The true strain distribution, for which $N = N_o$,
is found by modifying the value of ϵ_{tj} while ϵ_{ci} is kept constant
and repeating Steps 2 and 3 until a preset tolerance is satisfied.

$$N = \int_A \sigma \, dA \qquad (50)$$

$$|N| - |N_o| = \text{Tolerance} \simeq 0 \qquad (51)$$

4) The internal moment is then calculated by integration.

$$M = \int_A \sigma \, y \, dA \qquad (52)$$

5) With the value of M determined in Step 4, the load parameter W,
V and T are found from Eqs. 47, 48, 49

$$W = \frac{\int \sigma \, y \, dA}{C \, C_1 \, d} = \frac{M}{C \, C_1 \, d} \qquad (53)$$

$$V = \frac{\int \sigma \, y \, dA}{C_1 \, d} = C \, W \qquad (54)$$

$$T = C_2 \, d \, V = C \, C_2 \, d \, W \qquad (55)$$

6) The values of M, V and T are then used to compute the stresses in
each web subpanel (τ, σ_b, σ_c). The interaction formula of Eq. 8
is used to check the buckling condition.

7) The τ-γ relationships for the subpanels, as shown in Fig. 4, are
used to define the distribution of the shearing stresses in the
subpanels (same γ-parameter for all subpanels in each web at a
particular load) and to check for the ultimate shear strength of

31

each subpanel.

8) If the shearing stress in a particular subpanel is higher than the τ_{cr} or τ_u indicated in Fig. 4, ϵ_{ci} must be reduced and the same procefure repeated until a value acceptably close to τ_{cr} or τ_u is found.

9) After all controlling requirements are satisfied, ϵ_{ci} and its corresponding value of W_i represent one point on the W vs. ϵ_c curve.

10) The procedure of Steps 1 to 9 is repeated for increasing values of strain ϵ_c to obtain a complete W vs. ϵ_c curve, including the pre- and post-ultimate ranges.

In the examples of Figs. 18 and 19, the junction strain ϵ_c is nondimensionalized with respect to the yield strain ϵ_y. Contributions of the webs and flanges to the total load are shown by separate curves. The share for each was assumed to be proportional to the percentage of the moment carried by the respective component.

The method described above is not suitable for manual computations, and therefore, a computer program was written in accordance with the flow chart of Fig. 20.

32

3. TEST SPECIMEN

3.1 Types of Tests

In order to check the present theory, a test specimen was designed to conduct three tests under different combinations of moment, shear and torque. For each test, a particular segment (portion of the girder between transverse stiffeners) was tested to failure while the other two segments were reinforced.

Figure 21 shows the test arrangement for each of the tests and the corresponding combinations of moment, shear and torque defined in terms of the jack load W.

Test 1: The test segment is subjected to bending moment and shear force.

Test 2: The test segment is subjected to bending moment, shear force and torsional moment.

Test 3: The test segment is subjected to bending moment only.

In the present program, only Tests 1 and 2 were completed.

3.2 Scantlings of Test Specimen

The scantlings of the test specimen were selected to model portions of a typical hull girder. The relative proportions of each component were approximately the same as used in engineering practice. Two views and the principal cross sections are shown in Fig. 22. The overall scantlings are: length--2972 mm (117 in.),

width--667 mm (26.25 in.) and depth--508 mm (20 in.). In the middle

portion of 1372 mm (54 in.), the plate thickness is 1.59 mm (1/16 in.).

In the end portions, the thickness of the flange plate is 6.35 mm

(1/4 in.) and of the web plate 3.18 mm (1/8 in.).

The spacing of the longitudinal stiffeners and the thickness of

the plate in the middle test portion were selected so that plate

instability would occur before reaching the ultimate capacity.

The scantlings of the fabricated specimen were slightly

different than the design scantlings shown in Fig. 22. The most

significant change was in the plate thickness from 1.59 mm (1/16 in.)

to 1.85 mm (0.073 in.), and this was taken into account in the

analysis of the test results.

3.3 Material Properties

The test specimen was fabricated from ASTM A36 steel plate with

a nominal yield stress of 250 MPa (36 ksi). Eight standard 203 mm

(8 in.) gage tensile coupons (36) were fabricated from the plate to

determine the actual yield stress. Four coupons were in the longi-

tudinal direction of the specimen and four in the transverse. As

the first three coupon tests showed good agreement, the yield stress

was defined from these three coupons (two in the longitudinal and one

in the transverse direction). Four material properties were

determined:

F_{ys} - the static yield stress at a zero strain rate

34

F_{yd52} - the dynamic yield stress at the strain rate of 52 μm/m/sec

F_{yd1045} - the dynamic yield stress at the strain rate of 1045 μm/m/sec

F_u - the ultimate stress.

The most significant and reliable of these for analyzing test results is the static yield stress, F_{ys}. It was found by the following procedure (35), illustrated in Fig. 23. Shortly upon reaching the flattened portion of the stress-strain curve, that is, upon reaching the yield stress, the machine head is stopped to reduce the strain rate to zero and the load is allowed to stabilize within three to five minutes at a lower level. The resumption of straining leads to an increase of the load to a level dependent on the strain rate. At least two more stops are made within the plateau of yielding as shown in the figure. The average of the reduced stresses at the bottoms of the dips is defined as the static yield stress, that is, the yield stress at a zero strain rate. After this, the coupon test proceeds in the usual manner (36). Two non-zero strain rates are indicated by the different levels of the horizontal portions of the stress-strain diagram in Fig. 23.

The static yield stress and the dynamic yield stress at two different strain rates (52 μm/m/sec and 1042 μm/m/sec) are listed for the individual coupons in Table 2. The strain rate of 1042 μm/m/sec is the maximum testing rate permitted by ASTM A370 (36) and is commonly used by steel producers for determining mechanical material properties.

As shown in Table 2, the average static yield stress in the longitudinal direction is 237 MPa (34.34 ksi) and the dynamic yield stress, F_{yd1042} is 280 MPa (40.55 ksi). This represents an increase of 18.1%. The variation among the yield stresses at a given testing rate is relatively small (2% for a rate of 1042 μm/m/sec).

The yield stresses obtained for the coupon in the transverse direction of the specimen are a little larger than for the coupons in the longitudinal direction. The difference is of the order of 3 to 7%, depending on the strain rate.

No coupon tests were made for the material of the end portions of the specimen which were designed only to transmit loads and to have low stresses.

3.4 Fabrication Process

The middle portion of the specimen (the test portion) was fabricated as follows. First, the four sides of the box section were fabricated separately by welding the longitudinal and transverse stiffeners to the plate. Then, the four sides were put together and welded along the four corners to form a box section. The end portions were fabricated in the same way. The last operation consisted of joining the three portions of the specimen by transverse welding. All the welds were made manually by the submerged-arc process. Because of this and also because the small thickness of the plate in the middle test portion of the specimen (1.85 mm, 0.073 in.), the plates developed large initial imperfections. In order

36

to reduce these imperfections, the plate between longitudinal stiffeners was straightened out by hammering.

The residual stresses which were caused in the plates by the welding process, were not measured.

3.5 Initial Imperfections

Initial imperfections were measured for the plates of the webs and the compression flange. Imperfections of the tension flange and of the longitudinal and transverse stiffeners were not measured.

A standard measure of initial imperfections in plates is given by the out-of-flatness which is the maximum offset from a longitudinal straight line and the plate surface. The straight lines were defined by points at the transverse stiffeners.

The instrumentation for measuring initial imperfections consisted of a straight reference bar set on the transverse stiffeners and used as a guide for a movable dial gage. Readings were taken at different locations in the longitudinal direction of the test specimen. This was done over the full length of the test portion (1372 mm (54 in.)). This operation was repeated at each longitudinal profile where the initial imperfections were to be found. For the webs, readings were taken along the middle of each of the three subpanels. For the compression flange, thirteen profiles were used: at mid-subpanels, at longitudinals and at the edges.

37

Initial imperfections for the webs are shown in Figs. 24 and 25. The imperfections are plotted with respect to a straight line anchored at the extreme transverse stiffeners of the test portion. The maximum offsets are of the order of ± 4.8 mm (0.19 in.). This represents approximately 2.6 times the plate thickness.

Initial imperfections of the compression flange are shown in Fig. 26 by means of a contour map. The contour lines are plotted with respect to a reference plane defined by points A, B and C. The reference plane was adjusted so that the initial vertical imperfections along the web-flange junctions were minimized.

As can be seen in Fig. 26, most of the offsets are in the range of ± 2.54 mm (± 0.1 in.) which is equal to 1.4 of the plate thickness. The maximum values are of the order of ± 5.08 mm (± 0.2 in.), that is, 2.7 times the plate thickness. Thus, they have approximately the same order of magnitude as for the webs. The areas with the maximum values are rather small, but their influence on the flange behavior may be significant.

4. TEST PROCEDURE

4.1 Test Setup

4.1.1 General Arrangement

A general view of the test arrangement is shown in Fig. 28. The whitewashed specimen is in the middle. The loading jack is above the specimen and is attached to the loading frame. To the right of the right column of the loading frame and behind a table is the strain data acquisition unit.

The test setup is shown in Fig. 27. The specimen is positioned on two support pedestals so that there is a free space below it for placing instrumentation and making observations. The free span is 2970 mm (117 in.). A concentrated load is applied by means of a jack* attached to a transverse beam of the test frame. The load is transmitted to the test specimen by a spreader beam, set transversely on two plates welded to the transverse stiffeners of the webs as shown in Section A-A (Tests 1,2) of Fig. 27. Thus, the load is introduced to the box section through the webs. For Test 1, the cross section was loaded symmetrically (Section A-A) and for Test 2 with an eccentricity of 194 mm (7-5/8 in.).

There were three points of support for the specimen. The X-Y roller bearing at the right end of the specimen consisted of an

---

*Amsler hydraulic jack: Maximum dynamic load 250 kN (55 kips), maximum static load 475 kN (104.5 kips), maximum stroke 127 mm (5 in.), height 1.06 m (41.75 in.)

arrangement of two mutually perpendicular rollers separated by a plate so that rotation and translation were possible in the longitudinal and transverse directions. This arrangement and the bracing required in the specimen end frame to transmit the reaction are shown in Fig. 29.

At the left end in Fig. 27 there were two X-roller bearings, one on each side of the cross section, which permitted free rotation and one was also free to translate longitudinally (X-direction) as shown in Fig. 30a. In Test 2, one of these two supports was anchored down as shown in Fig. 30b to prevent uplift of the support due to torsion. The fixture consisted of a rigid corner angle positioned on the top bearing plate and tied down with two large bolts to the pedestal.

4.1.2 Reinforcements

To accomplish several tests on the same specimen (three tests were planned), it was necessary to reinforce the segments adjacent to the test segment. For Test 1, the adjacent segment was temporarily reinforced by using

a) small steel bars cee-clamped to the longitudinal stiffeners

b) corner angles at the web-to-compression flange junctions

c) pieces of wood on the compression flange

All these reinforcements were tightly wedged between the transverse stiffeners. Their function was to reduce the axial force in the compression flange.

For Test 2, the segment which failed in Test 1 was reinforced with four steel bars and two corner angles tack welded to the compression flange and wedged between transverse stiffeners. The webs were reinforced with steel bars in the direction of the tension diagonal as shown in Fig. 31a. All these reinforcements were welded to the transverse stiffeners. The segment reserved for Test 3 (to the left of the segment in Test 2 in Fig. 27) was reinforced by steel bars clamped to the longitudinal stiffeners and pieces of wood wedged between transverse stiffeners as shown in Fig. 31b.

4.2 Instrumentation

The instrumentation consisted of both mechanical dial gages and electric resistance strain gages. The dial gages set up underneath the specimen at transverse stiffeners were used to measure the vertical deflections of the specimen (Fig. 28). The deflection at the load point was used as an indicator of the overall behavior of the girder during the test.

Eighteen linear strain gages and seven three-branch rosettes were used in each test. The gages were cemented on the outside surface of the test segments and Figs. 32 and 33 show their location for tests 1 and 2, respectively.

Each strain gage, either as a uniaxial gage or as an element of a rosette, was read and recorded by means of an automatic data acquisition unit.* The digital strain output was typed and punched

*Multi-point strain gage plotting system with punched tape output,
 B&F Instruments, Inc., Philadelphia, Pa.

41

directly on paper tape.

The strain gages provided information about the transverse stress distribution in the compression flange and also about the tension field pattern which developed after the theoretical buckling of the webs. Three strain gages were also placed on the tension flange in order to get a complete picture of the stress distribution in the cross section of the box girder.

Diagonal deformations of the tested segments were measured by means of a variable length extensometer which consisted of an aluminum support bar and a dial gage mounted on a movable extension. The process of taking readings of diagonal deformations in Test 1 is shown in Fig. 28. This extensometer was also used at other points to measure the variation of length between the transverse stiffeners at the ends of a test segment.

Lateral deflections of the webs and vertical deflections of the compression flange were measured by means of two special dial gage rigs shown in Fig. 34. These rigs consisted of three mechanical dial gages attached to an aluminum angle bar for web deflections and to a steel bar for compression flange deflections. The positions of the dial gages corresponded to the 1/4, 1/2 and 3/4 of the spacing between two adjacent transverse stiffeners. The rigs were placed against the transverse stiffeners and held with magnets for the web rig and with point supports for the flange rig. The readings were taken while rigs were successively positioned at different sections.

42

The middle portion of the specimen was whitewashed prior to testing (Figs. 28 and 31). The flaking and cracking of the whitewash provided a means of visually observing the progress of yielding.

4.3 Testing Procedure

Each test started with a few cycles of loading between 0 and 23 kN (5 kips) (less than 10% of the expected ultimate load) in order to properly position the girder on its supports. A complete reading was taken of all gages at zero load to serve as an initial reference. The load was slowly incremented, generally in 23 kN (5 kip) steps. For Test 2, just before the ultimate condition was reached (it occurred at a lower load than expected), the specimen was unloaded to zero and then gradually reloaded up to the maximum strength level first in two larger increments of about 68 kN (15 kips) and then in two smaller increments of 13.6 kN (3 kips).

At all load levels, readings were taken of the dial gages measuring the vertical deflection of the specimen, the electrical strain gages and the variable length extensometer. Also at several load levels, readings of the dial gage rigs for measuring lateral deflections of the webs and of the vertical deflections of the compression flange were taken.

43

5. TEST RESULTS

5.1 Introduction

The procedure described in Art. 4.3 was followed in conducting
both tests, Test 1 under bending and shear (M+V) and Test 2 under
bending, shear and torque (M+V+T). Behavior of the specimen during
testing is presented here in the form of the following values plotted
against the applied load: (1) mid-span deflection, (2) diagonal
panel deformations, and (3) strain distributions. Some values of
the out-of-plane deformations of the compression flange and of the
webs are also given, but mainly in a descriptive form.

In both tests, the ultimate capacity was limited by the failure
of the compression flange characterized by large out-of-plane
deflections.

Some general comments apply to the interpretation of the results
of both tests. These pertain to the loads used in reporting the
results and to the strain readings.

Although the loading rate during testing was not recorded, it
was kept very low. Yet, the response of the girder was quite
sensitive to the rate of loading on approaching the ultimate load
and, especially, in the post-ultimate range. This sensitivity
manifested itself by the fact that after a desired load level was
reached and the testing machine stopped, the load gradually dropped
to a lower level while the data readings were taken. When testing
was resumed, the load climbed above the previously reached level,

44

but again fell when the machine was stopped. The reduction of the
load was about 0 to 4% in the nonlinear pre-ultimate range. This
reduction was about 8% in the post-ultimate range. For convenience,
the maximum load in each load increment was used in the description
of the test results.

Since the strain gages were placed only on the outside surface
of the plate, the gage readings were not indicative of the average
membrane stresses, but rather of the surface stresses which were
affected by local plate curvatures resulting from the initial or
buckling deformations. Yet, it is the membrane stresses which were
pertinent to the analysis of the girder cross section.

5.2   Test 1 (M,V)

5.2.1   General Behavior of Specimen

Since in Test 1 no torque was applied to the specimen, the
vertical deflections of the two webs must theoretically be the same.
This was approximately verified. In the test, Web 1 (the web seen
in the elevation of Fig. 27) deflected more than Web 2. However, the
difference was quite small; it did not exceed 8% when the load was
up to $0.67 \, W_u$. Then, the difference increased to reach 18% at the
ultimate.

The overall behavior of the segment is conveniently described
by referring to the load-deflection curve shown in Fig. 35 . The
deflection parameter is taken as the average of the deflections of
the two webs measured at the load location. As can be seen in Fig.

35, the curve exhibits four portions:

(1) Linear portion, up to $0.58\ W_u$.

(2) Gradually curving portion, up to the ultimate load at 272 kN
    (60 kips). The deviation of the curve from linearity appeared
    to be mainly due to the increase of the out-of-plane plate
    deflections of the compression flange and of the upper web
    subpanels and local yielding.

(3) Post-ultimate drop-down portion. After reaching the ultimate
    capacity, the load suddenly dropped and then stabilized at
    $0.75\ W_u$. When the machine valve was opened again, the load
    climbed somewhat and then dropped further to a stable level of
    $0.63\ W_u$.

(4) Unloading portion. After obtaining the post-ultimate range
    the girder was unloaded to zero in two steps as shown in Fig.
    35.

5.2.2 Diagonal Deformations of the Web

A good representation of the behavior of a test segment is
given by a diagram of deformations (changes in length) of the com-
pression and tension diagonals versus the applied load W. Figure
36 shows the relative diagonal deformations, respectively shortening
and elongation, of the compression and tension diagonals of Web 1
in Test 1. Some waviness of the curves is due to the inaccuracy
of the variable length extensometer which was used for measuring
diagonal deformations.

For the tension diagonal, the behavior is almost linear up
to the ultimate load. For the compression diagonal, the slope of
the linear portion is less steep than for the tension diagonal and
it extends up to about 0.75 W_u. Then, the curve gradually flattens
out up to 0.9 W_u and suddenly jumps to the ultimate load W_u. In
the post-ultimate range, both diagonals deformed much more readily
than in the pre-ultimate range, especially the compression diagonal.

A comparison of the diagonal deformations shown in Fig. 36
demonstrates the extent of the overall shearing distorsion of the
panel. The rigidity of the panel to the shear force was constant up
to 0.75 W_u and then started to decrease. At the ultimate load and
in the post-ultimate range, the shear force was mainly carried by
the tension diagonal since the large deformations of the compression
diagonal were mainly induced by the failure of the compression flange.

5.2.3 Deformations of Compression Flange and Webs

A comprehensive presentation of the out-of-plane deformations of the compression flange and webs was not warranted for the following reasons:

- The number of measurement points was relatively small to give an adequate picture of the irregular deformation patterns.

- The deformations of the compression flange at and after the ultimate load were too large to be measured with the dial gage rig.

In consequence, specific values are given only for the largest deflections of the plate and stiffeners of the compression flange and webs, and of the flange-web junction. They were measured at four load levels with respect to the deformation pattern at zero load (Figs. 24, 25 and 26) and are listed in Table 3.

All deformations increased gradually from the zero load to approximately $0.85\ W_u$ with the maximum deflection of 1.44 mm (0.057 in.) in a flange stiffener. This was about 30% of the maximum initial imperfection.

In the compression flange, the plate between longitudinals deflected more than twice as much as the longitudinals when the load was less than $0.5\ W_u$. Then, the deflections of the longitudinals suddenly accelerated so that at $0.67\ W_u$, they were of the same order of magnitude as of the plate. At the ultimate load, all deformations suddenly increased so that all of the middle portion of the flange panel came out as shown in Figs. 37 and 38. The maximum deflections were estimated to be more than 30 mm (1.2 in.). The fact that the

48

longitudinal stiffeners all exhibited almost the same maximum

deflection as indicated in Fig. 39 with respect to a ruler, supports

the validity of analyzing the compression flange as a beam-column.

For the webs, deflections were less than 1.2 mm (0.047 in.) at

0.85 W_u and then increased suddenly at the ultimate load, with some

local deflections reaching to 11 mm (0.433 in.). This dramatic change

was apparently induced by the failure of the compression flange.

As can be seen in Figs. 37 and 38. the web longitudinals buckled

since they were inadequate to resist the axial force redistributed

to them from the compression flange at the ultimate load. However,

they did not deflect more than 0.8 mm (0.03 in.) almost up to the

ultimate load (Table 3), and, therefore, they were sufficient to

enforce the redistribution of stresses between individual subpanels.

5.2.4 Strain Distribution

Figure 40 is a plot of the strain distribution in a half-width

of the compression flange. Location of the pertinent strain gages

is shown in the lower sketch (see also Fig. 32). Strain variation

between two middle longitudinals is shown dotted because the gage

there malfunctioned and the strain in the middle was averaged from

the strains of Gages 3 and 7.

For the loads not exceeding 0.5 W_u the strain was almost uniform.

For the loads over $0.5W_u$, the strain distribution was marked by the

local reduction which occurred between the longitudinal stiffeners

and indicated a change in the effectiveness of the plate due to

49

post-buckling deflections. Actually some reduction of the plate
effectiveness can be observed even at smaller loads due to the
influence of initial imperfections. The increasingly higher strain
at the edge of the flange (Gage 2) relative to the middle portion
points to the gradual reduction of the overall effectiveness of the
compression flange as the ultimate capacity was approached. Yet, a
large portion of the plate could reach the yield strain level as
indicated in Fig. 40.

Figure 41 shows the relationship between the strains in the
compression flange at several locations and the load. The strains
at the web-flange junctions at the mid-length of the panel (Gages
2 and 10) grow much faster than the strains at other points and are
almost identical to each other. A comparison of the curves for edge
gages (Gages 2 and 10) with the mid-width gage (Gage 9) further
confirms the observations made in connection with Fig. 40 about the
increasing nonuniformity of strains across the flange width. Yet
Gage 14 seems to violate this conclusion when compared with Gage 11.
The unexpectedly lower readings of Gage 14 may be due to some local
disturbances. A comparison of the strains of Gages 2, 9 and 10 with
the strains from the ordinary beam theory shows how erroneous the
results from the beam theory may be.

In Figure 42 are shown the longitudinal distribution of the
stresses in the plate at mid-width of the compression flange (Fig.
42c and the distribution of the bending strains in Web 1 (Fig. 42d).

The stresses along the flange (Fig. 42c) are relatively constant from one end to the other for loads smaller than 0.67 W_u. For higher loads, the strains decrease towards the ends of the panel because of the effect of the upward bending of the flange and the partial restraint at the ends by the transverse stiffeners and adjoining segments and their reinforcements. The restraining effect at the ends of the longitudinals cán be also observed in Figs. 37 and 38.

In Figure 42d, for the loads not exceeding 0.83 W_u, the neutral axis remains at its initial position (mid-depth). Then, as the ultimate load is approached, the neutral axis gradually shifts downward indicating a loss of capacity of the compression flange. Furthermore, the strain distribution remains more or less linear up to the ultimate load, except for the top subpanel which buckled quite early.

5.3 Test 2 (M,V,T)

5.3.1 General Behavior of Specimen

The overall behavior of the segment is described by the load-deflection curve shown in Fig. 43. The deflection parameter is the vertical deflection of Web 1 at the load location as shown in the insert. Five portions of the curve can be distinguished.

(1) Linear portion, up to 0.54 W_u.

(2) Nonlinear portion on approaching the ultimate load W_u. First the slope of the curve changed gradually; then, from 0.94 W_u, it suddenly became almost horizontal, indicating that the

51

ultimate capacity of the segment was being reached.

(3) Hysteresis loop. At 0.98 W_u, the effective eccentricity of the
load had increased due to the large angle of rotation of the
section and the distortion of the left end frame as shown in
Fig. 45. Furthermore, while gage readings were taken at 0.98
W_u, the load gradually dropped, first to 0.97 W_u, then to 0.87
W_u (reduction of 10%). At this point, the specimen was unloaded
in several steps to zero, the load eccentricity adjusted by
slightly shifting the loading point on the spreader beam, and
the specimen reloaded until the ultimate capacity was reached
at 168 kN (37 kips).

(4) Post-ultimate drop-down portion. After reaching the ultimate
load level, the load dropped and stabilized at 0.87 W_u.

(5) Unloading portion. The girder was unloaded to zero in several
steps of 22.7 kN (5 kips).

5.3.2 Diagonal Deformations of the Webs

Because of the load eccentricity, one web (Web 1) was subjected
to a higher shear than the other (Web 2), and, therefore, diagonal
deformations are plotted in Fig. 44 for both webs against the test
load W.

The response for the tension and compression diagonals for Web 2
and the tension diagonal for Web 1 are essentially linear up to 0.95
W_u. A sudden change in the slope occurs at this load before the
ultimate load is reached. Deformation of the compression diagonal

52

of Web 1 was much more pronounced. Although the curve was essentially linear up to $0.54 \, W_u$, the slope is much flatter than for other diagonals. The slope reduces further until $0.8 \, W_u$ and after $0.95 \, W_u$ becomes almost horizontal until the curve reaches the ultimate load W_u.

The load at which the response of the compression diagonal of Web 1 becomes nonlinear corresponds exactly to the beginning of the nonlinear portion of the load-deflection curve of Fig. 43. After this load, flaking of the whitewash was observed along the tension diagonal of the upper subpanel of Web 1 as shown in Fig. 46. (Note that the large deflections of the compression flange shown in Fig. 46 developed much later at the ultimate load.)

The larger deformation of the compression diagonal of Web 1 than of the tension diagonal demonstrates the extent of the overall shearing distortion of the panel caused by subpanel buckling and the shortening of the compression flange on this side. For Web 2, deformations of the tension and compression diagonal are approximately the same indicating a linear shearing deformation without buckling.

5.3.3 Deformations of Compression Flange and Webs

Maximum values of deformations of the web-flange junctions, the plate and the longitudinals with respect to initial imperfections are given in Table 4 for different load levels.

Out-of-plane deformations of the compression flange increased rapidly even at low loads. At 0.54 W_u, the maximum deflection of the plate already reached 0.99 mm (0.0389 in.). Deformations varied significantly across the width of the flange; they were larger at Web 1 than at Web 2 as can be seen in Fig. 46 at the ultimate load. Another illustration is given in Figs. 47 and 48 for the flange sides of Webs 1 and 2, respectively. For loads not exceeding about 0.81 W_u, the maximum out-of-plane deformations of the longitudinals were smaller by approximately 30% than for the plate in between. At the ultimate load, the maximum deflections of the plate and longitudinals became equal to each other, measuring 12.8 mm (0.0504 in.). For comparison, the longitudinal closest to Web 2, deflected less than 1 mm (0.039 in.). It is important that all deformations of the flange were downward (inward).

The results obtained for the diagonal deformations of the webs (Article 5.3.2) correlate with the out-of-plane deformations. Web 1 (the loaded web) exhibited larger deformations than Web 2. The deformation patterns at the ultimate load are shown for both webs in Figs. 47 and 48, and they very clearly point out the difference in behavior. Large deformations of Web 1 in Fig. 47, mainly in the top two subpanels are contrasted with the practically nonexistent deformations of Web 2 (Fig. 48) where they were smaller than 0.71 mm (0.028 in.). For loads not exceeding 0.81 W_u, the maximum deformations of the subpanel plate of Web 1 were twice as large as the deformations of the longitudinal stiffeners. However, at the ultimate load, similarly to what was observed in the compression

54

flange, the stiffener and plate deformations became of the same

order of magnitude.

5.3.4 Strain Distribution

Figures 49a and 49b show the strain distribution in the half-

widths of the tension and compression flanges next to the loaded web

(Web 1). The dotted lines in Fig. 49b indicate the strain dis-

tributions estimated from the averages of the readings of Gages 6

and 10 in the adjoining subpanels. The thinner lines in Fig. 50(b)

give the strain distribution computed by assuming the cross section

to be closed up to 0.41 W_u (theoretical buckling of two subpanels of

Web 1) and then to become an "open channel" section with Web 1

"removed" and including warping stresses for loads over 0.41 W_u.

In contrast to the strain distribution in Test 1 (Fig. 40

was relatively uniform except for small increases at the longitudinals

and a large increase at the edge, the strain distribution in Test 2

(Fig. 49b) was basically linear except for the variation between

subpanels and longitudinals and the increase at the edge, and is

thus analogous to the theoretical strains given by the thin lines

for an "open channel" section. This means that there was a gradual

transition from a closed to an open section as the heavier loaded

web (Web 1) was weakening. This behavior needs further investigation.

Figure 50 shows the load-strain relationships for strain gages

1, 5, 12 and 14, located on the compression flange as given in the

insert sketch. The strain at the gages along the mid-width of the

segment (Gages 1,12,14) is linear up to about 0.81 W_u. Then, the slope for the gages at the ends of the segment (Gages 1 and 14) progressively reduces as the load is increased toward the ultimate load, while the strain at mid-segment remains linear. This behavior is a direct consequence of the downward (inward) buckling of the longitudinals clearly seen in Figs. 46 and 47. The strain at Web 1 (web-flange junction, Gage 5) is linear up to 0.68 W_u and then suddenly increases. At the ultimate load, the strain was so large that no reliable reading could be taken. Figures 46 and 47 show the extensive deformations and yielding of the web-flange corner which led to such high strains. In contrast, the other corner (at Web 2) hardly deformed as can be seen in Fig. 48.

Figure 51 shows the strain distribution across Web 1 at mid-length of the segment. The strain distribution patterns for the individual loads are very irregular and can hardly be considered to support the "plane section remaining plane" hypothesis. However, except for the last two load increments, the neutral axis remained at essentially the same location, although below the mid-depth point. This indicates that the overall response of the cross section was essentially linearly elastic with the compression flange being weaker than in Test 1 from the start. The downward shift of the neutral axis for the loads over 0.68 W_u was mainly caused by the progressive failure of the compression flange and of the top web subpanel.

The unexpected bulge in the strain diagram for the bottom web subpanel apparently was caused by the straightening of the initial inward imperfection of the web at this location.

56

6. COMPARISON OF ANALYTICAL AND EXPERIMENTAL RESULTS

6.1 Analysis of Test Segments

The girder segments of Test 1 (M,V) and Test 2 (M,V,T) were analyzed by the method presented in Chapter 2.

Since the two segments had the same dimensions, the response of the compression flange to axial force was the same for both segments. The shearing stresses due to torque in Test 2 were assumed to have no effect on the axial behavior or ultimate strength. Figure 52 gives the resultant relationship between the axial force nondimensionalized with respect to the yield force vs. the total axial deformation nondimensionalized with respect to the yield strain. Also shown are the construction curves for non-zero lateral loading. This figure is analogous to Fig. 17 except that this time actual dimensions and yield stress of the specimen were used.

The internal forces, moment M, shear V and torque T, as well as the shear in each web, are listed in Table 5 for both tests in terms of the applied load W. The shear in Web 1 is the same for both tests, but in Web 2, it is much smaller for Test 2 than for Test 1. The moment for Test 2 is about 9% larger than for Test 1.

The relationship of Fig. 52 was used to analyze the two test segments, each under its own combination of internal forces (Table 5). The resultant test load vs. web-flange junction strain curves are shown in Fig. 53. For Test 1, the strain is the same at both flange edges and, for Test 2, the strain in the higher-stressed edge at Web 1 was used.

57

Both curves are linear up to the first kink which corresponds to the buckling of the top web subpanel (Webs 1 and 2 for Test 1 and Web 1 for Test 2). There is one more kink in each curve before the ultimate load is reached, and it reflects the buckling of the middle web subpanel. The computed ultimate test loads, W_u, were 314 kN (69 kips) and 287.5 kN (63 kips) for Tests 1 and 2, respectively. The post-ultimate range exhibits a rapid reduction in strength. It is noteworthy that the ultimate strength developed at approximately 0.89 ϵ_y on the abscissa, that is, before the junction had an average strain equal to the yield strain.

6.2 Test 1 (M,V)

The theoretical and experimental results are compared here with respect to the mode of failure, the ultimate load and the strain at the web-flange junction which was used to establish compatibility of axial deformations between the webs and flanges.

The test confirmed the analytical prediction that the strength of the box section in Test 1 was limited by the capacity of the compression flange. The upward motion of the compression flange (concave on the plate side) also agreed with the analysis.

The experimental ultimate load of 273.8 kN (60 kips) was lower than the theoretical load of 314.8 kN (69 kips) by 13%. It seems that the large initial imperfections and residual stresses in the plate, which were not taken into account in the analysis, had a much greater detrimental effect than originally expected. In fact, the

58

reduction would have been even greater if the compression flange
had not been rotationally restrained at the ends by the transverses
and adjoining segments.

Additional end restraint was provided by the temporary rein-
forcement of segment 2. Figures 37 and 38 indicate that the end
restraint was sufficient to develop plastic deformation at the
ends of the longitudinals, almost as if the ends were fixed rather
than simply supported as was assumed in the analysis.

The web-flange junction strains from the theory and experiment
can be compared only approximately since the overall shortening of
the compression flange could not be accurately measured and only the
plate surface strains at a few locations were available. Thus, only
the axial shortening component Δ_p of the total shortening Δ (Eq. 45)
could be estimated, but not the curvature component Δ_c.

However, since the curvature of the longitudinals was not very
large on approaching the ultimate load and since the centroid of the
flange cross section was very close to the top surface of the plate,
strain gage readings at points 1, 9, 10, 11 and 14 (Fig. 41) were
expected to give useful data. Figure 54 shows the plots of the
averages of the strains from gages 1, 9, 11 and from 10, 14 vs. the
test load W. For comparison, the theoretical curve is also included.

The curve for the average of gages 1, 9 and 11 not only agrees
quite well with the theoretical curve, but also lies to the correct
side of it by giving slightly lower values of strain since it does

59

not include the curvature shortening. The curve for gages 10 and 14 gives significantly higher values of strain than the theoretical curve mainly because the readings of gage 10 are so disproportionately large (see also Fig. 41).

Figure 39 shows that all longitudinal stiffeners exhibited almost the same maximum out-of-plane deflection. This means that the stiffeners made approximately equal contributions to the ultimate strength of the compression flange and, thus, strength of the compression flange and, thus, behaved in agreement with the beam-column approximation used in the analysis.

The approximately linear distribution of the strains in the web shown in Fig. 42d confirms the acceptability of the Navier-Bernoulli hypothesis about "plane section remaining plane" for box sections under symmetrical loads (T = 0).

6.3 Test 2 (M,V,T)

The experimental ultimate load of 168.8 kN (37 kips) was below the theoretical prediction of 287.5 kN (63 kips) by a substantial 41 percent.

Very soon after the start of the test it became obvious that the segment did not behave in the manner predicted theoretically. The consequent premature failure can be ascribed to the following causes:

60

(1)   As shown in Fig. 46, the compression flange buckled down at
       the ultimate load (convex on the plate side) instead of up as
       was expected under the assumptions of theoretical analyses. The
       apparent reason for this behavior is the eccentricity of the
       compression applied to the longitudinals. The eccentricity was
       produced by the reinforcements in the neighboring segments,
       welded permanently in segment 1 and wedged temporarily in
       segment 3, as well as by residual end moments. The reinforce-
       ments of segment 3 not only caused an upward shift of the
       centroid at the left end, but also introduced a negative
       residual moment (causing compression in the stiffener) by the
       process of wedging. At the right end next to segment 1, there
       was a similar upward shift of the centroid and a moment which
       remained from the plastification of the longitudinals in Test 1
       (see Figs. 37 and 38). The net result was that the flange was
       subjected to flexure forcing it to deflect down.

(2)   Eccentricity of the load on the specimen increased in the course
       of testing due to the large angle of rotation as indicated by
       the slope of the spreader beam in Fig. 45 as well as due to the
       distortion of the end frame and the corresponding lateral shift
       of the top flange, also seen in Fig. 45. As indicated in Fig.
       43 by the hysteresis loop, an adjustment was made to compensate
       for the increase in eccentricity.

(3)   End distortion shown in Fig. 45 indicates the possibility that
       the shape of the cross section of the tested segment was not
       maintained during the test, especially at the end (no measurements

61

were made) and this may have affected the strength.

(4) The previously conducted Test 1 introduced additional imper-
fections in the plate of segment 2 in spite of the temporary
reinforcements cee-clamped and wedged to prevent such imper-
fections from occurring.

(5) Although the warping normal stresses due to torsion were
expected to be very insignificant in the closed section of
segment 2, Fig. 49 shows that this theoretically verifiable
assumption was not supported by the test observations. Instead
of being uniformly distributed across the width of the flanges
or at least being symmetrical about the mid-width, the normal
stresses vary linearly from one side to the other. This is
particularly clear in Fig. 49a for the tension flange.

A stress distribution of this type indicates the presence of warping

stresses in addition to the stresses caused by the bending moment.

Since the warping stresses in a closed section could not be of the

intensity measured, a gradual transformation must have taken place

from a closed box section to an open channel section as Web 1 was

loosing its rigidity under a higher shear force than in Web 2 (see

Table 5). This transformation not only forced the section to carry

an increasing portion of the torque by warping torsion (vs. the pure

St. Venant torsion) but also amplified the torque itself as the shear

center shifted away from the weaker web (Web 1) toward the more rigid

web (Web 2). The resultant increase of stresses in the Web 1 side of

the compression flange (Fig. 49b led to the collapse of the web-

flange junction corner and of the longitudinals closest to it much

before the predicted ultimate load was reached. Figure 46 illustrates this mechanism of failure. As shown in Fig. 48, the other side of the flange was hardly disturbed.

The first four of the above possible causes for the reduction in the ultimate strength of segment 2 can be either corrected during testing or taken into account in the analytical method by some minor modifications. However, the fifth cause, the change of a closed cross section into an open one and the resultant shift of the shear center, will require considerable realignment of the formulation and a modification of the computer program. For one, the compression flange can no longer be treated as a single beam-column.

7. SUMMARY, CONCLUSIONS AND RECOMMENDATIONS

7.1 Summary

A theoretical and experimental study was performed on the pre- and postultimate behavior of longitudinally and transversely stiffened box girders of the scantlings typical for ship hulls. Two loading conditions were considered: (1) moment and shear, and (2) moment, shear and torsion. Two tests were conducted on a hull girder specimen to verify the analytical method.

The principal feature of the analytical method was the consideration of continuous interaction between the components of a hull girder cross section through the compatibility of axial strains at the junction lines between the components. This was needed for the following reasons:

a) The danger of computing the maximum strength of a hull cross section by adding the maximum strengths of the individual components rests on the fact that the segments reach their maximum strengths at different levels of deformation. Thus, some segments may be already in the post-ultimate range of reduced capacity when some others just attain their maximum strength.

b) Redistribution of internal forces, specifically, of the bending moment between the webs and flanges could be considered by maintaining compatibility of strains at the junction lines and requiring that "plane sections remain plane".

The behavior and ultimate strength of individual components of the cross section was established by adapting and extending available methods. The compression flange was analyzed by using a substitute beam-column which consisted of a stiffener and a plate and was subjected to axial and lateral loads. Buckling and post-buckling response of the plate, plastification and large deformations were considered. The webs were analyzed by using an ultimate strength theory previously developed for longitudinally stiffened plate girders and box girders.

The following assumptions were made in the method:

(1) Effect of warping torsion is negligible for a box section.

(2) Transverse rings (formed by transverse stiffeners) or diaphragms are sufficiently rigid to prevent deformation of the box cross section and to allow buckling and large deformations to occur only between the transverse rings.

(3) Compression flange panels (portion of the flange between two adjacent transverse stiffeners) are wide enough so that lateral interaction between longitudinals (plate action in the transverse direction) is negligible.

(4) Ultimate strength of a box girder segment (portion between transverse rings) is limited by the capacity of the compression flange or of the web by shear or the yielding of the tension flange.

The two tests conducted on separate segments of the hull girder specimen led to the following observations:

65

Test 1 (moment and shear)

1) The experimental ultimate load was 13% below the theoretical load and, as predicted, it was limited by the capacity of the compression flange.

2) The theoretical and experimental strains at the junction between the web and the compression flange were in agreement up to the ultimate load.

3) The experimental stress distribution in the compression flange agreed well with the theoretical, up to 50% of the ultimate load. Then, there was a predictable deviation, with the stresses at the web-flange junction becoming significantly higher than in the middle portion of the flange.

Test 2 (moment, shear and torque)

1) The experimental ultimate load was 41% below the predicted load.

2) The compression flange buckled downward (convex on the plate side) rather than upward. This unforeseen mode of failure was apparently caused by the residual moments and eccentricities from the reinforcements in the neighboring segments and by the initial deformations resulting from Test 1.

3) Contrary to the analytical prediction, the stresses measured in the tension and compression flanges were not distributed uniformly or symmetrically. They varied linearly across the width as if they were partially produced by warping torsion of an open channel section rather than by pure torsion of a closed box section as was assumed in the analysis. Apparently, the rigidity of the web

66

subjected to a greater shear than the other web was deteriorating much faster than anticipated. The consequent redistribution of internal forces made the cross section to behave as if it was gradually transformed from a closed box to an open channel section.

7.2 Conclusions and Recommendations for Improvement of the Method

7.2.1 Moment and Shear

Comparison of the theoretical and experimental results (Test 1) for the case when only moment and shear are acting on the girder segment leads to the following conclusions:

1) The analytical method is acceptably accurate although it is somewhat optimistic. Partially, the discrepancy can be ascribed to the assumption that the residual stresses were set equal to zero since they were not measured in this program.

2) Many assumptions of the analytical method were confirmed:

   - The behavior of the compression flange can be computed from the beam-column analysis.

   - "Plane section remained plane" (Navier-Bernouilli hypothesis).

   - Transverses were sufficiently strong to remain undeformed and enforce the compression flange to fail in the "panel mode".

3) The following refinements of the method are recommended to improve its accuracy with respect to experimental results:

   - Inclusion of the effect of residual stresses and initial imperfections. Only minor modifications of the program are needed for this.

- More careful consideration of the actual end conditions of the
compression flange.

7.2.2 Moment, Shear and Torque

The method was found to be inadequate when the girder segment was
subjected to the general loading of moment, shear and torque (Test 2).
Even if there were no disturbances at the end of the compression
flange (eccentricity and residual moments due to reinforcements of
the segments adjacent to the tested segment), there would have been
a significant reduction of the maximum strength due to the development
of warping stresses. (In the method, these stresses were assumed to
be negligible.) Results of Test 2 have shown that the torsional
stiffness and the ultimate strength of a box girder segment under
general loading are detrimentally affected when a component (Web 1
in this case) of the segment experiences nonlinear post-buckling
behavior leading to the yielding along the tension diagonal.

7.2.3 Recommendations for Extension of Present Research

In order to meet the original objective of developing a reliable
method for hull girders under moment, shear and torque the following
improvements are recommended:
1) Tests on hull girder segments under combinations of moment, shear
   and torque (M,V,T), specifically that Test 3 planned for the
   present test specimen be conducted under M,V,T rather than under
   moment M alone.

2) Inclusion of the effect of shearing stresses on the strength of flanges, especially of the compression flange.

3) Refinement of the strength formulation for the webs.

4) Inclusion of the effect of warping torsion by the consideration of nonuniform but linearly varying normal stresses across the width of the flanges.

5) Consideration of the change of the shape of the cross section when transverse rings (diaphragms, transverse bulkheads) are not sufficiently rigid.

7.3 Recommendations for Future Work on Ship Hull Strength

The following recommendations on the extension of research beyond the objectives of the present research are made:

1) Consideration of weak transverse stiffeners and lateral loading so that the flange may fail in the "grillage mode".

2) Behavior and ultimate strength of hull girders with non-rectangular cross section.

3) Behavior and ultimate strength of double-bottom and partially open hull girders.

4) Development of a design procedure for hull girders based on the ultimate strength concepts. This will be in the form of tables, charts and simple formulas rather than complex computer programs.

8. NOMENCLATURE

A	area of cross section
A_o	enclosed area of cross section ($= bd$)
a	length of test segment
b	width of test segment
b_c	spacing between longitudinal stiffeners on the compression flange
b_t	spacing between longitudinal stiffeners on the tension flange
C	proportionality factor between the cross-sectional shear and the applied load W (load parameter)
C_1	bending moment-shear ratio
C_2	torque-shear ratio
d	depth of test segment
d_i	variable spacing of longitudinals in webs
d_p	distance from plate to the point of application of axial load P
d_s	stiffener depth
E	Young's modulus of elasticity
E_t	tangent modulus
e	eccentricity of the load
F_{bcri}	critical bending buckling stress in the case of bending acting alone for the i-th web supbanel
F_{ccri}	critical compressive buckling stress in the case of pure axial compression acting alone for the i-th web subpanel

70

F_{vcri} critical shear buckling stress in the case of shear stress acting alone for the i-th web subpanel

F_u ultimate stress

F_y yield stress

F_{ys} static yield stress at zero strain rate

F_{yd52} dynamic yield stress at the strain rate of 52 μm/m/sec

F_{yd1045} dynamic yield stress at the strain rate of 1045 μm/m/sec

G   shear modulus

H   horizontal stress resultant

$\underline{H}$ $H/(\sigma_o A)$

I   moment of inertia

k   buckling coefficient or constant (Eq. 15)

L   length of specimen and any length of the beam-column

$\underline{L}$ $2\ s_{end}$

L_{max} length of the beam-column with given cross section and end conditions for which specified P and q are ultimate loads (P_u and q_u)

M   bending moment

$\underline{M}$ $M/(\sigma_o A\ d_s)$

M_w bending moment on webs

$\underline{M}_o$ mid-span moment computed from other assumed variables for the integration process of the beam-column

N   axial force, resulting from the stress distribution in the box section

N_o given axial force

P   axial force in the beam-column

$\underline{P}$ $\qquad$ $P/(\sigma_o A)$

P' $\qquad$ axial force acting in the compression flange

P_u $\qquad$ ultimate axial force for the beam-column of length L_{max}

q $\qquad$ lateral loading acting per unit length of beam-column

$\qquad$ $(q = q'b_c)$

$\underline{q}$ $\qquad$ $\dfrac{q\ r}{\sigma_o A}$

q' $\qquad$ distributed lateral loading

q_t $\qquad$ shear flow = $T/(2A_o)$

q_u $\qquad$ ultimate lateral loading for the beam-column of length

$\qquad$ L_{max}

r $\qquad$ radius of gyration = $\sqrt{I/A}$

s_{end} $\qquad$ half-length of the beam-column for simply supported or

$\qquad$ fixed end conditions

T $\qquad$ torque

t $\qquad$ plate thickness of flanges

t_w $\qquad$ thickness of web plate

V $\qquad$ shear force

$\underline{V}$ $\qquad$ $V/(\sigma_o A)$

V_{bi} $\qquad$ $\tau_{vcri}\ d_i\ t_w$ - buckling strength of the i-th subpanel

V_{FT} $\qquad$ shear force in flanges due to torque

V_{tfi} $\qquad$ $\tau_{tfi}\ d_i\ t_w$ - tension field strength of the i-th subpanel

V_W $\qquad$ shear force in web

V_{WT} $\qquad$ shear force in webs due to torque

V_{wu} $\qquad$ ultimate shear capacity of web

W $\qquad$ load parameter equivalent to a concentrated transverse

$\qquad$ load acting on a simply supported beam

72

W_u	ultimate load
x	horizontal coordinate axis
$\underline{x}$	s/r
y	vertical coordinate axis or vertical deflection
$\underline{y}$	y/r
z	distance from any point of the section to the geometric centroid of the cross section
α	aspect ratio (= a/d)
α_{min}	aspect ratio of the widest web subpanel (= a/d_{imax})
Δ	total axial shortening of the beam-column or compression flange
Δ_c	axial shortening due to curvature
Δ_p	axial shortening due to axial strain (effect of P)
Δ_{pu}	axial shortening which exists under the ultimate load P_u
Δ_s	segment length
$\underline{\Delta_s}$	Δ_s/r
Δx	change in x in segment length Δ_s
$\underline{\Delta x}$	$\Delta x/r$
Δy	change in y in segment length Δ_s
$\underline{\Delta y}$	$\Delta y/r$
ϵ	axial strain
ϵ_{cr}	plate buckling strain
ϵ_{f1}	strain in stiffener flange of the beam-column
ϵ_o	buckling or yield strain, ϵ_{cr} or ϵ_y, depending on whether buckling occurs or not in the plate of the compression flange

ϵ_{pl} edge strain in the plate

ϵ_y yield strain

θ slope

ν Poisson's ratio

γ shearing deformation

γ_{cri} critical shearing deformation at point of buckling of the i-th subpanel $(\gamma_{cri} = \tau_{cri}/G)$

γ_{ui} ultimate shearing deformation of the i-th subpanel

σ_{avg} average stress for the plate of the compression flange

σ_{bcri} pure bending stress which causes buckling of the i-th web subpanel when acting simultaneously with σ_{ccri} and τ_{vcri}

σ_{cr} plate buckling stress of the compression flange

σ_{ccri} pure compression stress which causes buckling of the i-th web subpanel when acting simultaneously with σ_{bcri} and τ_{vcri}

σ_o buckling or yield stress, σ_{cr} or F_y, depending on whether buckling occurs or not in the plate of the compression flange

σ_{ti} tension field stress at the ultimate condition for the i-th web subpanel

τ shearing stress

τ_{tfi} equivalent shearing stress in the i-th web subpanel (tension field action)

τ_{vcri} shearing stress which causes buckling of the i-th web subpanel when acting simultaneously with σ_{bcri} and σ_{ccri}

φ curvature $\left(= d\epsilon/ds = \dfrac{\epsilon_{pl} - \epsilon_{fl}}{d_s} \right)$

$\overline{\varphi}$ $\varphi \, d_s / \epsilon_o$

$\overline{\varphi}_o$ assumed mid-span curvature

74

9. REFERENCES

1. Vasta, J.
   LESSONS LEARNED FROM FULL SCALE STRUCTURAL TESTS,
   Transactions S.N.A.M.E., Vol. 66, p. 165, 1958.

2. Koiter, W. T.
   THE EFFECTIVE WIDTH OF FLAT PLATES FOR VARIOUS LONGITUDINAL
   EDGE CONDITIONS AT LOADS FAR BEYOND BUCKLING LOAD,
   National Luchtvaartlaboratorium, Netherlands, Rep. S287
   (in Dutch), 1943.

3. Lee, T. T.
   ELASTIC-PLASTIC ANALYSIS OF SIMPLY SUPPORTED RECTANGULAR
   PLATES UNDER COMBINED AXIAL AND LATERAL LOADING, Fritz
   Engineering Laboratory Report No. 248.7, Lehigh University,
   1961.

4. Moxham, K. E. and Bradfield, C. D.
   THE STRENGTH OF WELDED STEEL PLATES UNDER INPLANE COMPRES-
   SION, University of Cambridge, Department of Engineering,
   Technical Report No. CUED/C-Struct/TR.65, 1977.

5. Dwight, J.
   COLLAPSE OF STEEL COMPRESSION PANELS, in Developments in
   Bridges Design and Construction, University College, Cardiff,
   1971.

6. Kondo, J.
   ULTIMATE STRENGTH OF LONGITUDINALLY STIFFENED PLATE PANELS
   SUBJECTED TO COMBINED AXIAL AND LATERAL LOADING, Fritz
   Engineering Laboratory Report No. 248.13, Lehigh University,
   1965.

7. Becker, H. and Colao, A.
   COMPRESSIVE STRENGTH OF SHIP HULL GIRDERS (Part III, Theory
   and Additional Experiments), SSC No. 267, Ship Structure
   Committee, Washington, 1977.

8. Rutledge, D. R. and Ostapenko, A.
   ULTIMATE STRENGTH OF LONGITUDINALLY STIFFENED PLATE PANELS
   (Large and Small b/t, General Material Properties), Fritz
   Engineering Laboratory Report No. 248.24, Lehigh University,
   1968.

9. Rutledge, D. R.
   COMPUTER PROGRAM FOR ULTIMATE STRENGTH OF LONGITUDINALLY
   STIFFENED PANELS, Fritz Engineering Laboratory Report No.
   248.23, Lehigh University, 1968.

10. Parsanejad, S. and Ostapenko, A.
    ULTIMATE STRENGTH ANALYSIS OF PLATE GRILLAGES UNDER
    COMGINED LOADS, Fritz Engineering Laboratory Report No.
    323.11, Lehigh University, 1972.

11. Maquoi, R.
    ETUDE THEORIQUE ET EXPERIMENTALE DE LA RESISTANCE POST-
    CRITIQUE DES SEMELLES COMPRIMEES RAIDIES DES PONTS METAL-
    LIQUES EN CAISSON (Theoretical and Experimental Study of
    the Post-Buckling Strength of Stiffened Flanges of Steel
    Box Girder Bridges under Compression) (in French), Faculté
    des Sciences, Report No. 54, Université de Liège, 1975.

12. Herzog, M.
    DIE TRAGLAST EINSEITIG LANGVERSTEIFTER BLECHE MIT IMPERFEK-
    TIONEN UND EIGENSPANNUNGEN UNTER AXIALDRUCK NACH VERSUCHEN
    (Ultimate Strength of Longitudinally Stiffened Plates
    According to Test Results—Consideration of Initial Imper-
    fections and Residual Stresses) (in German), Verein Deutscher
    Ingenieure-Zeitung, Vol. 118, No. 7, 1976.

13. Basler, K.
    STRENGTH OF PLATE GIRDERS IN SHEAR, Journal of the Struct.
    Div., ASCE, Vol. 87, No. ST7, Proc. Paper 2967, October 1961.

14. Basler, K.
    STRENGTH OF PLATE GIRDERS UNDER COMBINED BENDING AND SHEAR,
    Journal of the Struct. Div., ASCE, Vol. 87, No. ST7, Proc.
    Paper 2968, October 1961.

15. Basler, K. and Thurlimann, B.
    STRENGTH OF PLATE GIRDERS IN BENDING, Journal of the Struct.
    Div., ASCE, Vol. 87, No. ST7, Proc. Paper 2913, August 1961.

16. Schueller, W. and Ostapenko, A.
    TESTS ON A TRANSVERSELY STIFFENED AND ON A LONGITUDINALLY
    STIFFENED UNSYMMETRICAL PLATE GIRDER, WRC Bulletin No. 156,
    November 1970.

17. Ostapenko, A. and Chern, C.
    ULTIMATE STRENGTH OF LONGITUDINALLY STIFFENED PLATE GIRDERS
    UNDER COMBINED LOADS, IABSE, Proceedings, Vol. 11, II,
    London, 1971.

18. Ostapenko, A., Chern, C. and Parsanejad, S.
    ULTIMATE STRENGTH DESIGN OF PLATE GIRDERS in Developments in
    Bridge Design and Construction, Crosby, Lockwood & Son, Ltd.,
    University College, Cardiff, 1971.

19. Massonnet, Ch., Skaloud, M. and Donea, J.
    COMPORTEMENT POSTCRITIQUE DES PLAQUES CISAILLEES RAIDIES
    (Postbuckling Behavior of Stiffened Plates Subjected to Pure
    Shear), IABSE, Proceedings, Vol. 28, II, Zurich, 1968.

20. Rockey, K. C., Evans, H. R. and Porter, D. M.
    A DESIGN METHOD FOR PREDICTING THE COLLAPSE BEHAVIOR OF PLATE
    GIRDERS Proc. Institution of Civil Engineers, Part 2,
    Vol. 65, p. 85-112, March 1978.

21. Herzog, M.
    ULTIMATE STRENGTH OF PLATE GIRDERS FROM TESTS, Journal of
    the Struc. Div., ASCE, Vol. 100, No. ST5, Proc. Paper 10530,
    May 1974.

22. Höglund, T.
    DESIGN OF THIN PLATE I GIRDERS IN SHEAR AND BENDING, Royal
    Institute of Technology Bulletin, No. 94, Stockholm, 1973.

23. Massonnet, Ch.
    DESIGN OF STEEL PLATE AND BOX GIRDER BIRDGES, Journal of
    Struc. Div., ASCE, Vol. 101, No. 11, Proc. Paper 11686,
    p. 2477, 1975.

24. Vernarr, J. D.
    COMPARISON STUDY OF PLATE GIRDER ULTIMATE STRENGTH METHODS,
    Report CE 481, Department of Civil Engineering, Lehigh
    University, September 1977.

25. Deutscher Ausschuss fuer Stahlbau
    "Beulsicherheitsnachweise für Platten, DAST-Richtlinie
    012, October 1978.

26. Wolchuk, R. and Mayrbaurl, R.
    PROPOSED DESIGN SPECIFICATIONS FOR STEEL BOX GIRDER
    BRIDGES, Report No. FHWA-TS-80-205, U.S. Federal Highway
    Administration, Washington, 1980.

27. Caldwell, J. B.
    ULTIMATE LONGITUDINAL STRENGTH, Proceedings of the Royal
    Institution of Naval Architects, Vol. 107, London, 1965.

28. Mansour, A. E.
    DESIGN CHARTS FOR BUCKLING AND POST-BUCKLING OF STIFFENED
    PLATES UNDER COMBINED LOADING, SSC No.   , Ship Structure
    Committee, Washington, 1976.

29. Frey, F.
    L'ANALYSE STATIQUE NON LINEAIRE DES STRUCTURES PAR LA METHODE
    DES ELEMENTS FINIS ET SON APPLICATION A LA CONSTRUCTION
    METALLIQUE (Nonlinear Structure Analysis by the Method of
    Finite Elements and its Application to Steel Structures),
    in French, Faculté des Sciences, Doctoral Thesis, Univer-
    sité de Liège, 1978.

30. Smith, C. S.
    COMPRESSIVE STRENGTH OF WELDED STEEL SHIP GRILLAGES,
    Proceedings of the Royal Institution of Naval Architects,
    Vol. 117, London, 1975.

31. Ostapenko, A.
    SHEAR STRENGTH OF LONGITUDINALLY STIFFENED PLATE GIRDERS,
    Proceedings of Structural Stability Research Council, 1980.

32. Corrado, J. A.
    ULTIMATE STRENGTH OF SINGLE-SPAN, RECTANGULAR STEEL BOX
    GIRDERS, Ph.D. Dissertation, Fritz Engineering Laboratory
    Report No. 380.3, Lehigh University, University Microfilms
    Ann Arbor, 1971.

33. Walker, A. C. and Davies, P.
    AN ELEMENTARY STUDY OF NON-LINEAR BUCKLING PHENOMENA IN
    STIFFENED PLATES, in Proceedings of Symposium on Structural
    Analysis, Non-Linear Behavior and Techniques, Transport and
    Road Research Laboratory (TRRL) Supplementary Report 164 UC,
    p. 19, 1975.

34. Ostapenko, A.
    ULTIMATE STRENGTH DESIGN OF WIDE STIFFENED PLATES LOADED
    AXIALLY AND NORMALLY, in Proceedings of Symposium on
    Structural Analysis, Non-Linear Behavior and Techniques,
    Transport and Road Research Laboratory (TRRL) Supplementary
    Report 164 UC, p. 175, 1975.

35. Rao, N. R., Lohrman, M. and Tall, L.
    EFFECT OF STRAIN RATE ON THE YIELD STRESS OF STRUCTURAL
    STEELS, Journal of Materials, Vol. 1, No. 1, p. 241,
    March 1966.

36. American Society for Testing and Materials
    1971 ANNUAL BOOK OF ASTM STANDARDS, Part 31, ASTM Specifi-
    cation E8-69, American Society for Testing and Materials,
    Philadelphia, Pa., 1971.

10. ACKNOWLEDGMENTS

Table 1 Reference Buckling Stresses

Pure Stress	Aspect Ratio $\alpha=a/d_i$	Buckling Coefficient K	Relative Plate Slenderness	For λ	Buckling Stress
Shear		$k_v = 5 + \dfrac{5}{\alpha^2}$	$\lambda_v = 0.8\,\dfrac{d_i}{t_w}\sqrt{\dfrac{F_y}{E\,k_v}}$	≤ 0.58	$F_{vcr} = 0.58\,F_y$
				≥ 0.58 ≤ 1.41	$F_{vcr} = \left[0.58 - 0.357(\lambda_v - 0.58)^{1.18}\right]F_y$
				> 1.41	$F_{vcr} = 0.58\,F_y/\lambda_v^2$
Bending	$>\dfrac{2}{3}$	$k_b = 24$	$\lambda_b = \dfrac{d_i/t_w}{0.95}\sqrt{\dfrac{F_y}{E\,k_b}}$	≥ 0.65 ≤ 1.5	$F_{bcr} = \left[0.072(\lambda_b - 5.62)^2 - 0.78\right]F_y$
	$<\dfrac{2}{3}$	$= 24 + 13(2/3-\alpha)^2$		≥ 1.5	$F_{bcr} = \left[1/\lambda_b^2\right]F_y$
Axial	>1	$k_c = 4$	$\lambda_c = \dfrac{d_i/t_w}{0.95}\sqrt{\dfrac{F_y}{E\,k_c}}$	≥ 0.65 ≤ 1.5	$F_{ccr} = \left[0.072(\lambda_c - 5.62)^2 - 0.78\right]F_y$
	<1	$= \left(\alpha + \dfrac{1}{\alpha}\right)^2$		≥ 1.5	$F_{ccr} = \left[1/\lambda_c^2\right]F_y$

80

TABLE 2 Material Properties of Plate
in Test Segments

| Direction | Longitudinal | | Transverse | Longitudinal |
Coupons	LP3	LP4	TP1	Coupons Average
Thickness (mm)	1.853	1.855	1.866	1.854
F_{ys} (MPa)	236.83	236.66	245.12	236.75
F_{yd52} (MPa)*	256.25	258.48	274.63	257.37
F_{yd1042} (MPa)**	277.88	281.35	292.46	279.61
F_u (MPa)	349.89	348.07	353.13	348.98
$\dfrac{F_{yd52}}{F_{ys}}$	1.082	1.092	1.120	1.087
$\dfrac{F_{yd1042}}{F_{ys}}$	1.173	1.189	1.193	1.181

*Strain rate = 52 μm/m/sec
**Strain rate = 1042 μm/m/sec (ASTM)

TABLE 2A Material Properties of Plate
in Test Segments

Direction Coupons	Longitudinal		Transverse	Longitudinal Coupons
	LP3	LP4	TP1	Average
Thickness (in.)	0.07297	0.07304	0.07348	0.07301
F_{ys} (ksi)	34.348	.34.324	35.557	34.336
F_{yd52} (ksi)*	37.165	37.488	39.830	37.327
F_{yd1042} (ksi)**	40.301	40.805	42.416	40.553
F_{u} (ksi)	50.746	50.482	51.216	50.614
$\dfrac{F_{yd52}}{F_{ys}}$	1.082	1.092	1.120	1.087
$\dfrac{F_{yd1042}}{F_{ys}}$	1.173	1.189	1.193	1.181

*Strain rate = 52 μ in./in./sec
**Strain rate = 1042 μ in./in./sec (ASTM)

82

Table 3. Out-of-Plane Deformations of the Compression

Flange and Webs for Test 1

Maximum Out-of-Plane Deformations of the Compression Flange

Load [kN]	Web-Comp. Fl. Junct.	Plate	Stiffener
0	0.0	0.0	0.0
133.4	+0.21	-0.71	-0.44
177.9	+0.25	-1.00	-1.10
222.4	+0.27	-1.30	-1.44

(+) inward deflection (mm)
(-) outward deflection (mm)

Maximum Out-of-Plane Deformations of Webs

Load [kN]	Web-Comp Fl Junct		Plate		Stiffener	
	Web 1	Web 2	Web 1	Web 2	Web 1	Web 2
0	0.0	0.0	0.0	0.0	0.0	0.0
133.4	+0.19	+0.08	+0.19	+0.64	+0.50	+0.09
177.9	+0.32	+0.37	+0.38	+0.86	+0.58	-0.02
222.4	+0.40	+0.62	+0.61	+1.18	+0.76	-0.10
266.9	+1.64	+3.70	+7.80	+5.85	+11.0	-5.60

Table 3A. Out-of-Plane Deformations of the Compression
Flange and Webs for Test 1

Maximum Out-of-Plane Deformations of the Compression Flange

Load [kips]	Web-Comp. Fl. Junct.	Plate	Stiffener
0	0.0	0.0	0.0
30	+0.0083	-0.0279	-0.0173
40	+0.0099	-0.0394	-0.0433
50	+0.0105	-0.0512	-0.0567

(+) inward deflection (in.)
(-) outward deflection (in.)

Maximum Out-of-Plane Deformations of Webs

Load [kips]	Web-Comp Fl Junct		Plate		Stiffener	
	Web 1	Web 2	Web 1	Web 2	Web 1	Web 2
0	0.0	0.0	0.0	0.0	0.0	0.0
30	+0.0075	+0.0032	+0.0075	+0.0252	+0.0197	+0.0035
40	+0.0126	+0.0146	+0.0149	+0.0339	+0.0228	-0.0008
50	+0.0157	+0.0244	+0.0240	+0.0465	+0.0299	-0.0039
60	+0.0646	+0.1457	+0.3071	+0.2303	+0.4331	-0.2205

84

Table 4.. Out-of-Plane Deformations of the Compression

Flange and Webs in Test 2

Maximum Out-of-Plane Deformations of the Compression Flange

Load [kN]	Web-Comp. Fl. Junct.	Plate	Stiffener
0.0	0.0	0.0	0.0
88.9	-0.46	+0.99	+0.76
133.4	-0.51	+2.11	+1.62
162.4	-0.92	+12.79	+12.71

(+) inward deflection (mm)
(-) outward deflection (mm)

Maximum Out-of-Plane Deformations of Webs

Load [kN]	Web-Comp Fl Junct		Plate		Stiffener	
	Web 1	Web 2	Web 1	Web 2	Web 1	Web 2
0.0	0.0	0.0	0.0	0.0	0.0	0.0
88.9	+0.52	+0.03	+1.07	-0.21	+0.61	-0.02
133.4	+0.59	+0.03	+2.27	-0.53	+0.80	-0.42
162.4	+2.41	+0.15	+7.53	-0.71	+6.43	-0.42

Table 4A.   Out-of-Plane Deformations of the Compression

Flange and Webs in Test 2

Maximum Out-of-Plane Deformations of the Compression Flange

Load [kips]	Web-Comp. Fl. Junct.	Plate	Stiffener
0.0	0.0	0.0	0.0
20.0	-0.0182	+0.0389	+0.0298
30.0	-0.0202	+0.0834	+0.0636
36.5	-0.0362	+0.5036	+0.5005

(+) inward deflection (in.)
(-) outward deflection (in.)

Maximum Out-of-Plane Deformations of Webs

Load [kips]	Web-Comp Fl Junct		Plate		Stiffener	
	Web 1	Web 2	Web 1	Web 2	Web 1	Web 2
0.0	0.0	0.0	0.0	0.0	0.0	0.0
20.0	+0.0203	+0.0010	+0.0423	-0.0083	+0.0241	-0.0008
30.0	+0.0234	+0.0010	+0.0894	-0.0210	+0.0316	-0.0164
36.5	+0.0949	+0.0059	+0.2966	-0.0280	+0.2532	-0.0166

Table 5. Forces Acting in Test Segment for Tests 1 and 2

A-A (Test 1: M,V)   A-A (Test 2: M,V,T)
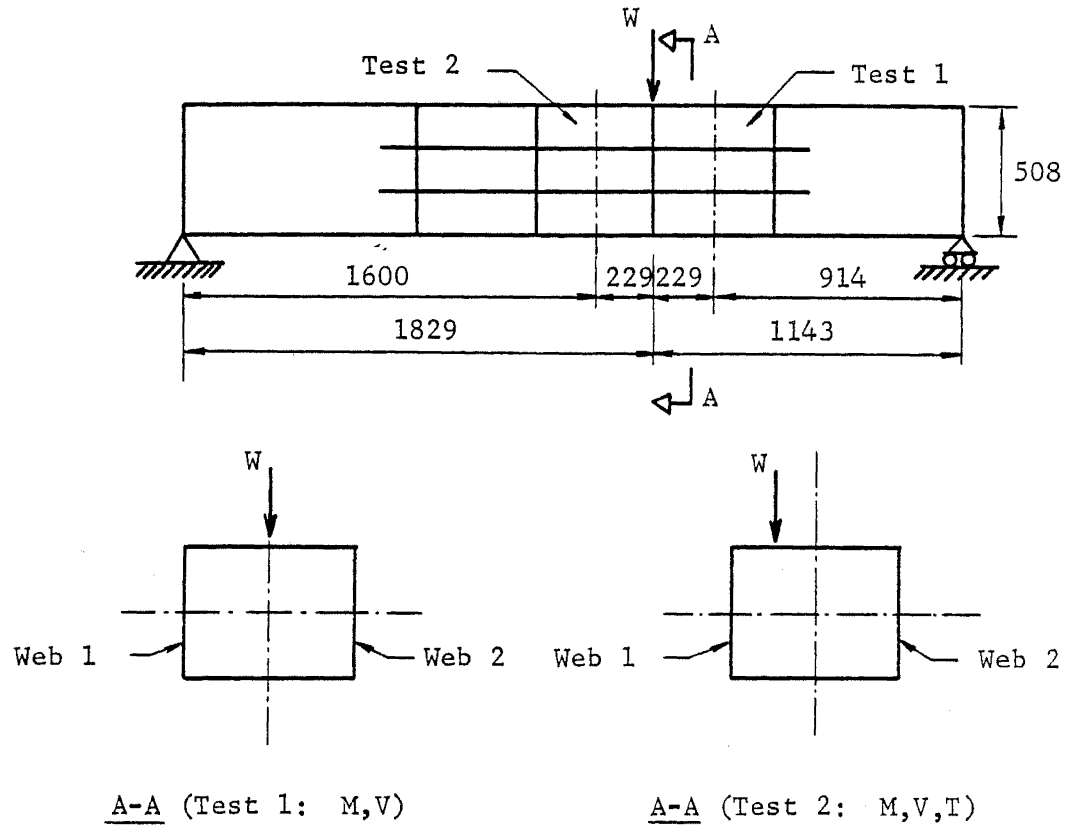
Forces	Test 1	Test 2
Moment M	562 W	616 W
Total Shear V	0.615 W	0.385 W
Torque T	0.0	194 W
Shear in Web 1	0.3075 W	0.3092 W
Shear in Web 2	0.3075 W	0.0758 W

87

FIGURES
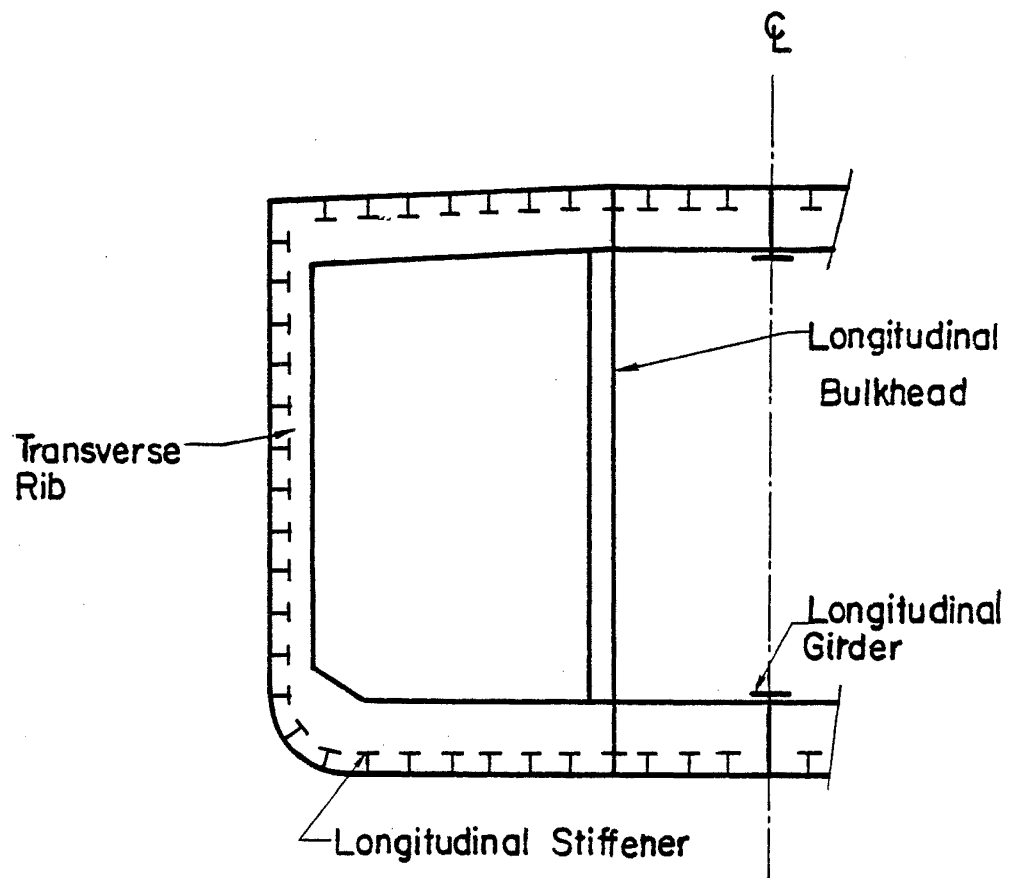
Fig. 1 Typical Mid-Ship Cross Section
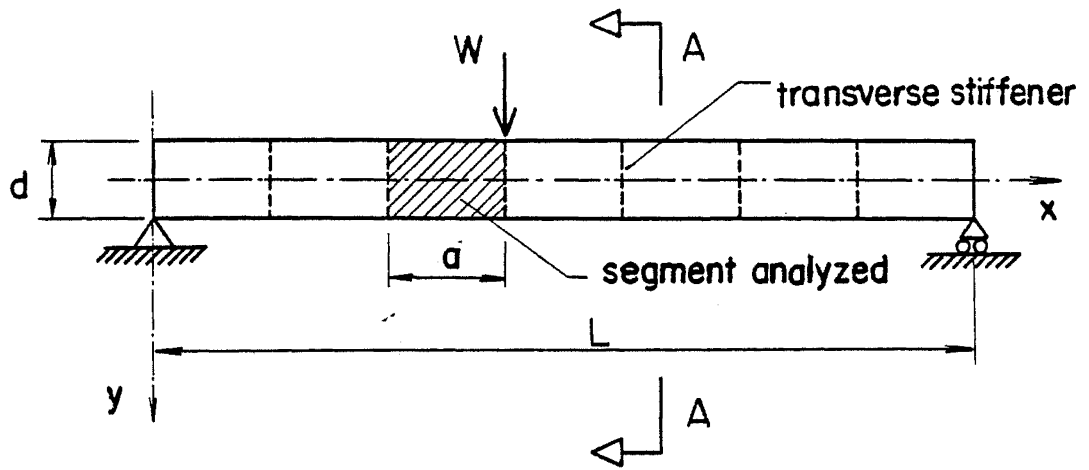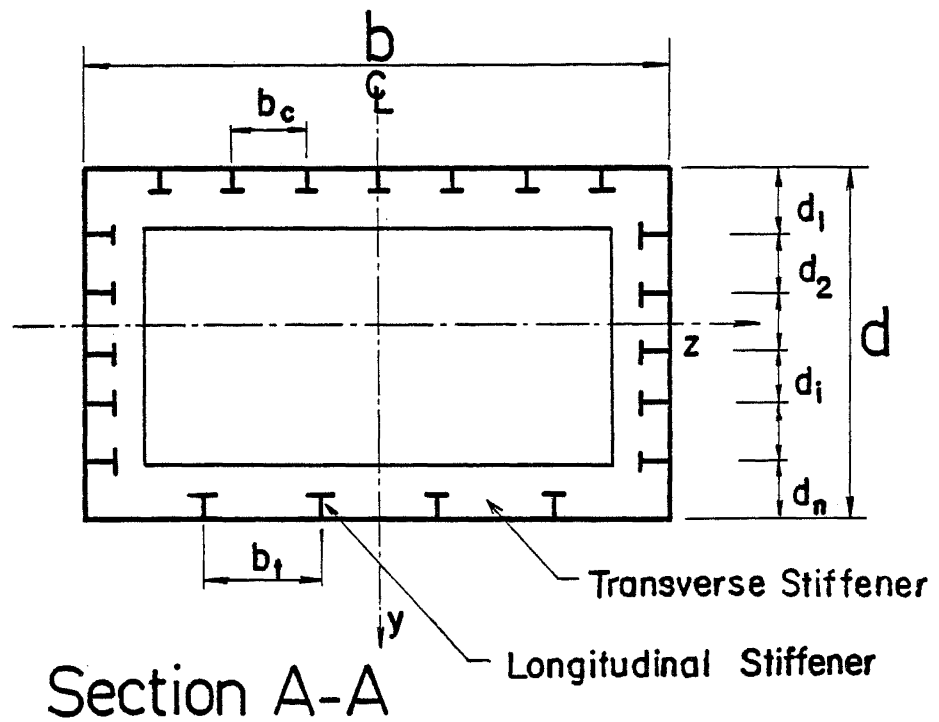
Fig. 2   Idealization of a Hull Girder
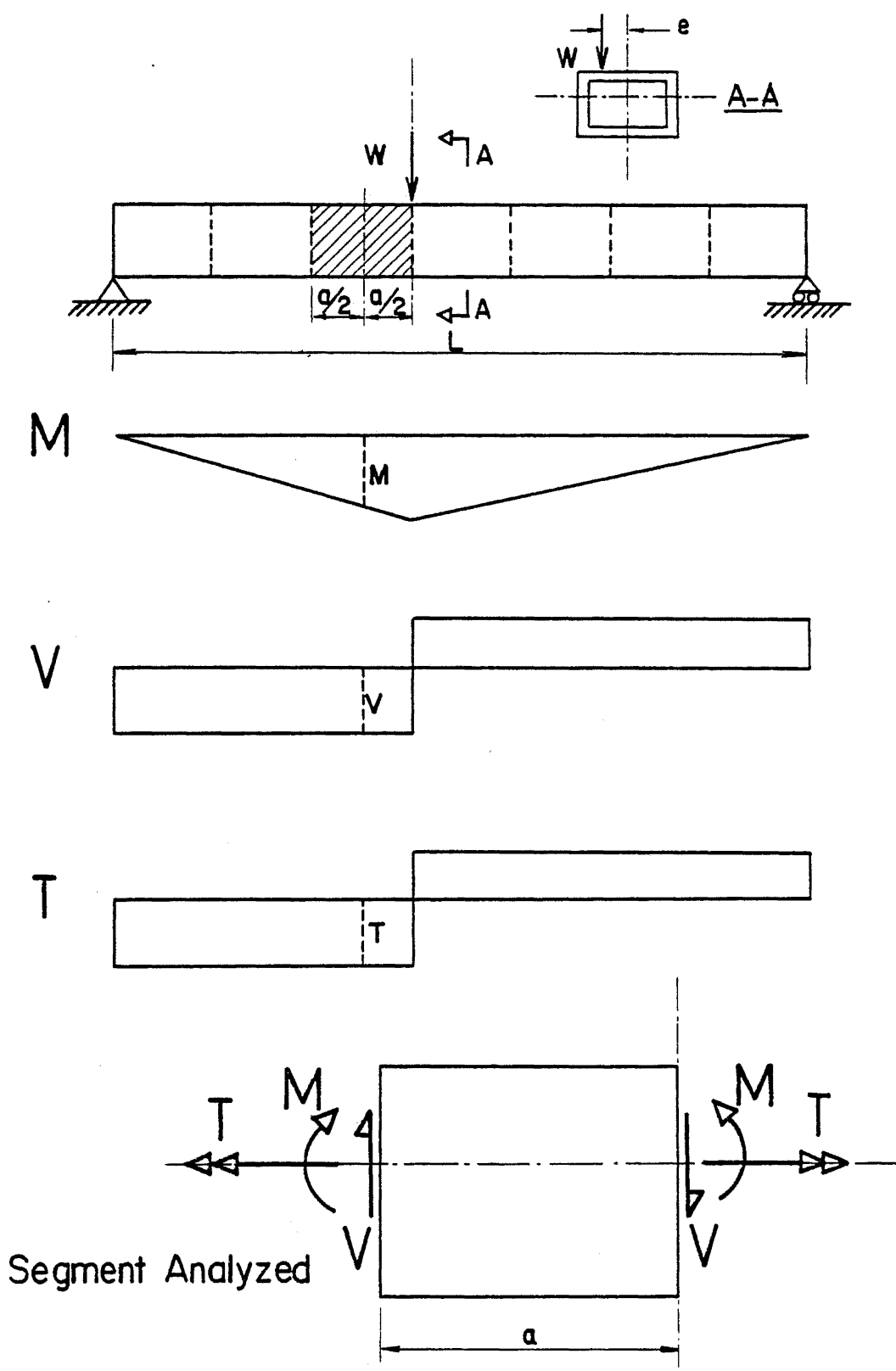
Fig. 3 Forces in Segment of Hull Girder Test Specimen

91
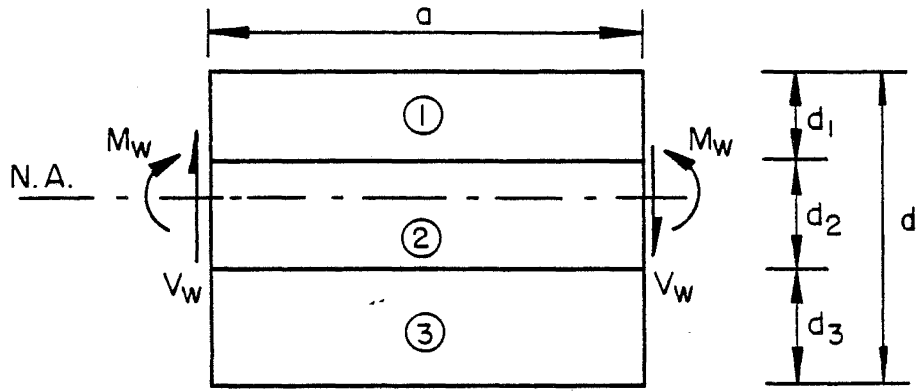
Segment of Web $\textcircled{i}$: Subpanel No.
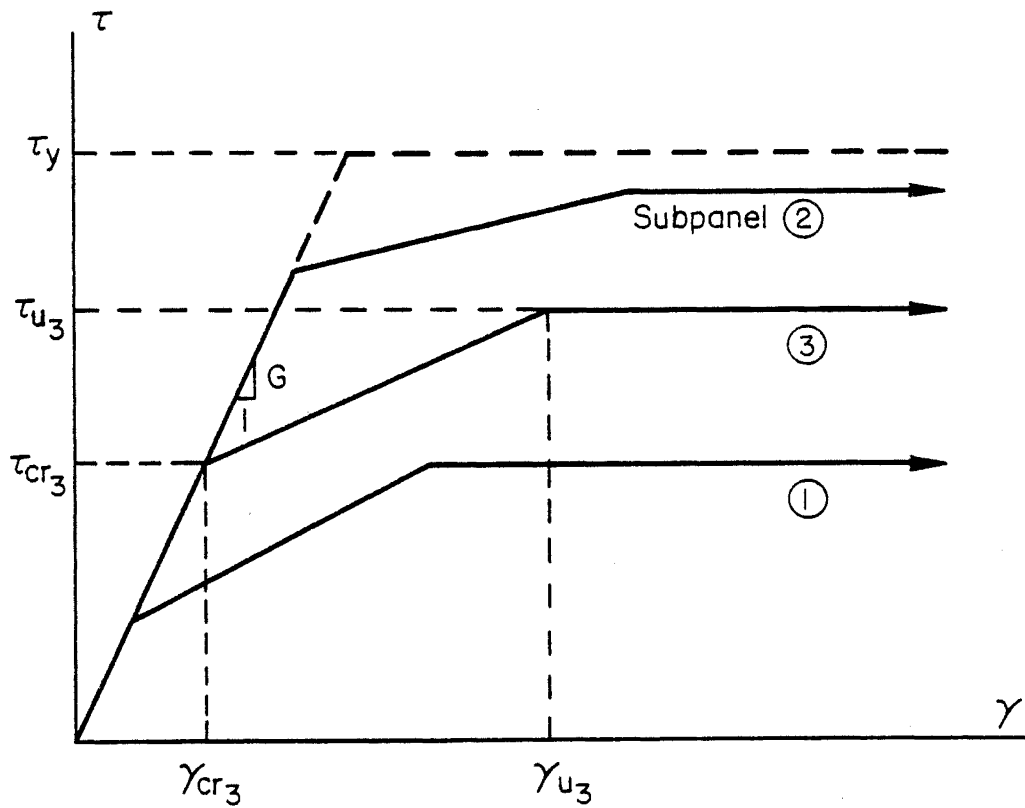
Fig. 4 $\mathcal{T}$-γ Relationship for Each Subpanel
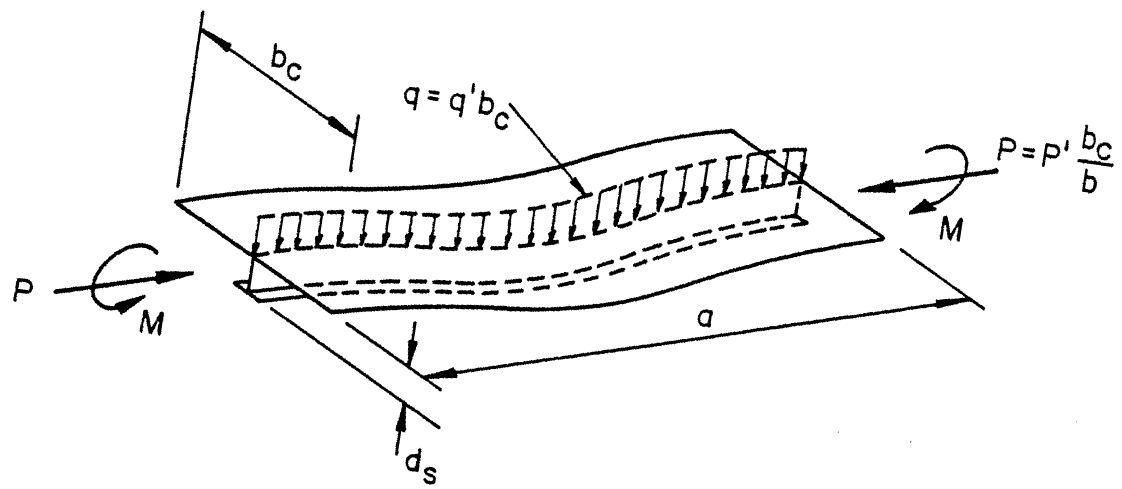
Fig. 5 Beam-Column Idealization
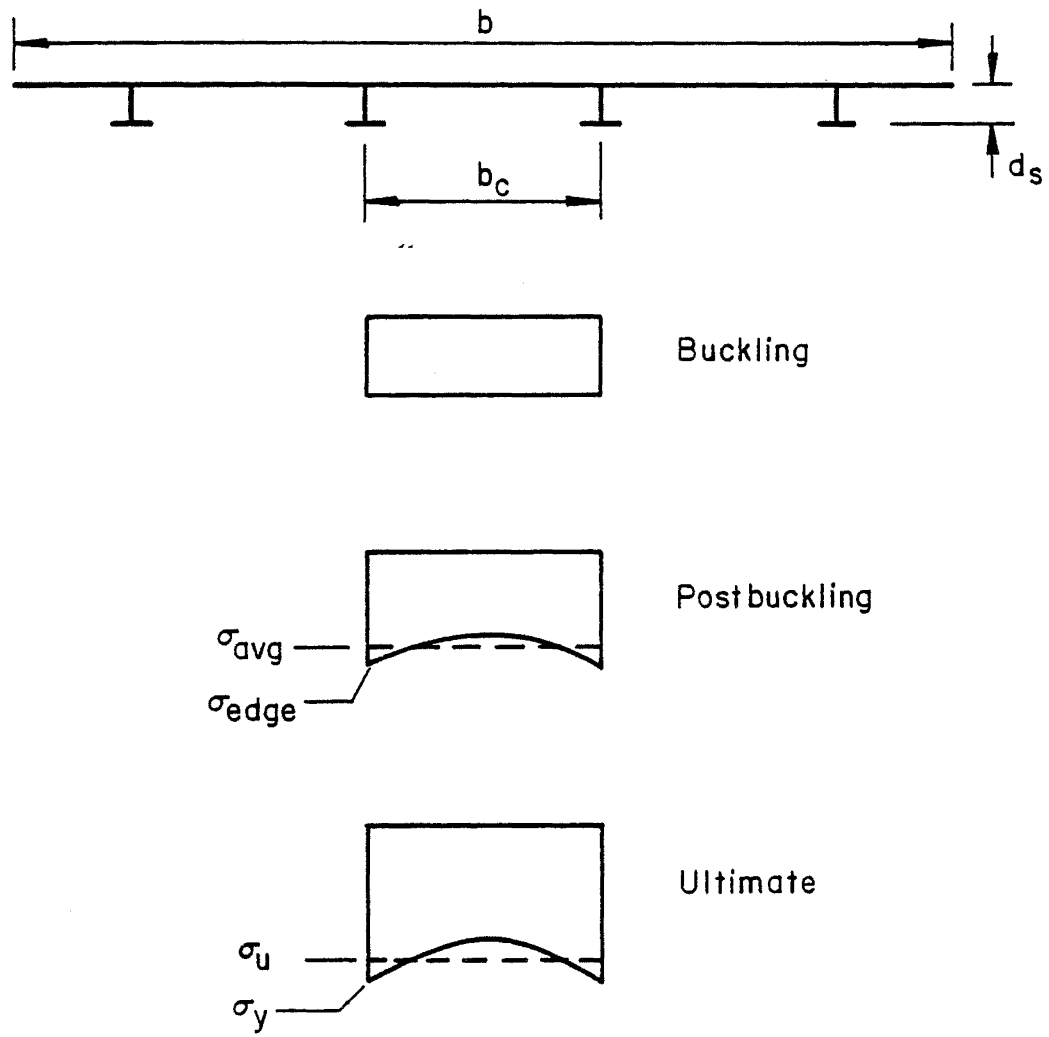
Fig. 6   Stress Distribution in Subpanel of Compression Flange

94
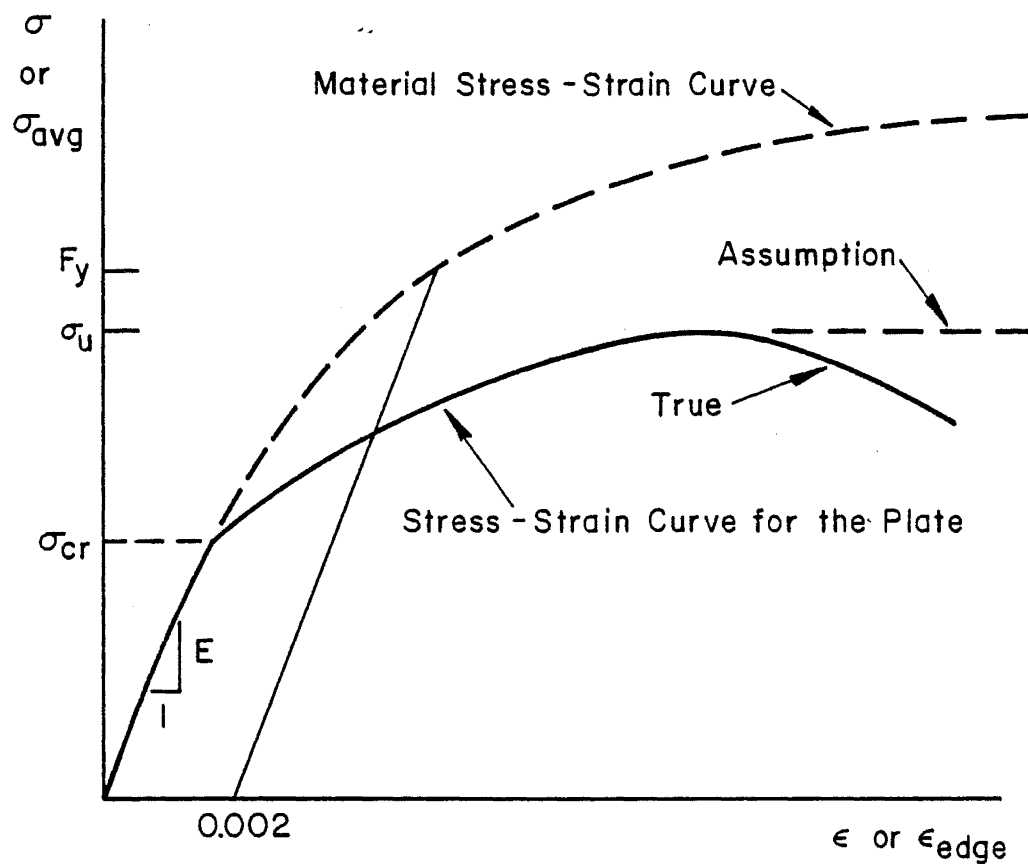
Fig. 7 Average Stress vs. Edge Strain Relationship for Plate
under Compression
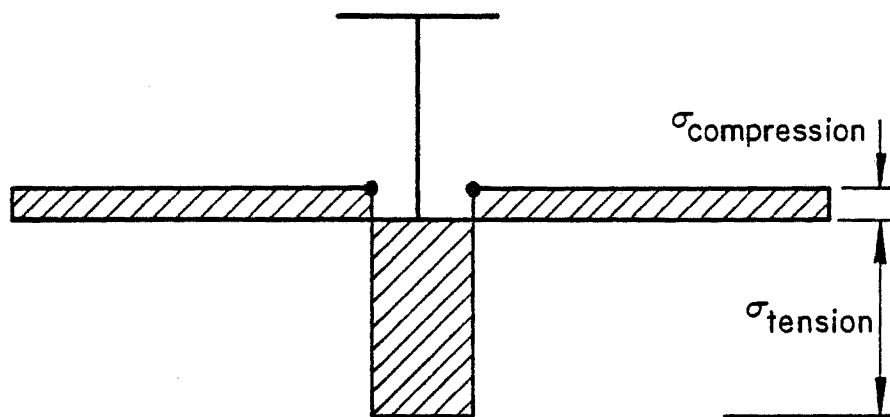
Fig. 8   Residual Stress Pattern in Plate
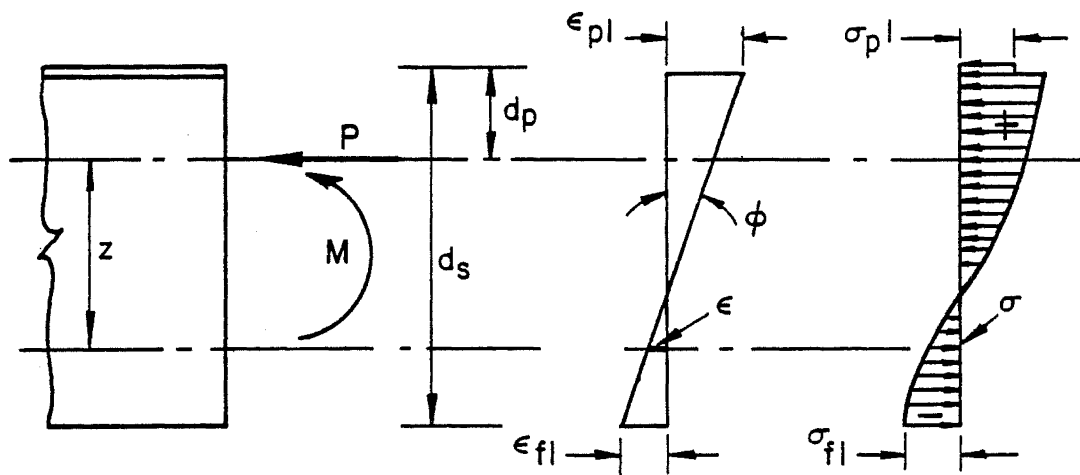
Fig. 9 Distribution of Strains and Stresses in Cross Section

Fig. 10 Moment-Curvature Relationship

Mid-Span of Beam-Column

End Boundary Conditions

$$\frac{d^2y}{dx^2} = 0 \quad \text{or} \quad \frac{dy}{dx} = 0$$

Forces On Element
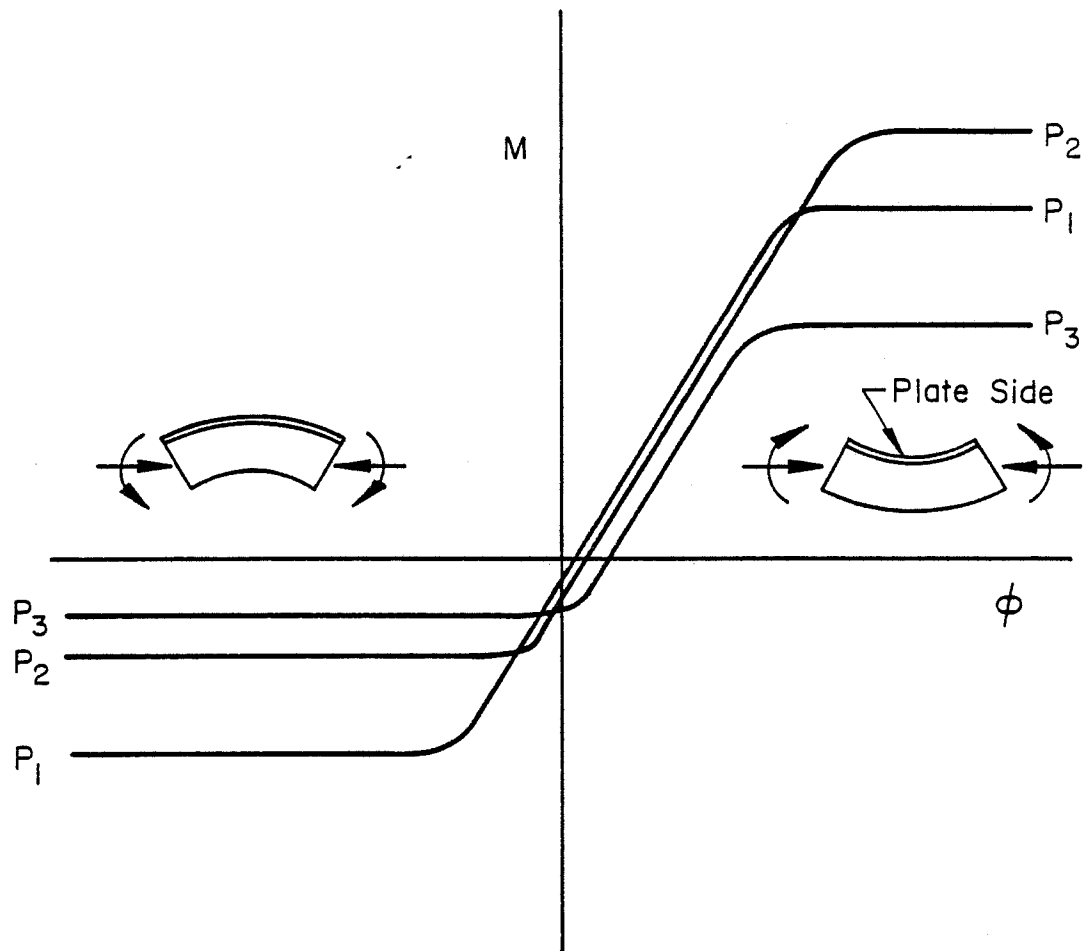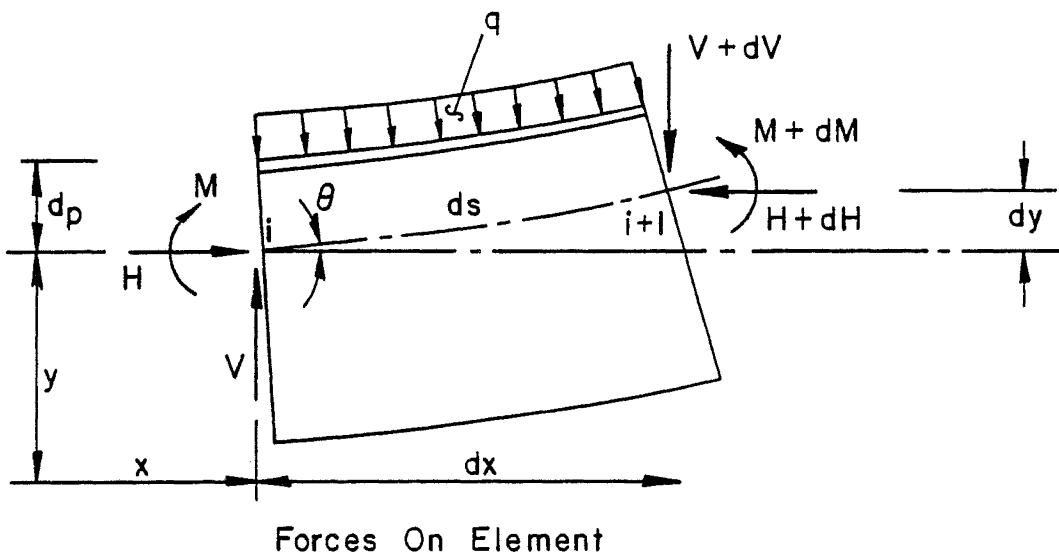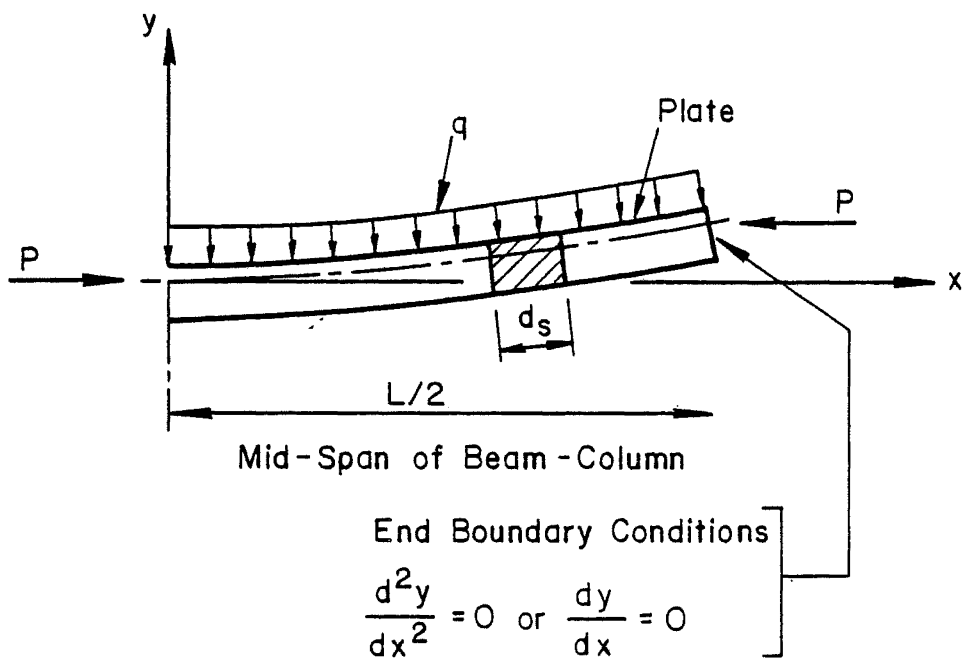
Fig. 11 Stepwise Integration

99
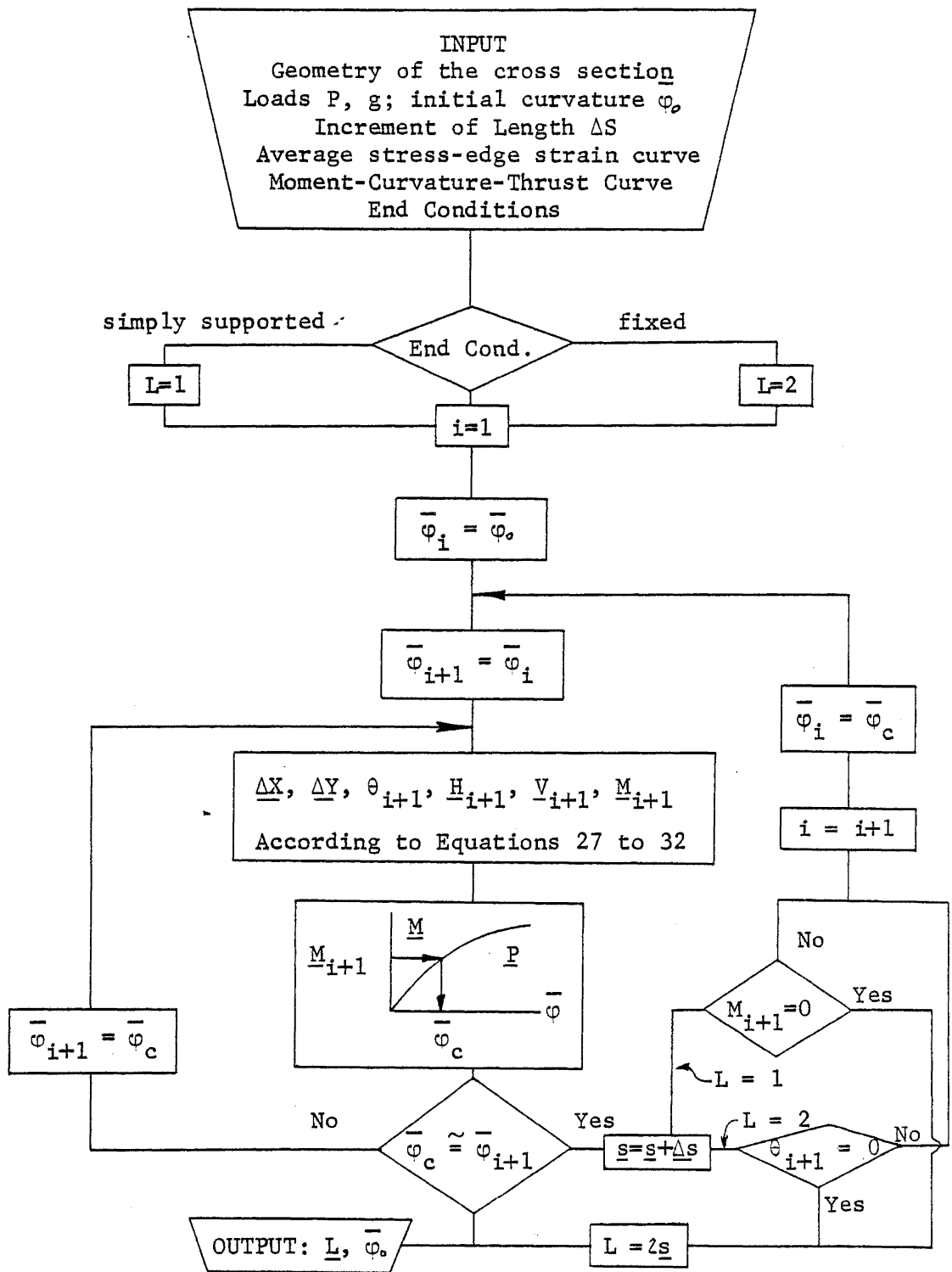
Fig. 12 Flow Chart of Integration Process for
the Length of Beam-Column
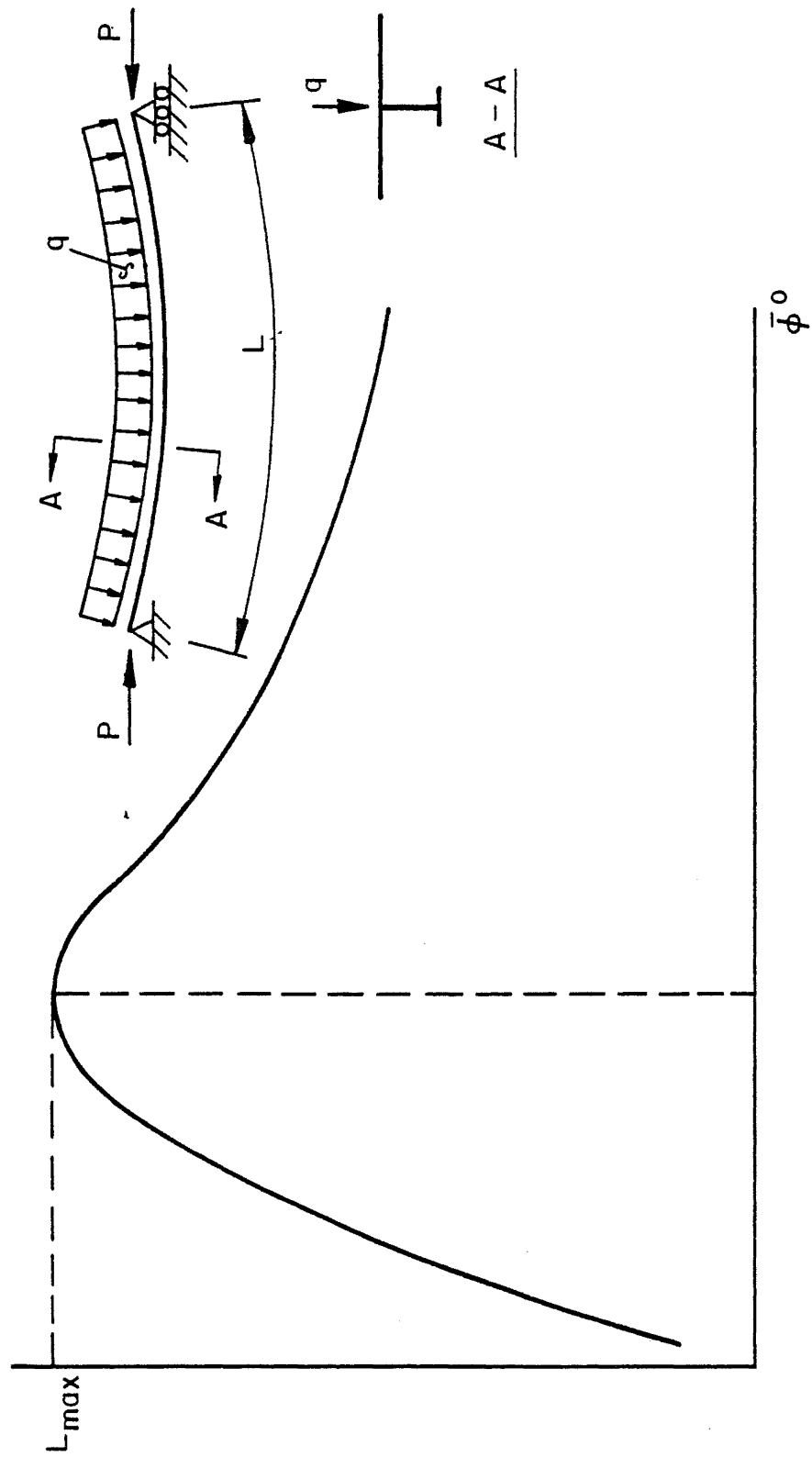
Fig. 13 Length vs. Mid-Span Curvature for Beam-Column
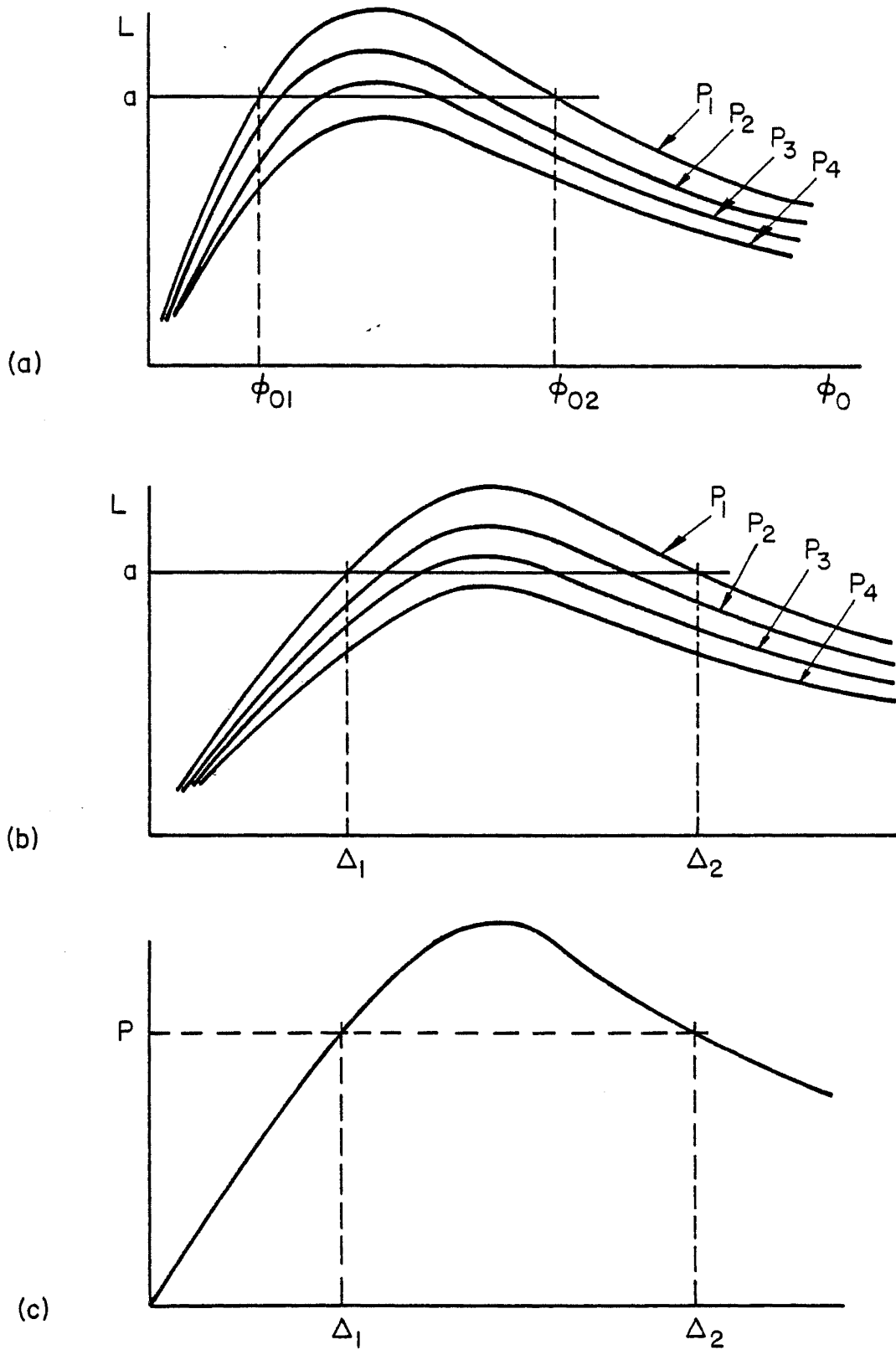
Fig. 14 Procedure of Obtaining P vs. Δ Relationship for Given q
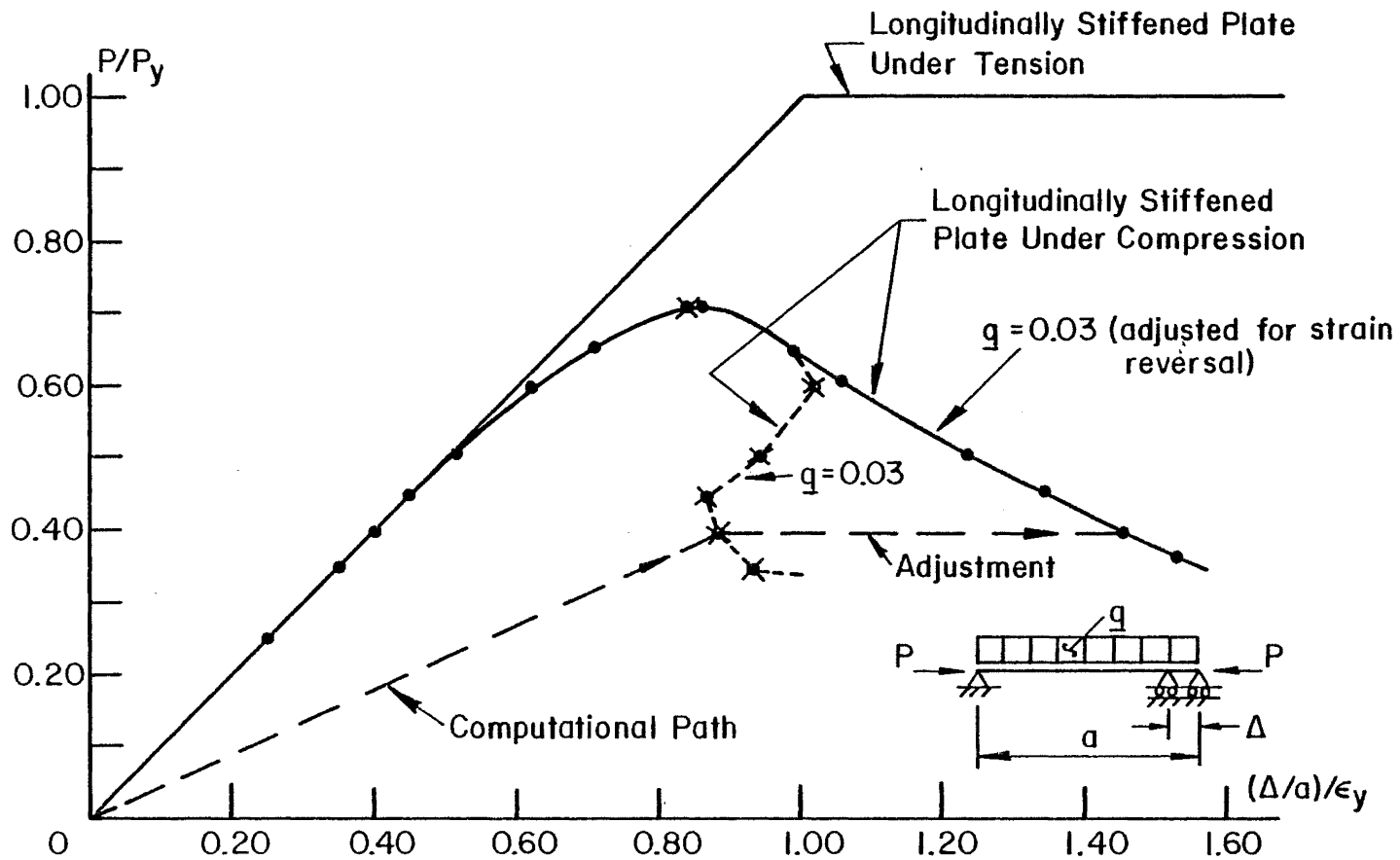
Fig. 15 Load vs. Axial Shortening Adjusted for Strain Reversal
(example for $\underline{q}$ = 0.03)
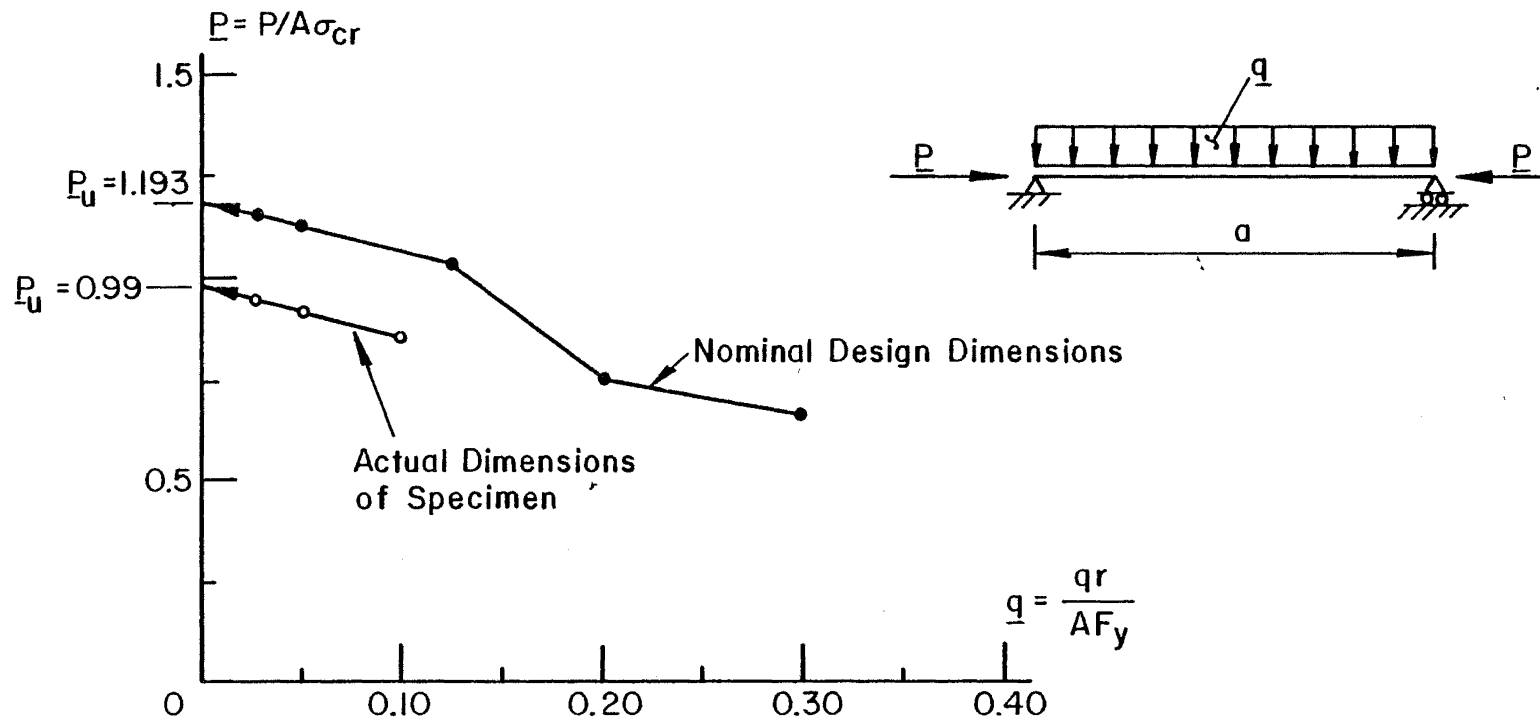
Fig. 16   Extrapolation of Pure Axial Strength from Beam–Column
Strengths (Axial and Normal)
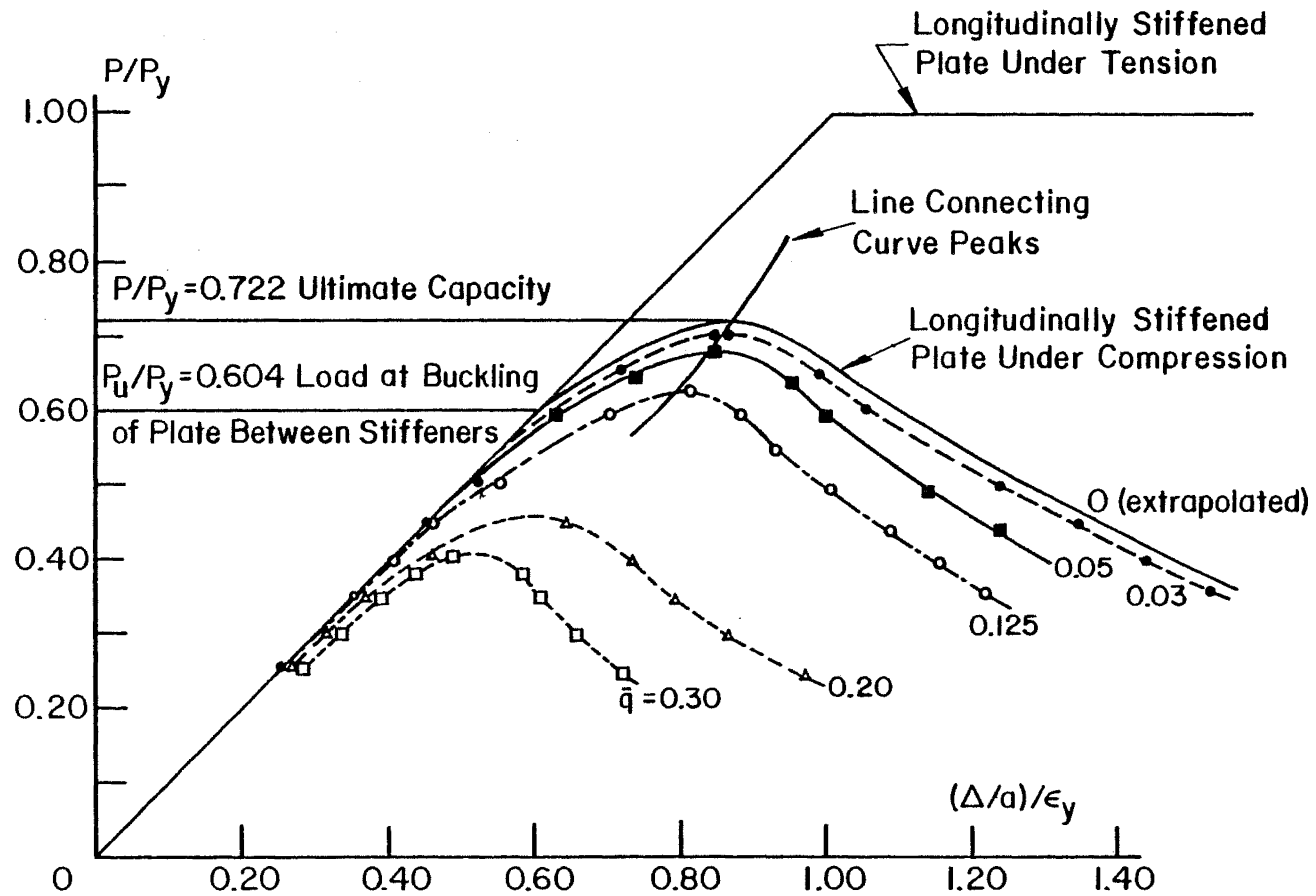
Fig. 17   Load vs. Axial Shortening of Stiffened Plate under Axial
Compression and Normal Loading
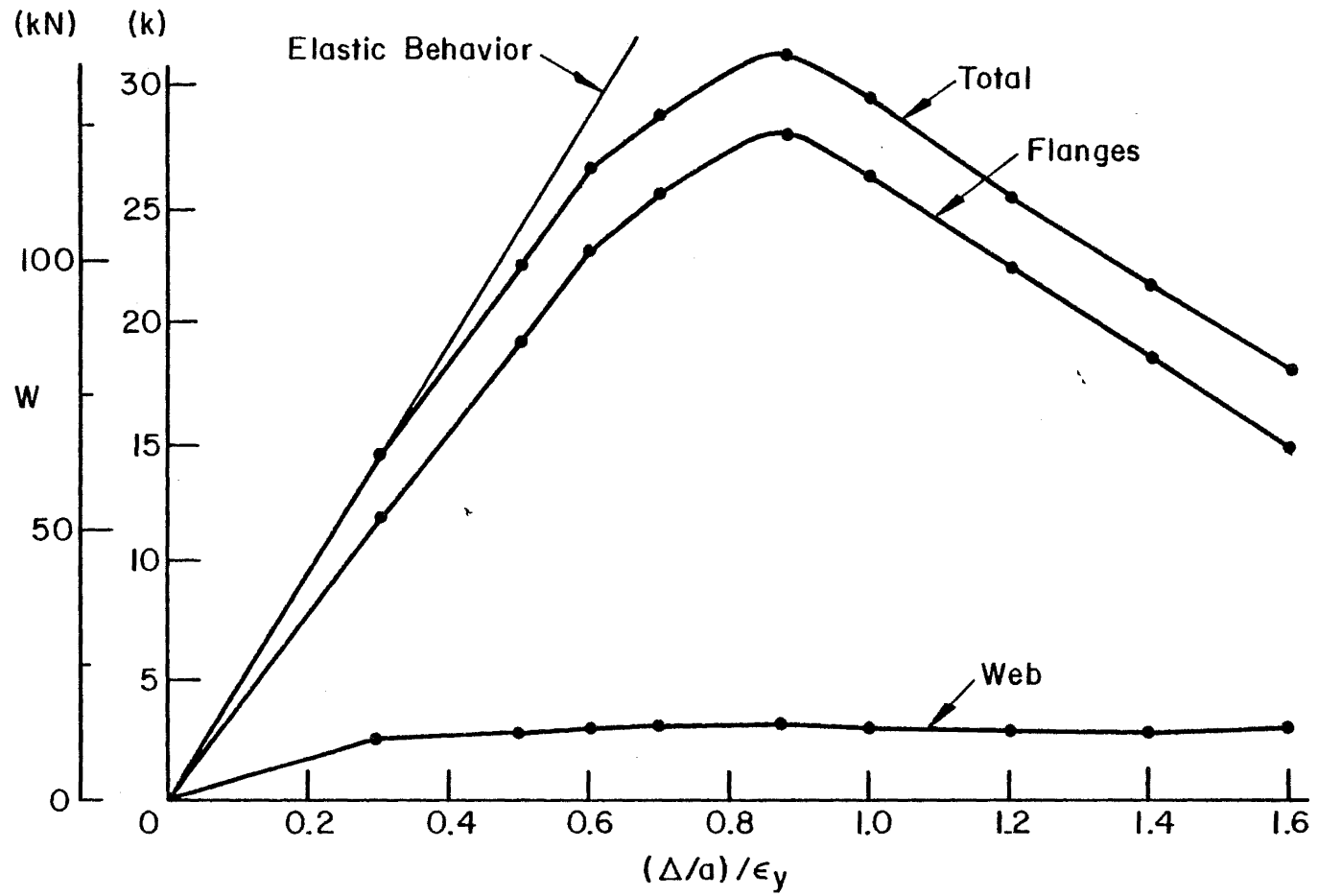
Fig. 18   Load Distribution between Webs and Flanges for Box Section
under Shear and Bending
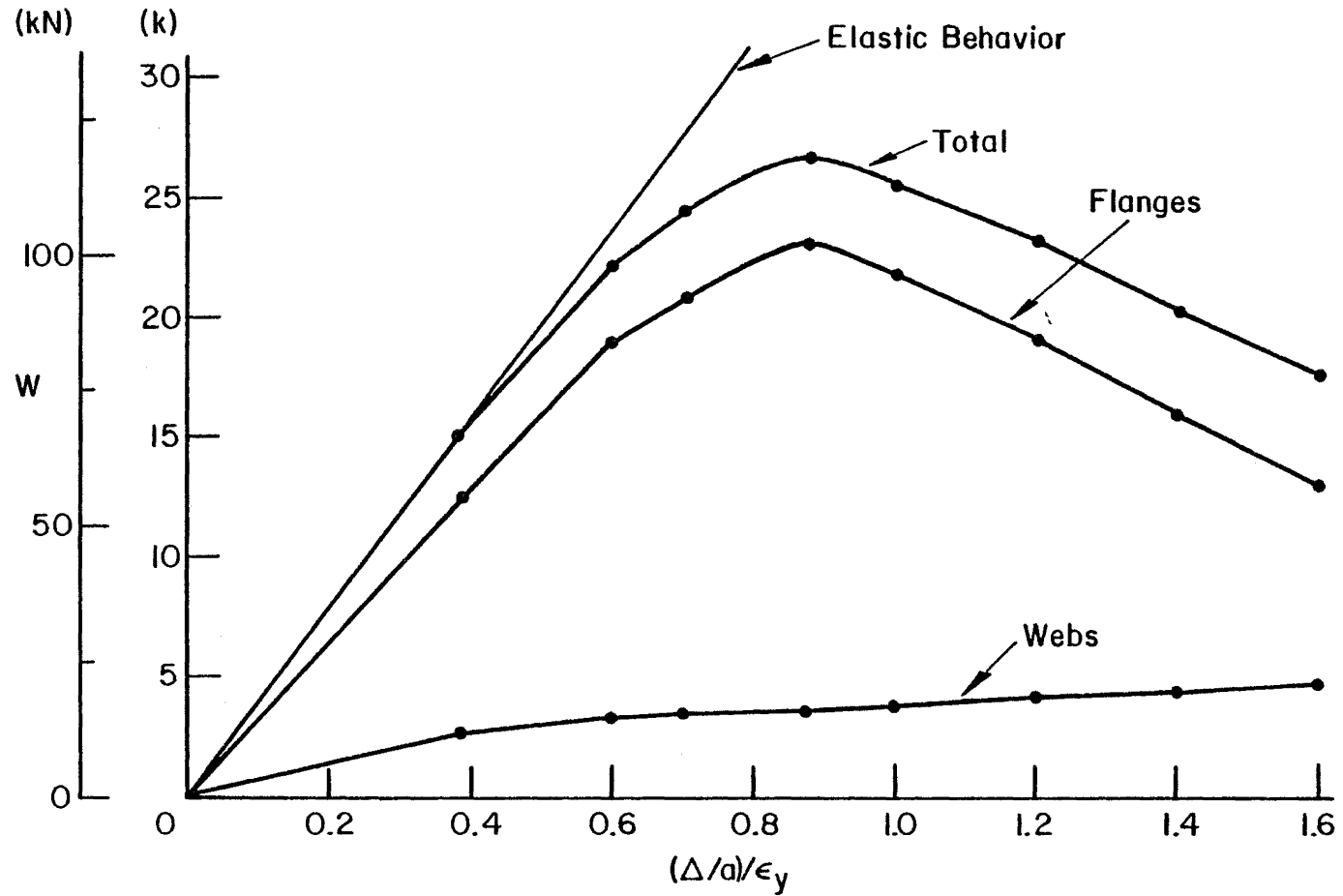
Fig. 19   Load Distribution between Webs and Flanges for Box Section under Bending

START
i=1   j=1

$\varepsilon_{ci}, \varepsilon_{tj}$

Linear Strain Distr.

INPUT
Response of
indiv. components
——
Stress Distribution

j=j+1

INPUT
Cross Section
Geometry
——
$N = \int_A \sigma \, dA$

Change
ε_t

$N \cong 0$ No

Yes

$M = \int_A \sigma \, y \, dA$

INPUT
$M = M(W) = C\ C_1 d\ W$
$V = V(W) = C\ W$
$T = T(W) = C\ C_2 d\ W$
——
$W = \dfrac{M}{C\ C_1 d}$
$V = C\ W$
$T = C\ C_2 d\ W$

i=i+1

For each subpanel
σ_b, σ_c, τ

Reduction of
ε_{tj}, then
get buckling
condition

≤ 1 Buckling
Equ. (8) > 1

OUTPUT
$W, \varepsilon_{ci},$
$\tau_{vcr}, \sigma_{bcr}, \sigma_{ccr}$

$i = i_{max}$

Yes

END

Tension field action
developed.
$\tau - \gamma$ needed

Fig. 20 Flow Chart of the Procedure for Load-Deformation Relationship
of Girder Segment

108

Test Segment

508

3 @ 457

1829   1143

2972

M = 0.562 W (kN-m)
V = 0.615 W (kN)
T = 0 (kN-m)

a) Test l : Moment + Shear

W

M = 0.616 W (kN-m)
V = 0.385 W (kN)
T = 0.194 W (kN-M)
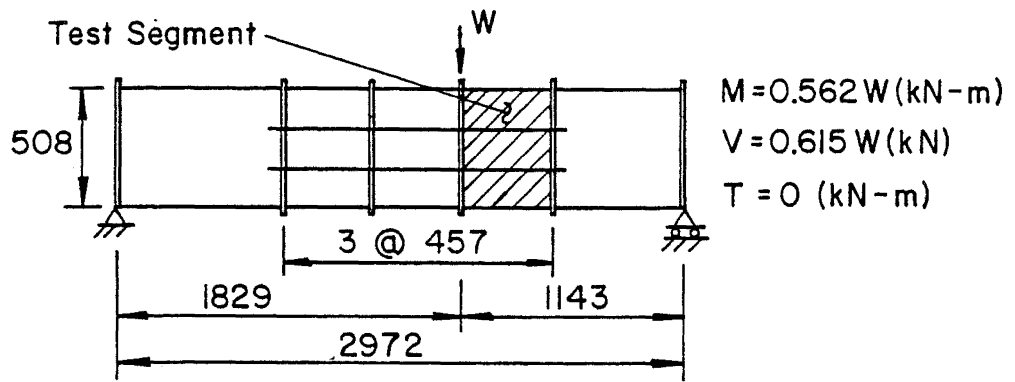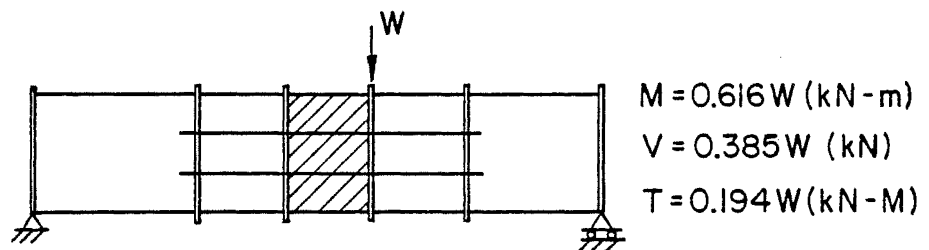
b) Test 2 : Moment + Shear + Torque

W   W

M = 1.143 W (kN-m)
V = 0
T = 0

1143   1829   1143
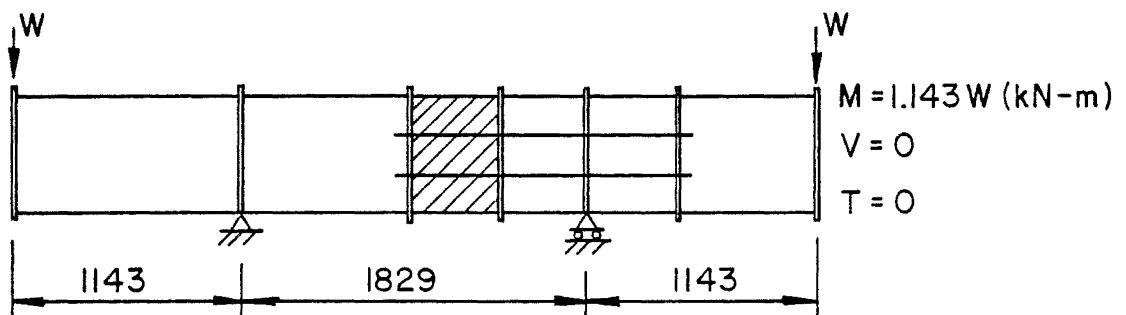
c) Test 3 : Moment Only (future test)

Fig. 21 Test Segments

109

ELEVATION

3.2 Web ℙ   1.6 Web ℙ   3.2 Web ℙ

A→   B→

508

19 x 3.2 (typ)

152   152

915   3 @ 457 =1371   686

2972

ELEVATION   A⏋   B⏋

TOP AND BOTTOM VIEWS

6.4 Flange ℙ   1.6 Flange ℙ   6.4 Flange ℙ

666

51x 9.5 (typ)

19 x 3.2 (typ)

915   3 @ 457 = 1371   686

TOP AND BOTTOM VIEWS

SECTION A-A

51 x 9.5 (typ)

19 x 3.2 (typ)   1.6 (typ)

508   168 172 168

51   6@111=666   51

SECTION A-A

SECTION B-B

6.4

508   3.2   3.2

6.4

666

SECTION B-B
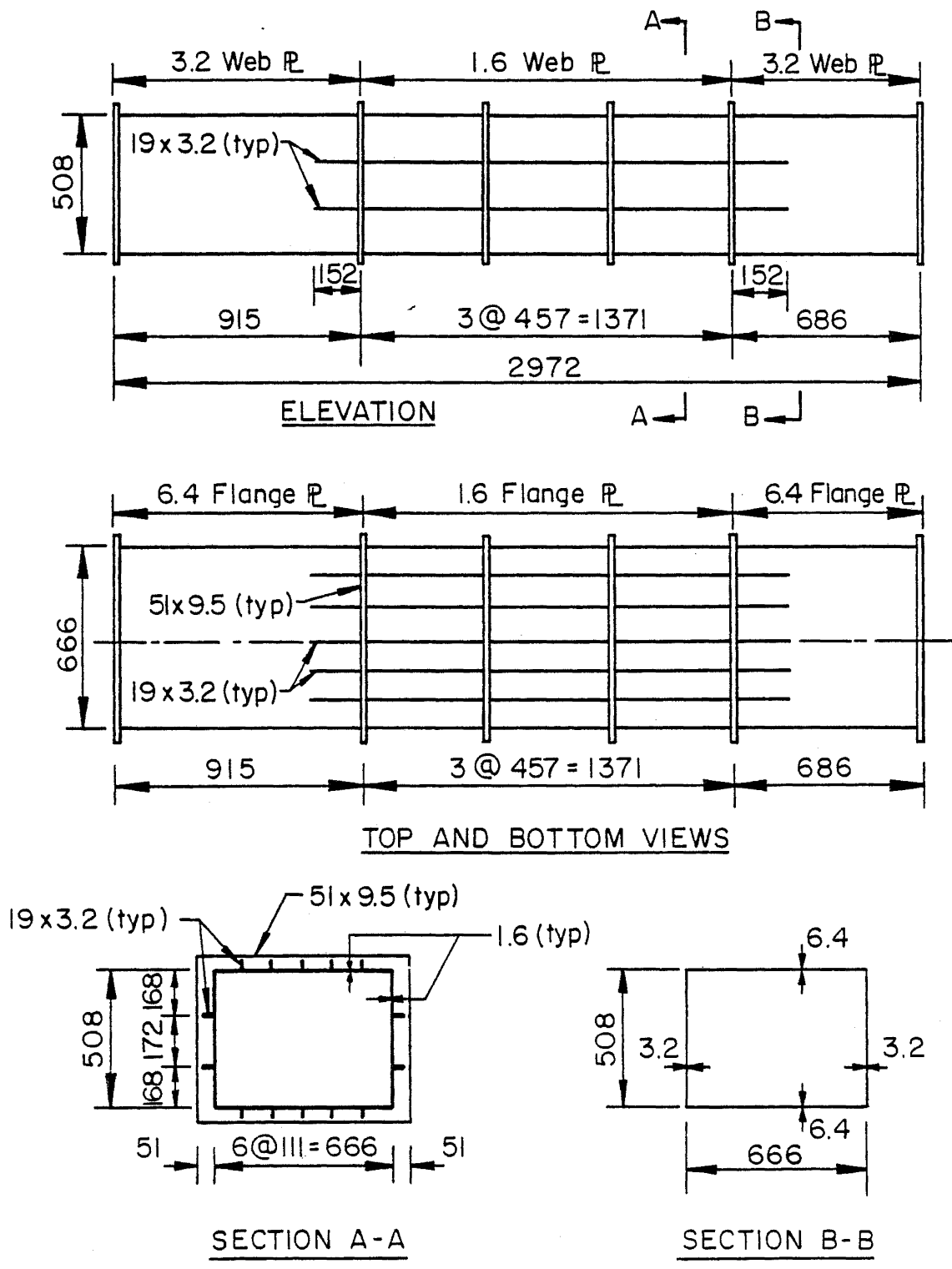
Fig. 22   Test Specimen Scantlings

110
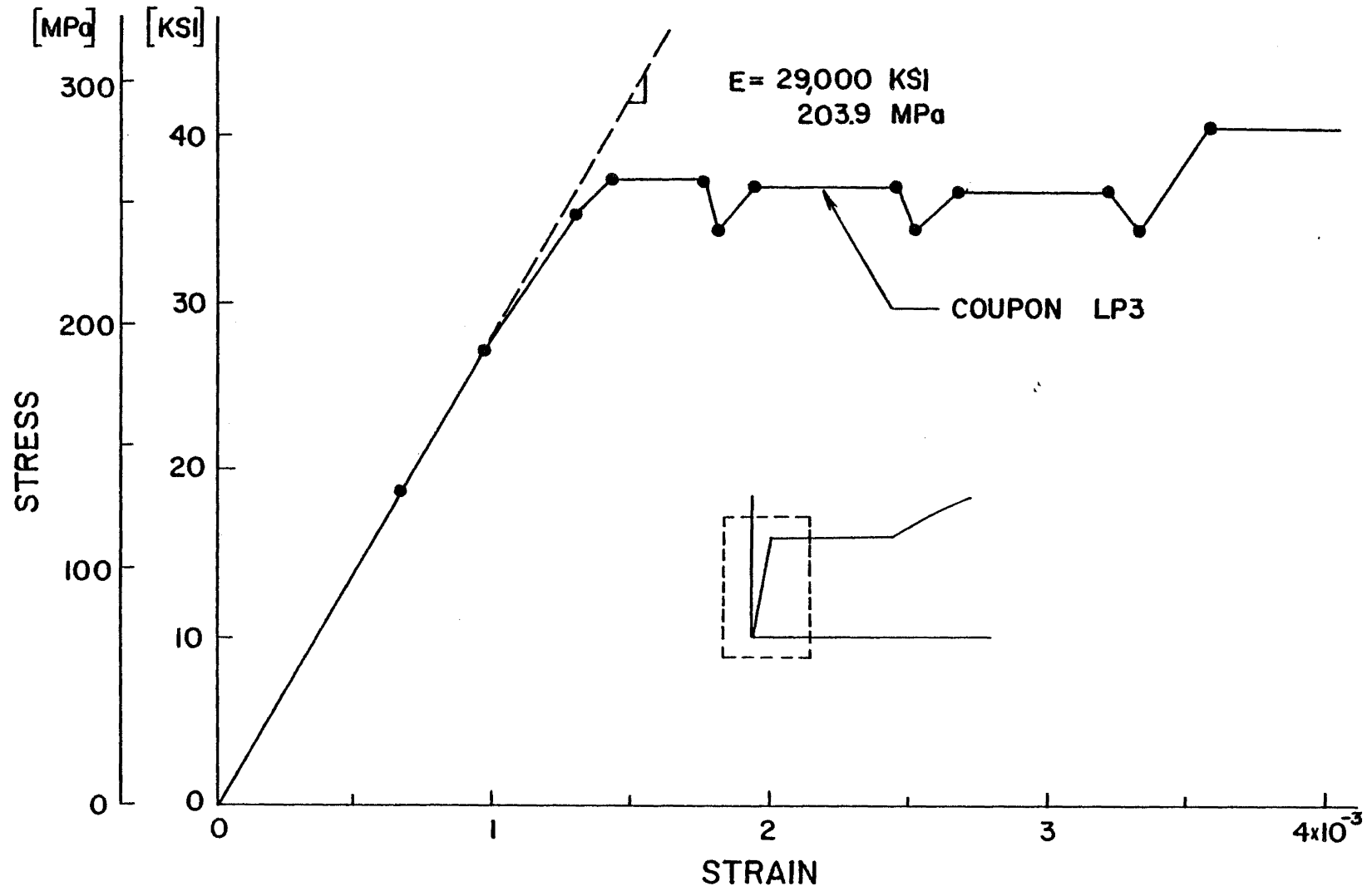
Fig. 23 Typical Coupon Stress-Strain Diagram

ELEVATION

Web I

Segments

3 2 I

508

915

3 @ 457

686

Segments

(mm)

4

2

0

-2

-4

3 2 I

Bottom

Top

Middle
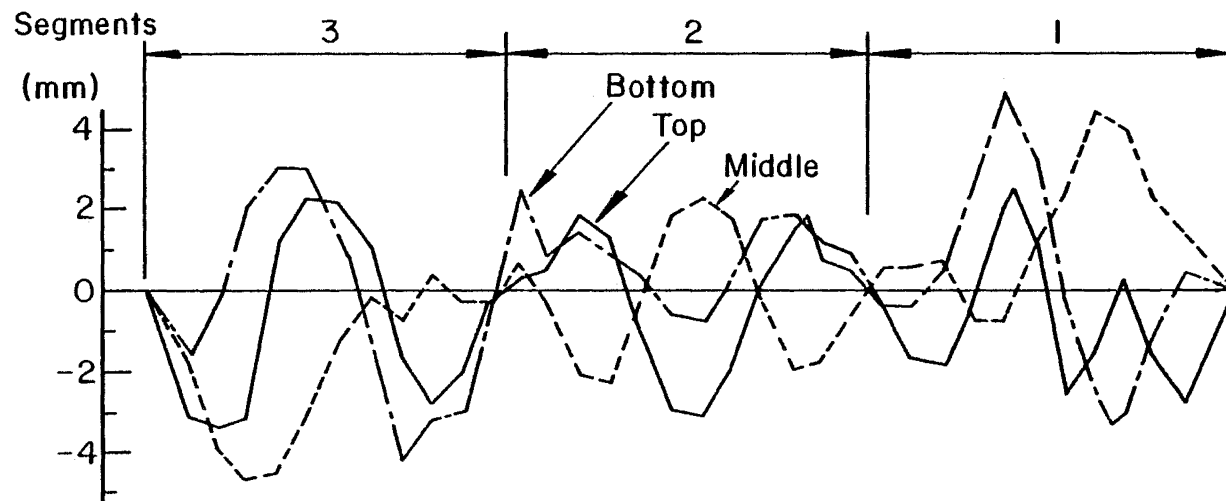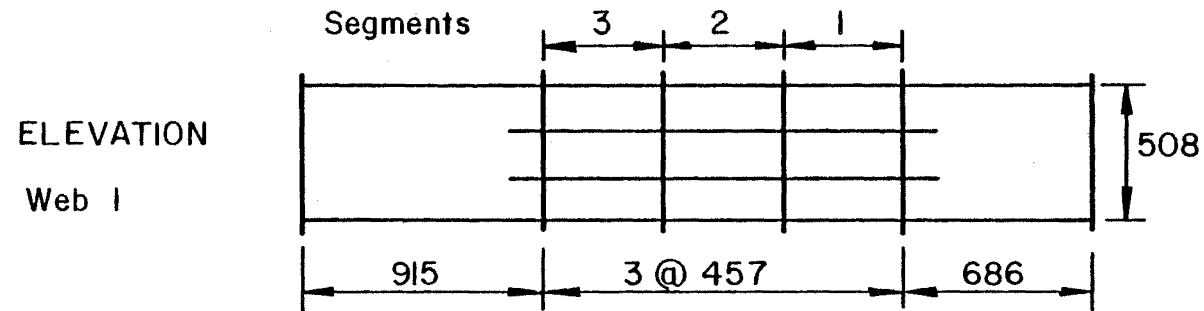
Fig. 24 Initial Imperfection Profile along Mid-Subpanels of Web 1
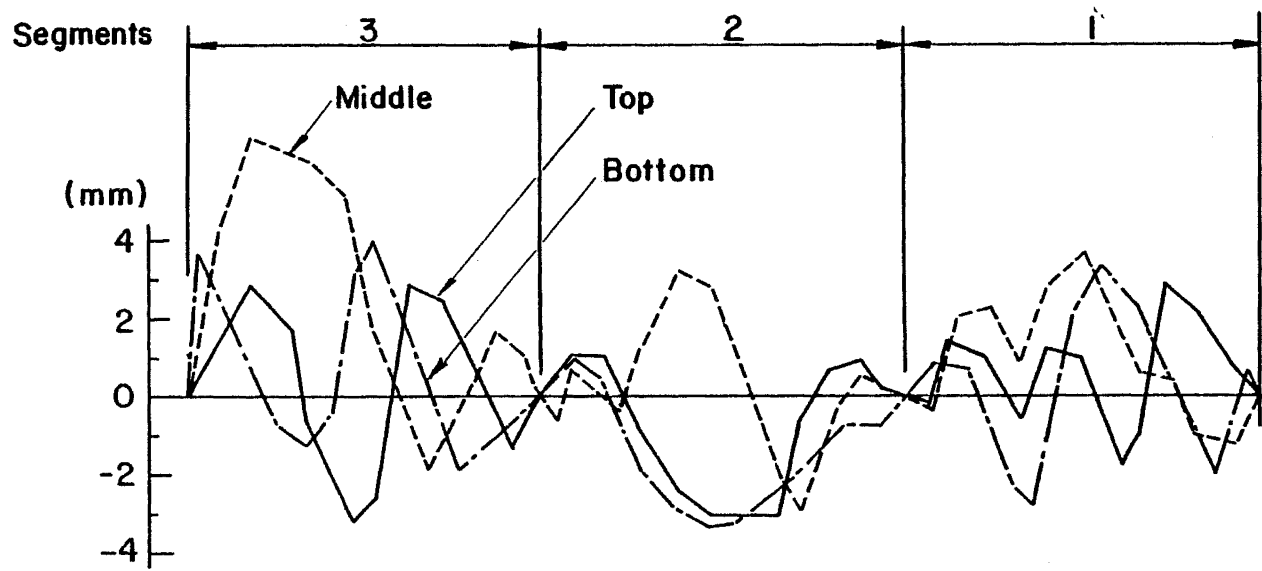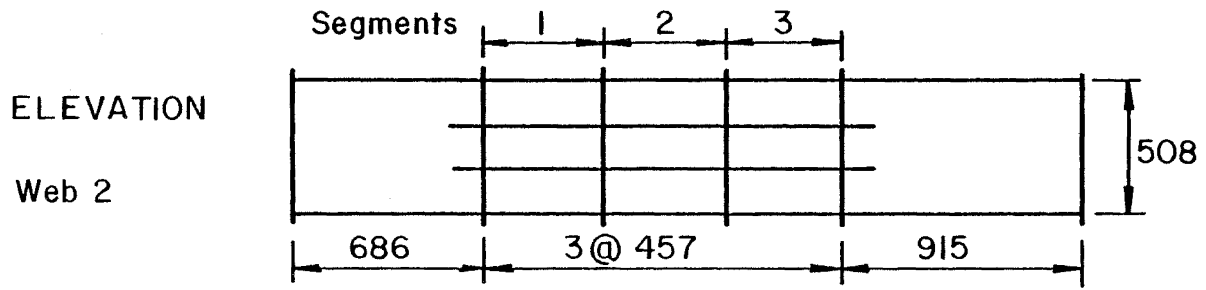
Fig. 25   Initial Imperfection Profile along Mid-Subpanels of Web 2

113

Points A,B,C, Define

Reference Plane

666

915 B 3 @ 457 686
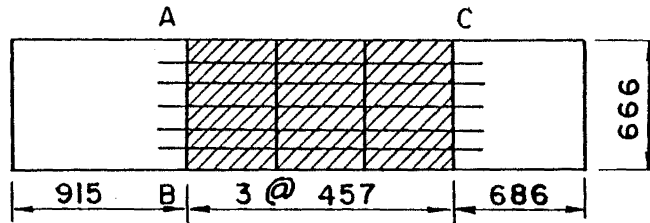
Contours

——— Inward

------ Outward

A Segment ③   ②   ① C

114

B
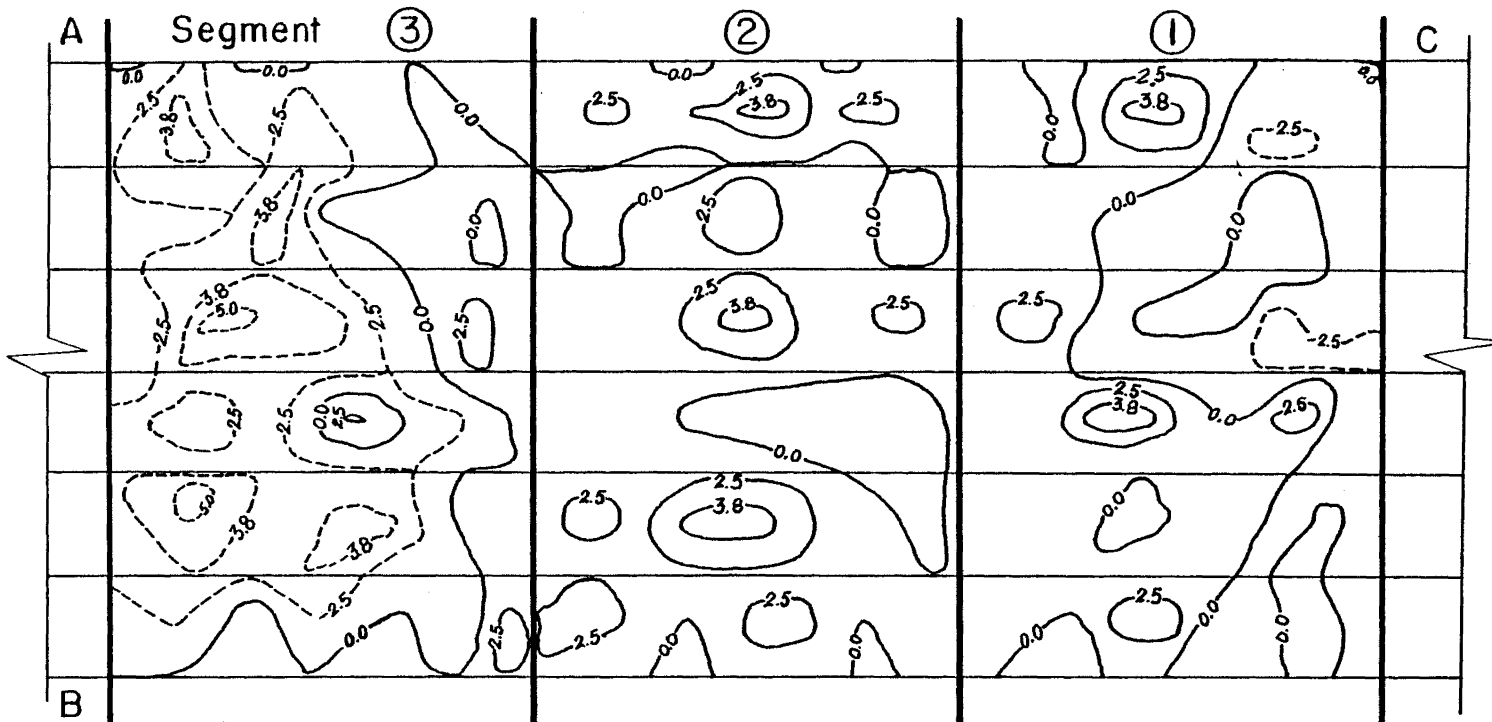
Fig. 26   Initial Imperfections in the Compression Flange (all
dimensions in mm)

ELEVATION

SECTION A-A(Test I)   SECTION A-A(Test 2)

Fig. 27   Test Setup

115
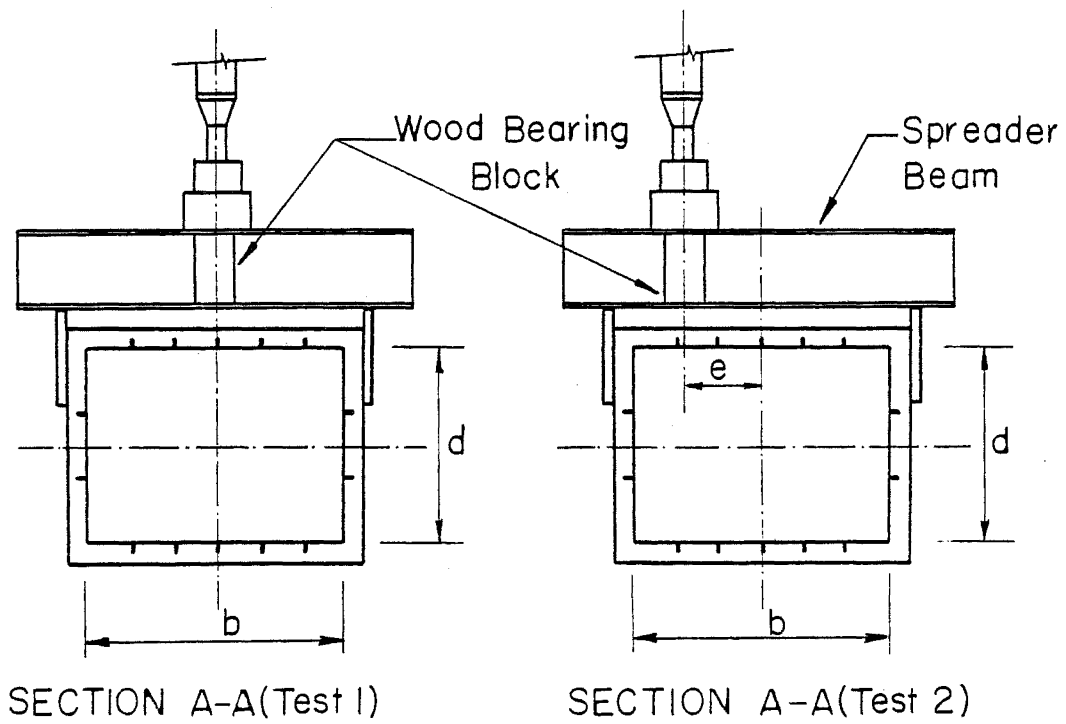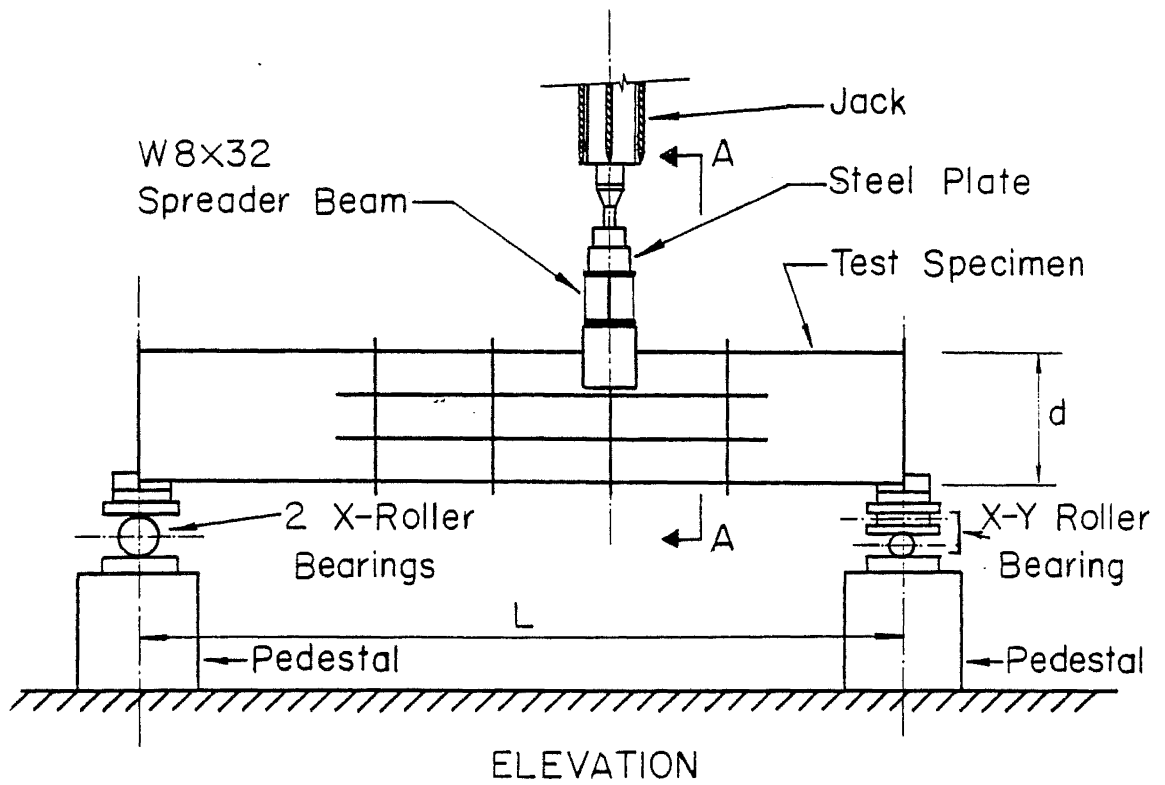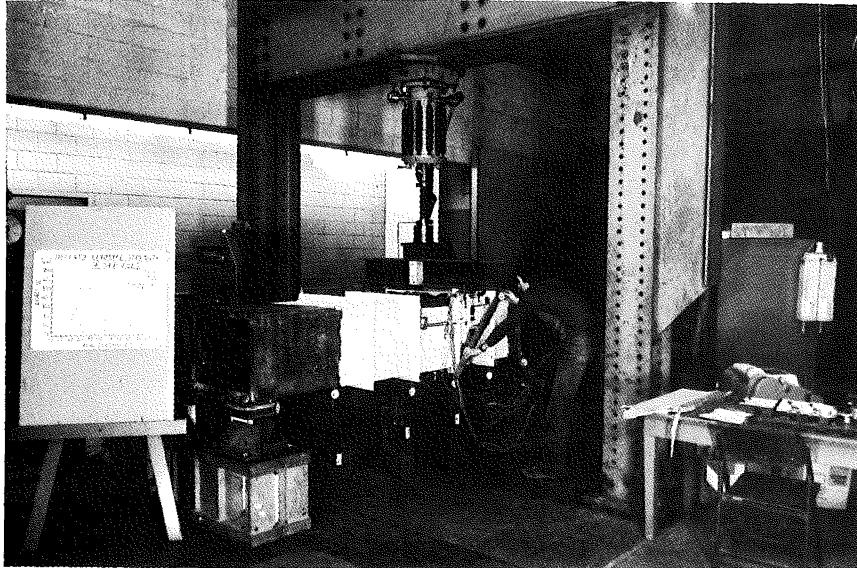
Fig. 28   General Test Arrangement
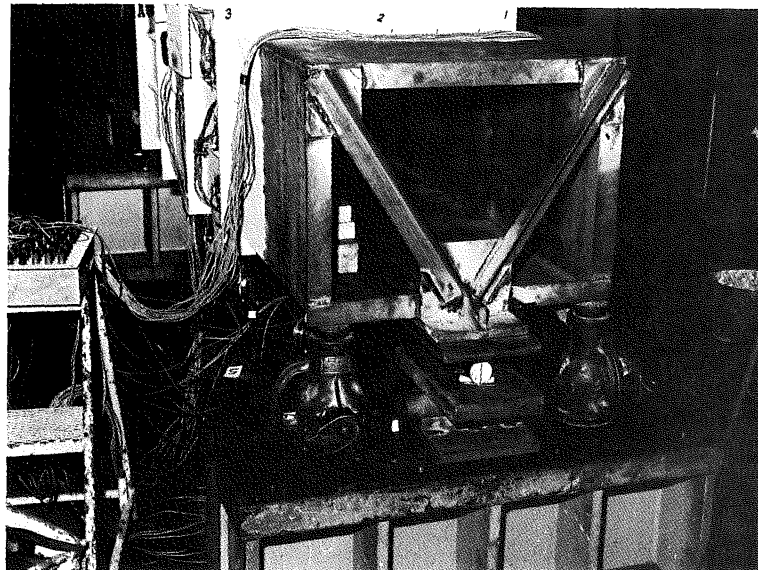
Fig. 29   X-Y Roller Bearing and Bracing at
Specimen End
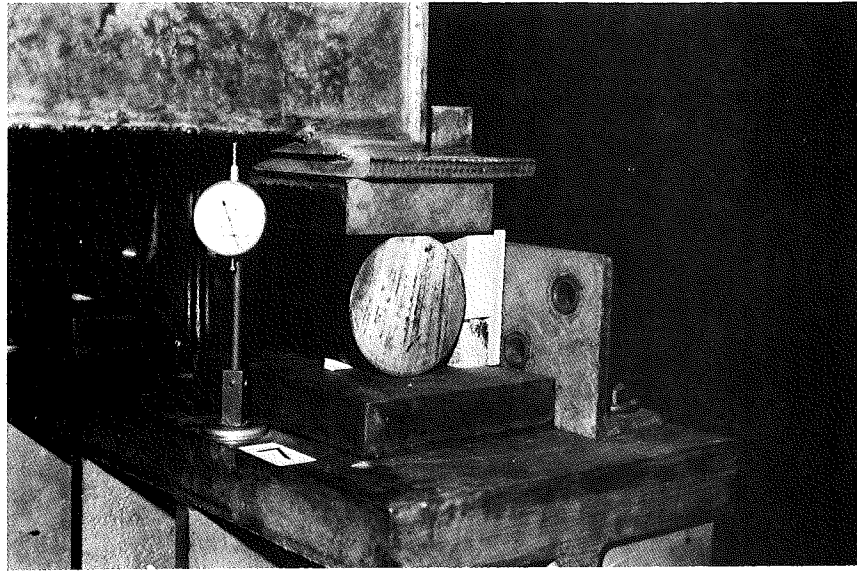
a.   X-Roller Bearing
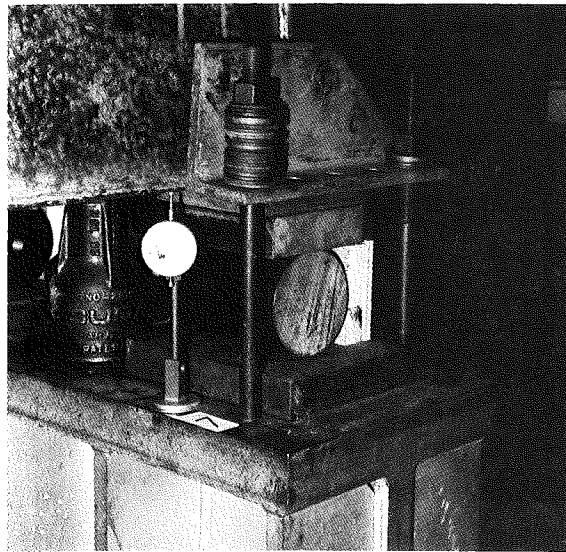
b.   Anchor Bolt to Prevent Uplift of Support

Fig. 30   X-Roller Bearings
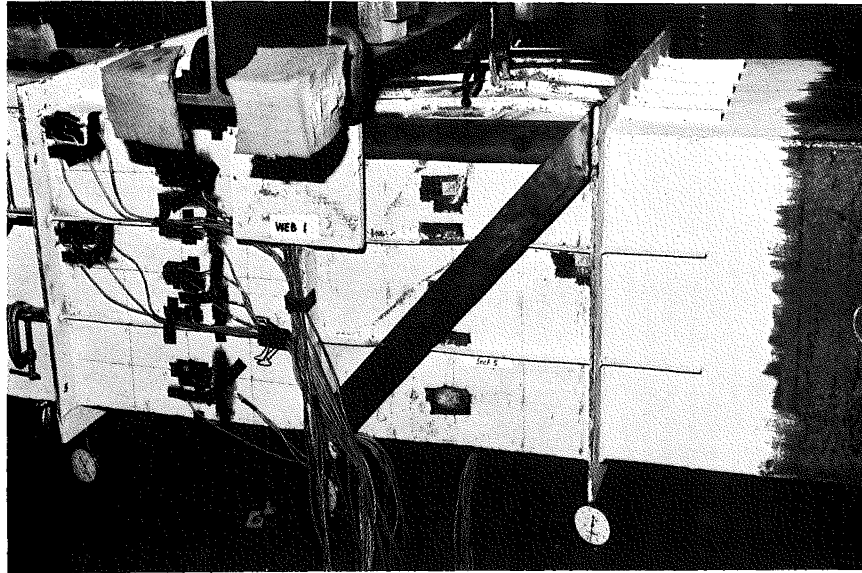
a. Reinforcement of Segment Failed in Test 1
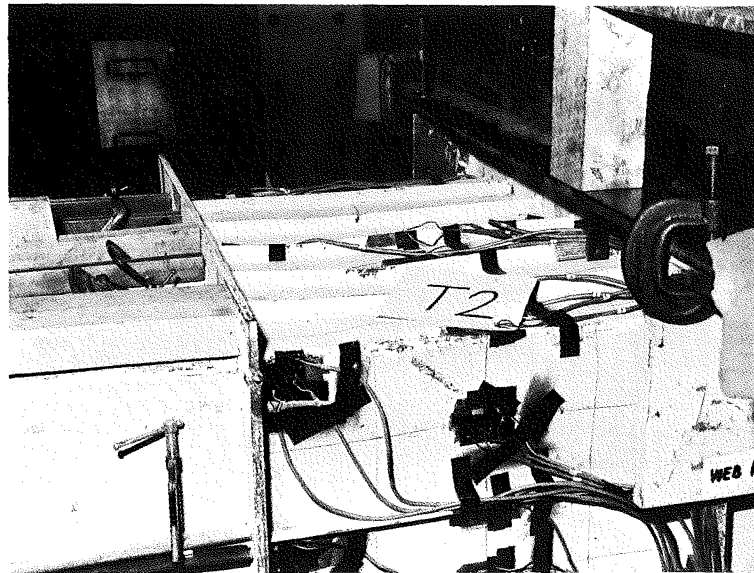
b. Temporary Reinforcement of Segment 3 (at Left)

Fig. 31 Reinforcements of Adjacent Segment Prior to Test 2

ELEVATION

SECTION A-A

TOP FLANGE

WEB I

BOTTOM FLANGE

WEB 2

SECTION B-B
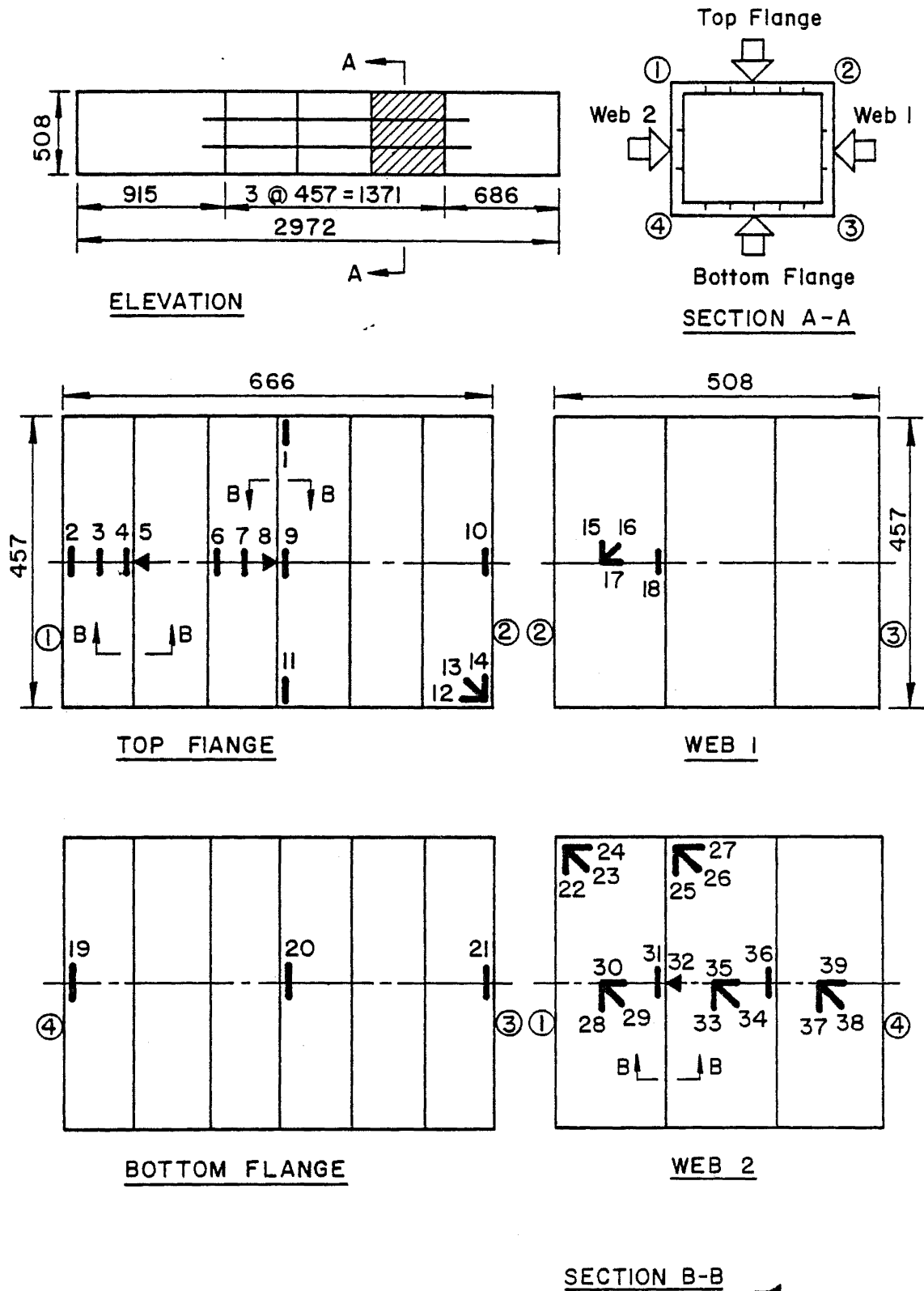
Fig. 32   Location of Strain Gages (Test 1)

119

ELEVATION

508

915   3 a 457=1371   686

2972

A

SECTION A-A

Top Flange

① ②

Web 2   Web 1

④ ③

Bottom Flange

TOP FLANGE

666

457

2 3 4
1

B   B

5 6 7 8   9 10 11 12   13

B   B

14

①

WEB 1

508

457

17 18

15 16

②

③

BOTTOM FLANGE

19   20   21

④   ③

WEB 2

B   B

22 23   26 27 28   31 32

24 25   29   30   33

34 35   37 38

36   39

①   ④

SECTION B-B
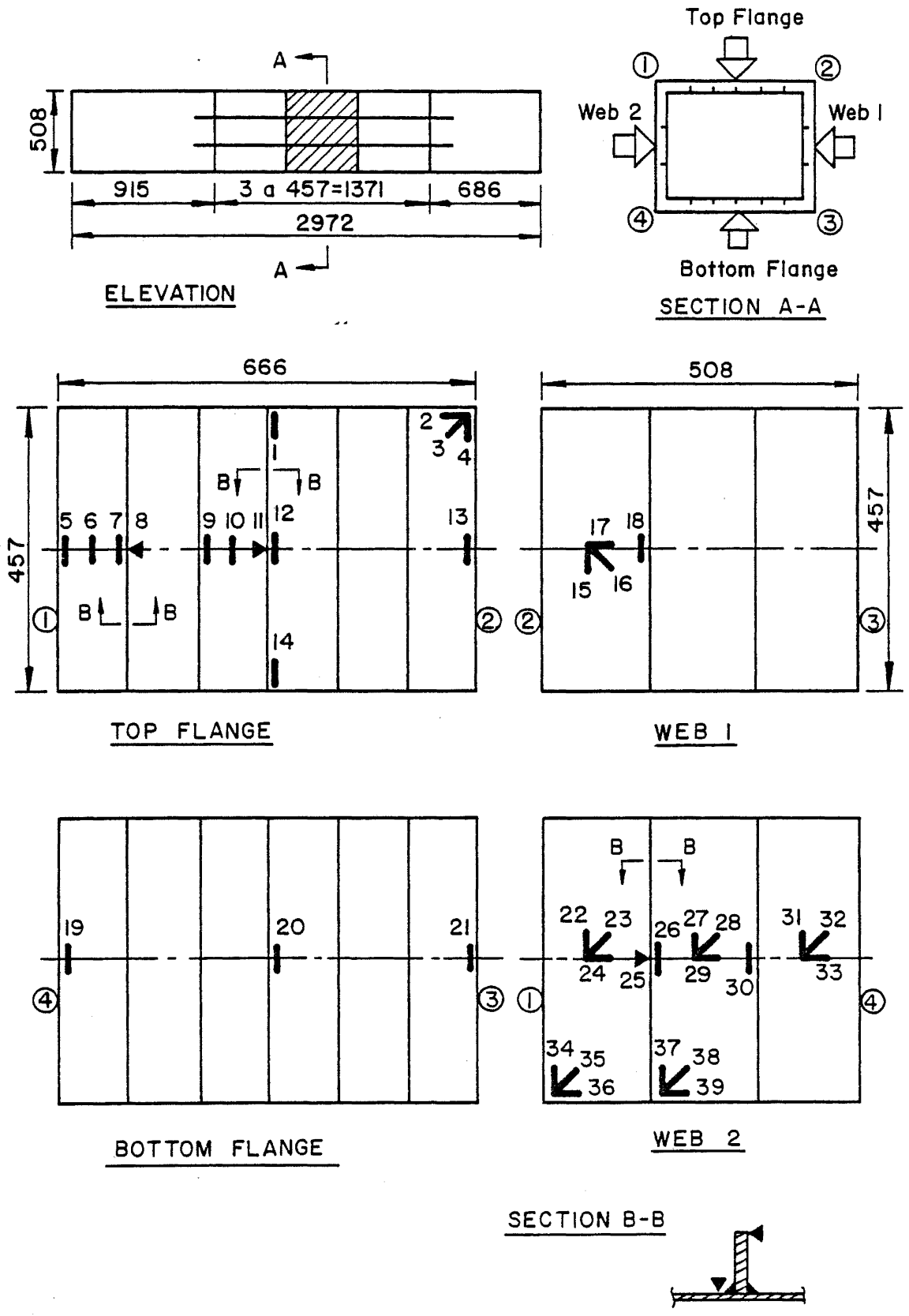
Fig. 33   Location of Strain Gages (Test 2)

120

Segment 3 2 1

51

508

51

914   3 @ 457   687

2972

ELEVATION WEB I

Dial Gage Rig for Web Deflections

Dial Gage Rig for Comp. Flange Deflections

Magnet

ELEVATION SEGMENT I
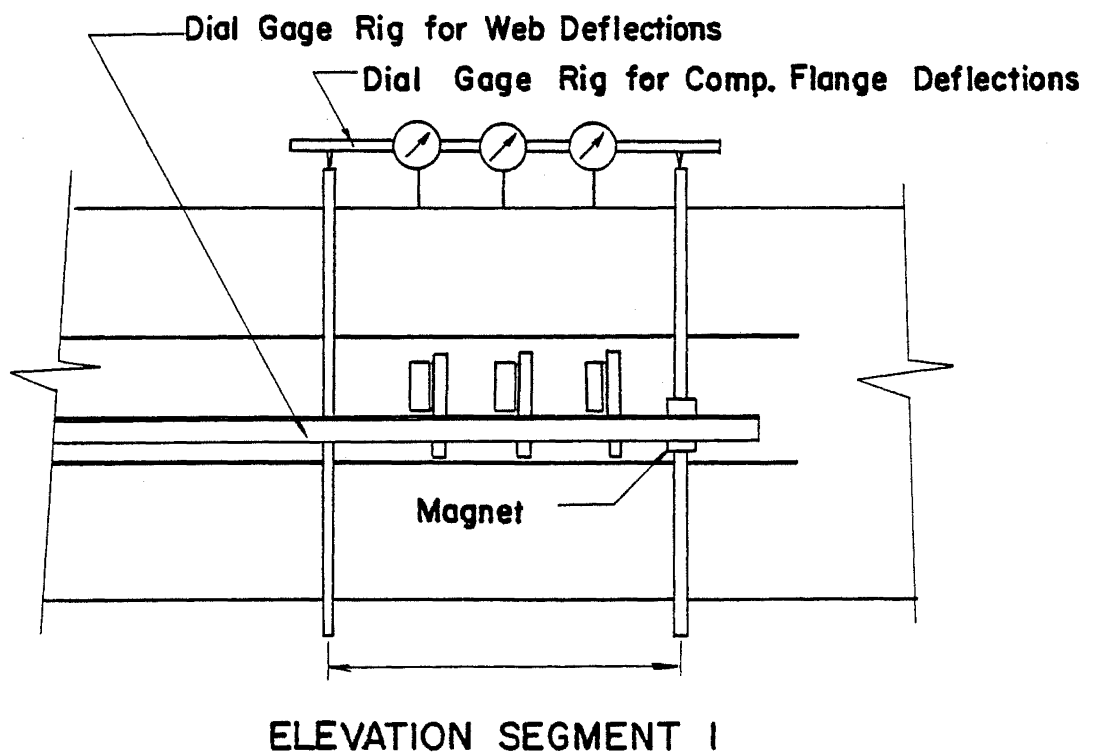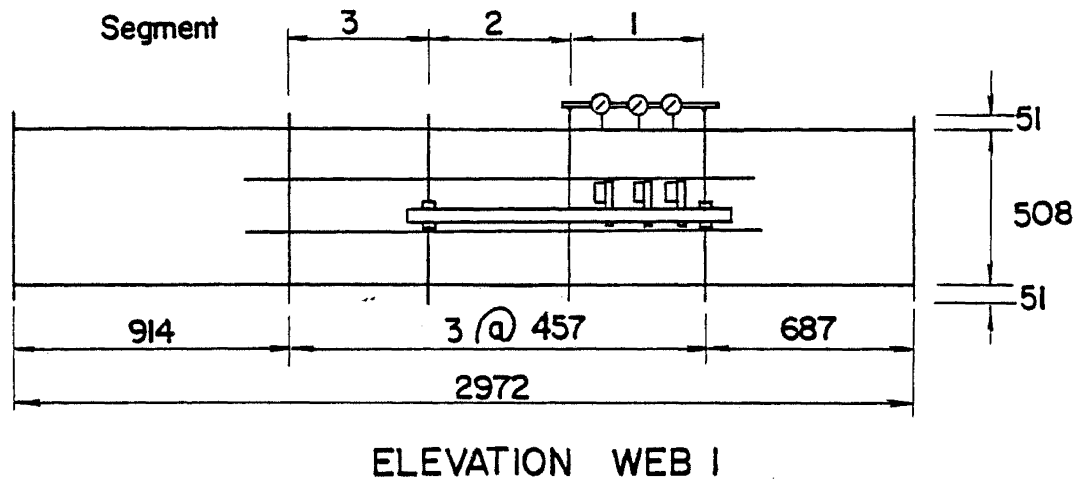
Fig. 34   Dial Gage Rigs for Web and Flange Deflections
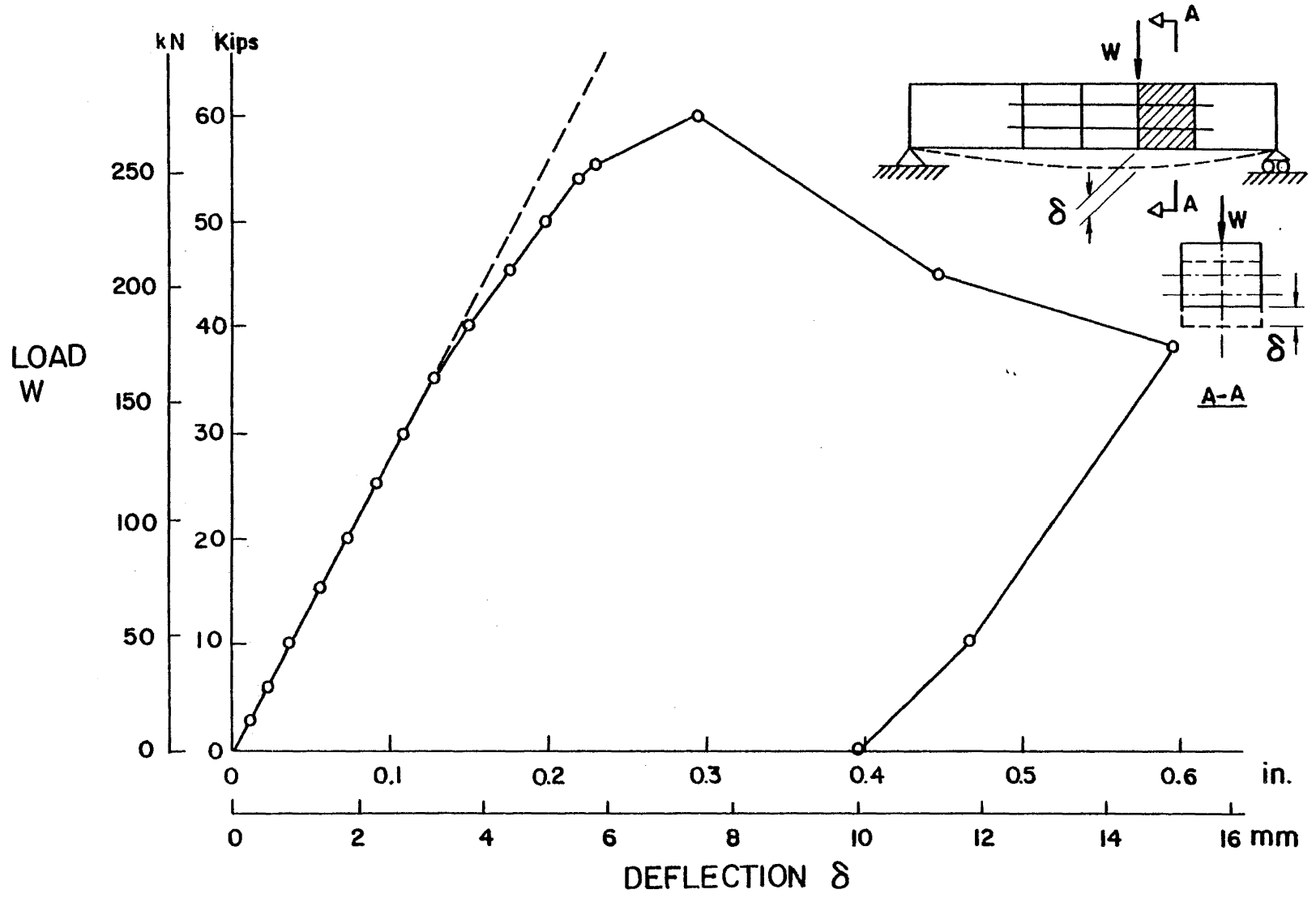
Fig. 35 Load vs. Deflection Curve for Test 1

122
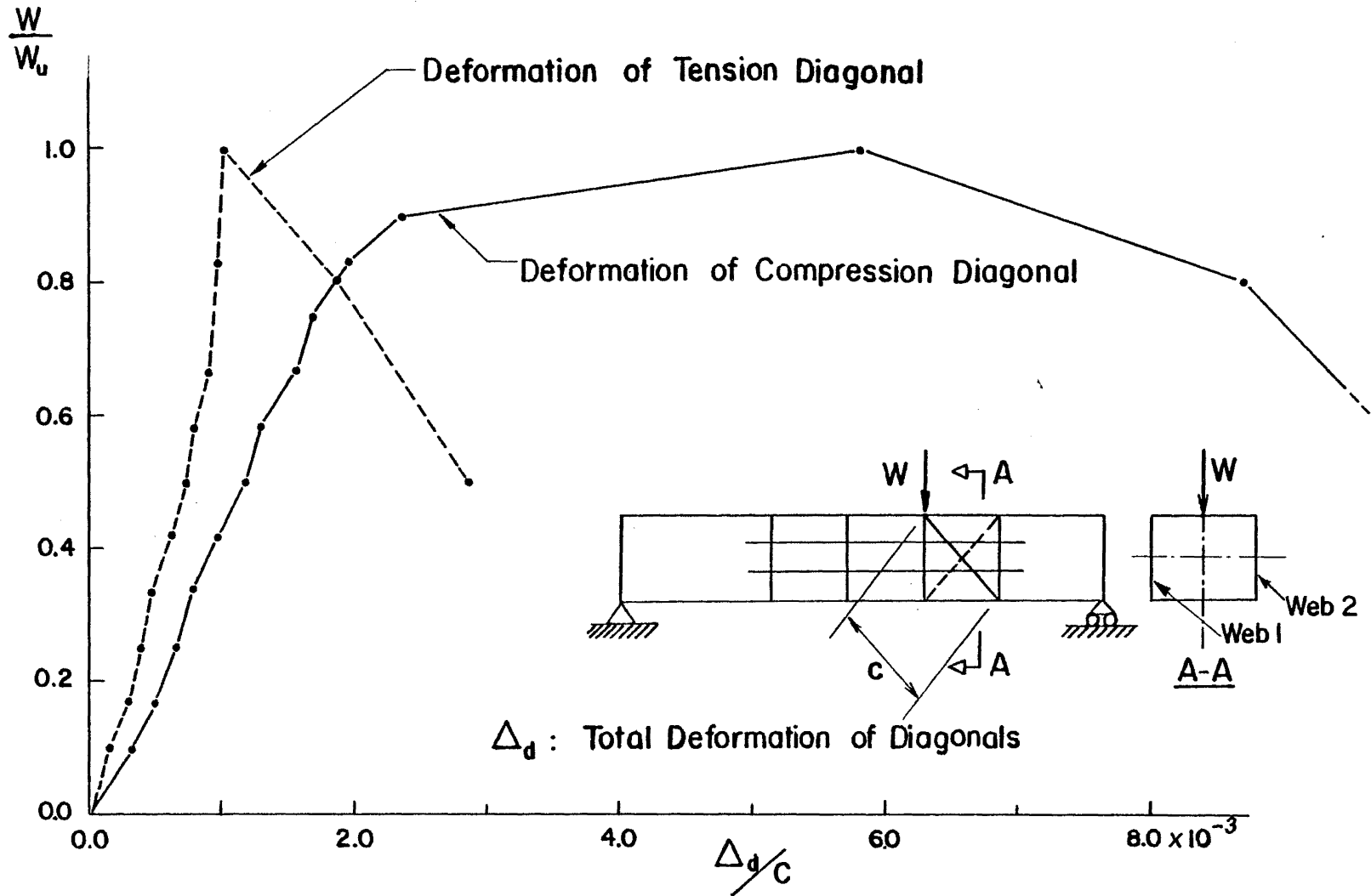
Fig. 36 Diagonal Deformations of Web 1 (Test 1)

123

Fig. 37   Deformations of Compression Flange
and Web 1 (Test 1)

Fig. 38   Deformations of Compression Flange
and Web 2 (Test 1)
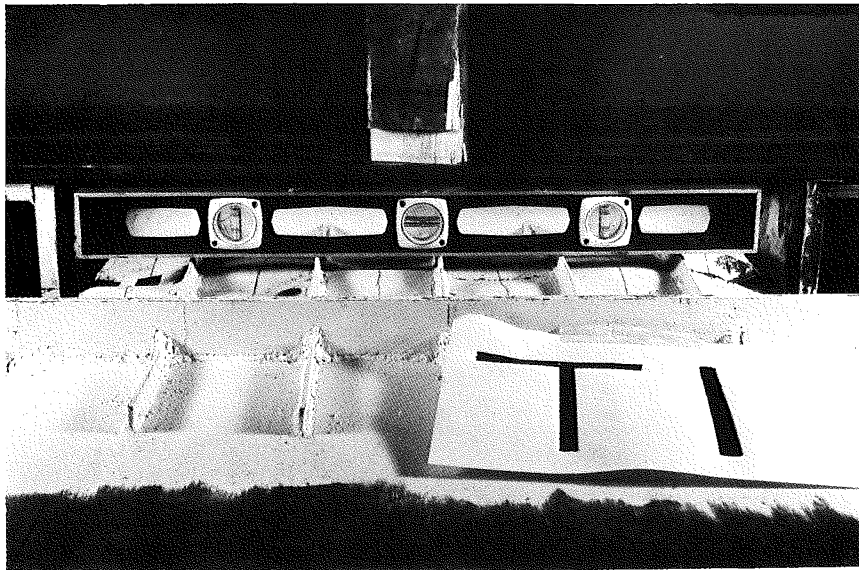
Fig. 39   Uniformity of Deflection of Compression Flange
          Stiffeners at Ultimate Load (Test 1)
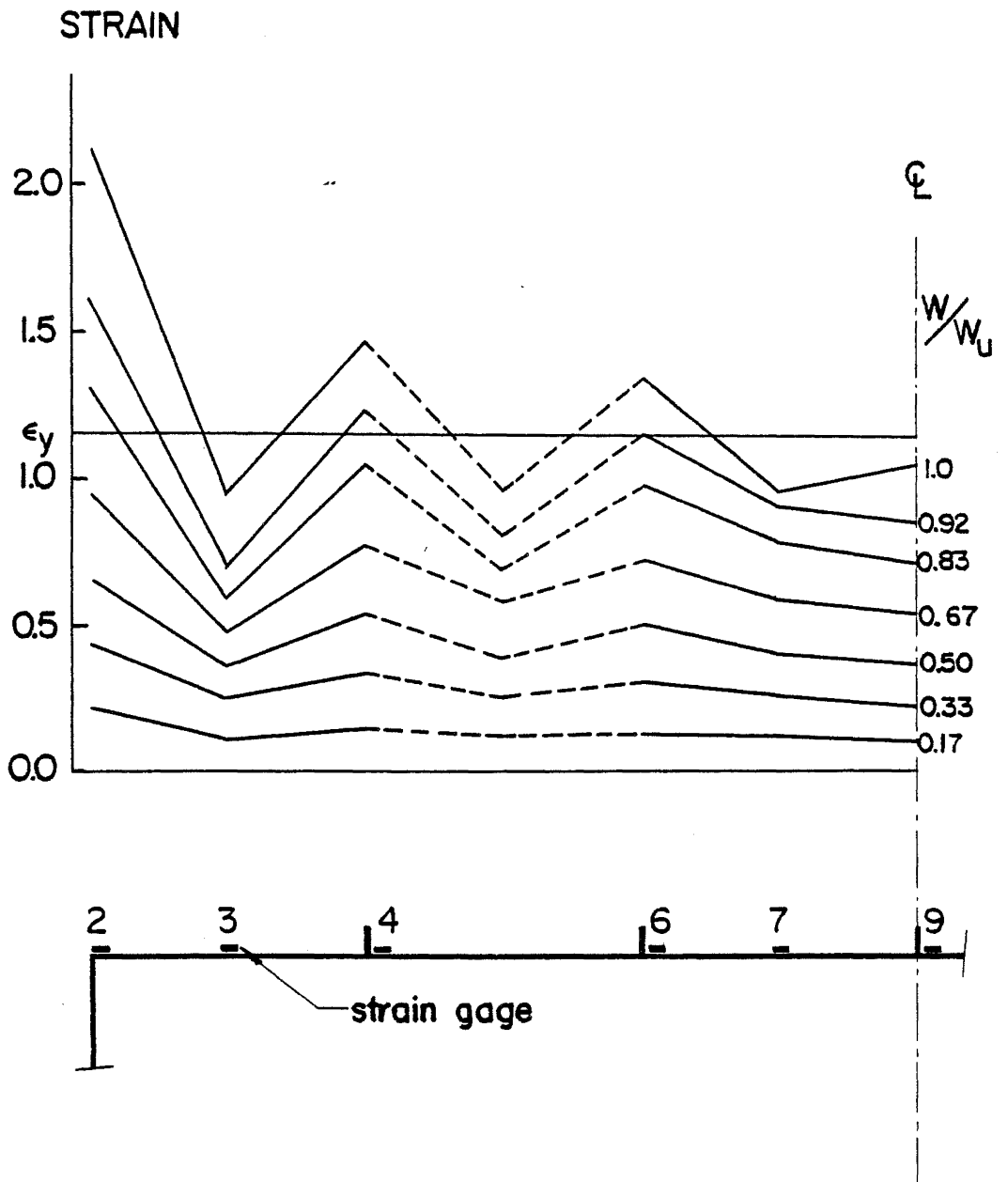
Fig. 40   Strain Distribution at Mid-Length of Compression Flange
(Test 1)

126
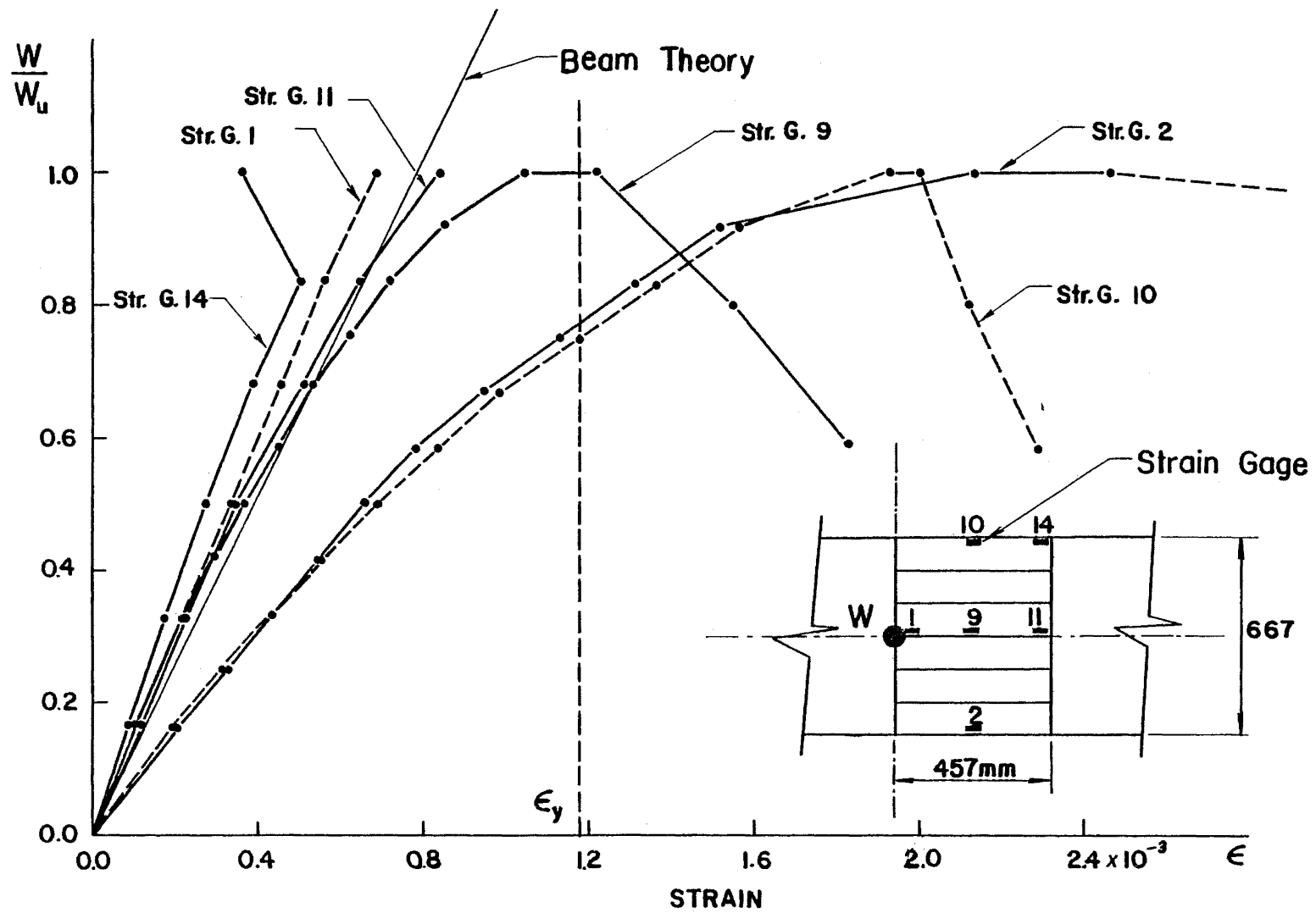
Fig. 41 Load–Strain Relationships for Different Points of
Compression Flange

W

A

a. ELEVATION

A

B

B

Web 1 ——   —— Web 2

b. SECTION A-A

c. AXIAL STRESS
   IN FLANGE
   (Section B-B)

1.0

0.6

0.2

0

W/W_u

1.0

0.83

0.67

0.50

0.33

0.17

Gage 1   Gage 9   Gage 11

W/W_u 1.0   0.83 0.67 0.50 0.33 0.17

d. AXIAL STRESS
   IN WEB
   (Section A-A, Web 1)
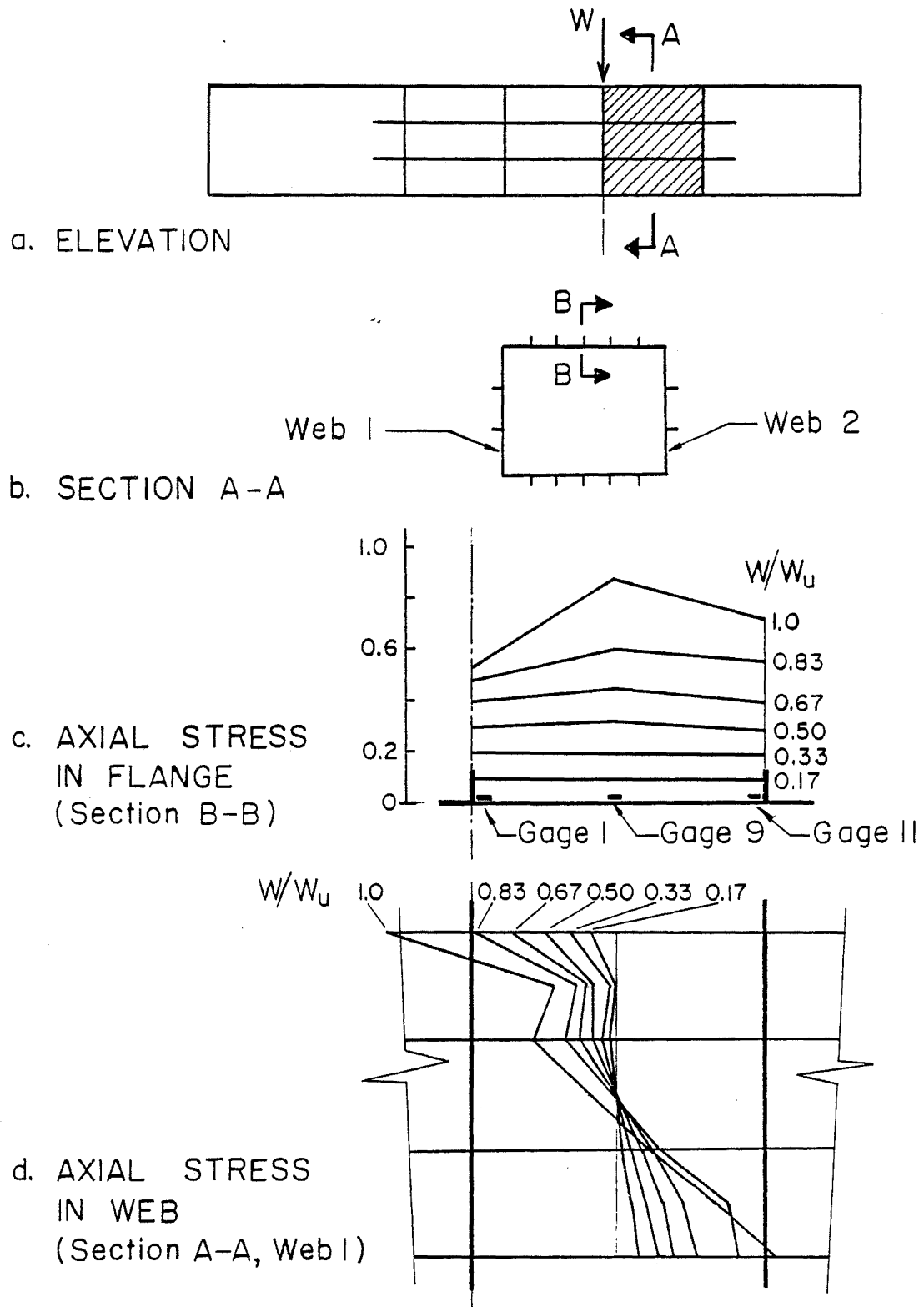
Fig. 42 Longitudinal Stress Distribution in Compression Flange and
Strain Distribution in Web 1 (Test 1)

128
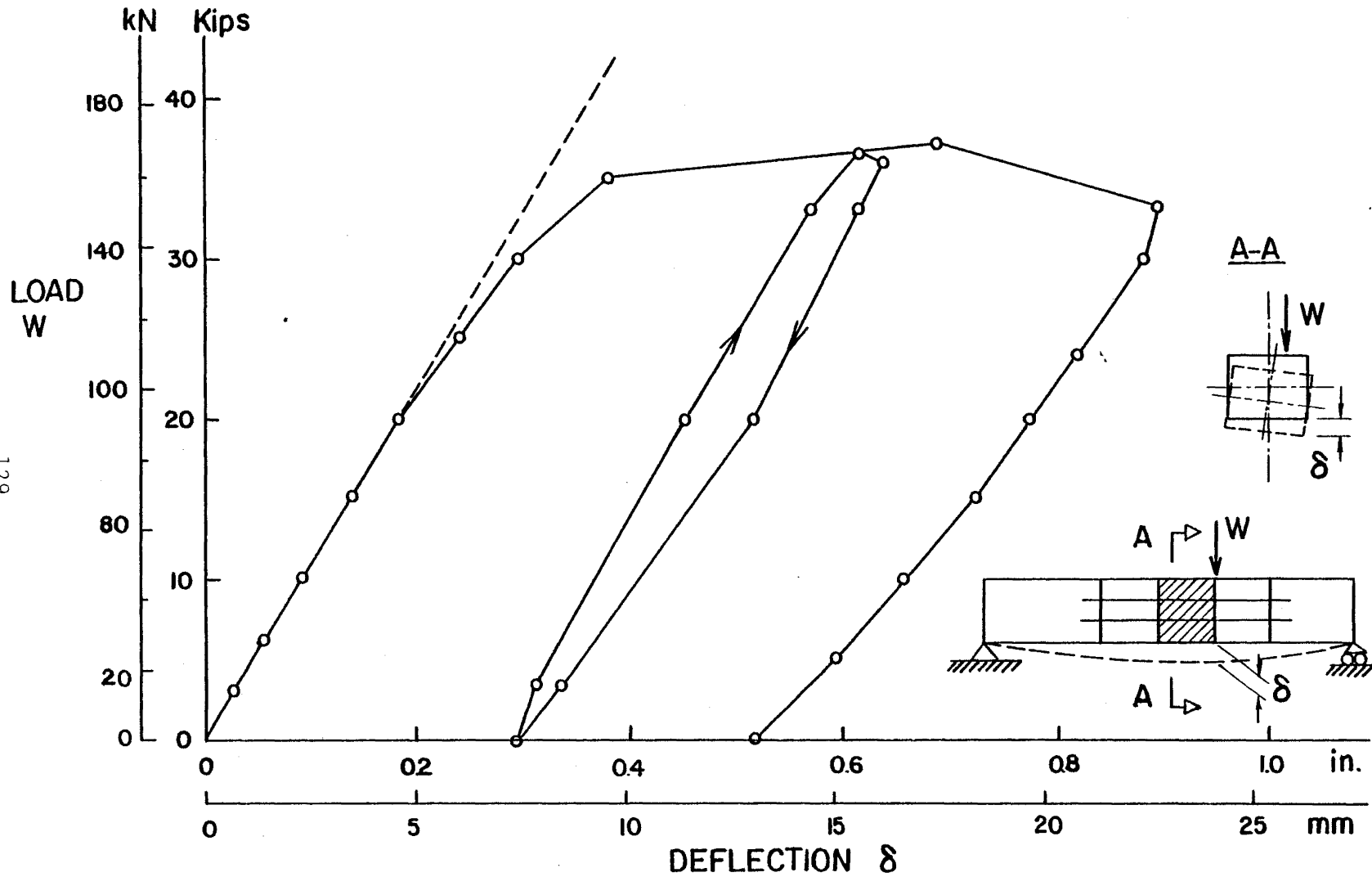
Fig. 43 Load vs. Deflection Curve for Test 2
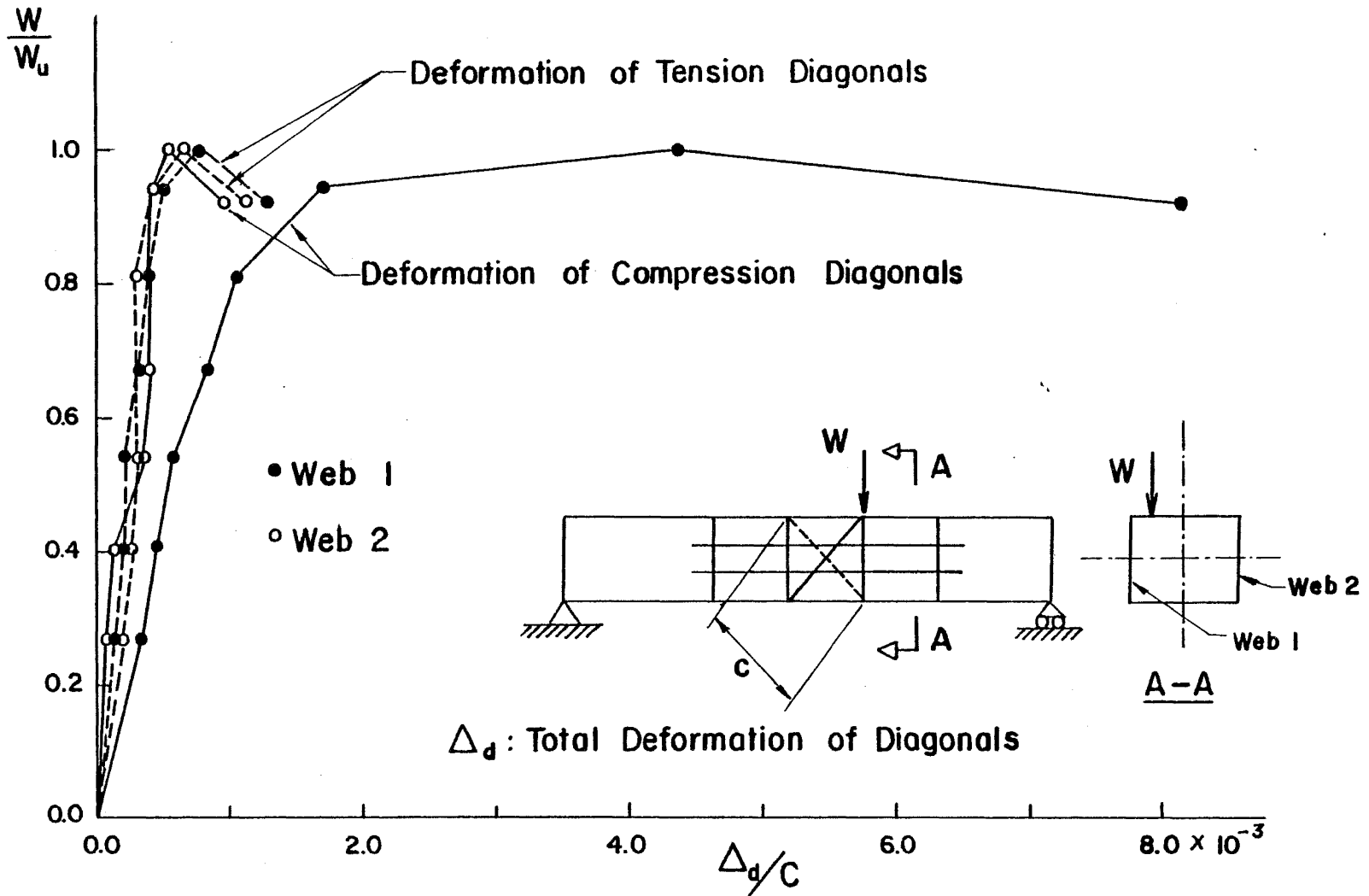
Fig. 44 Diagonal Deformations of Webs 1 and 2 (Test 2)

130
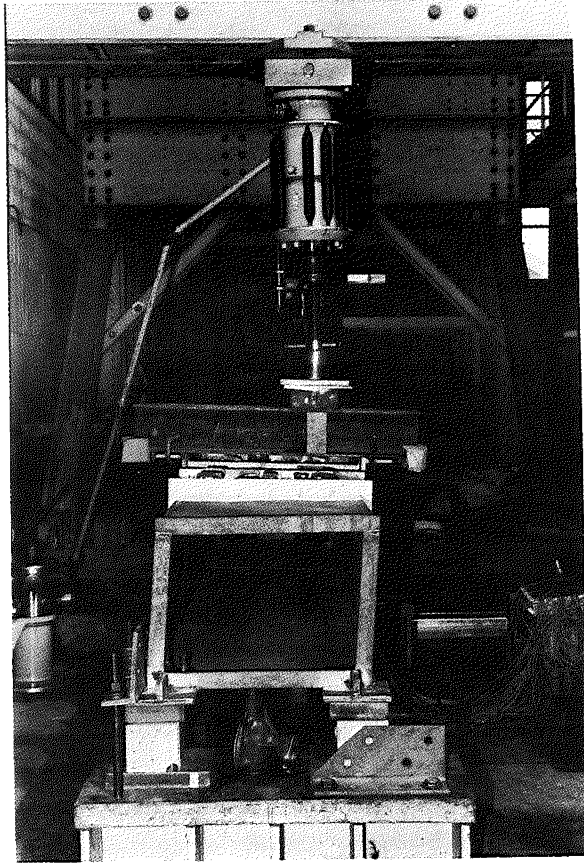
Fig. 45   Load Eccentricity and End
           Distortion (Test 2)
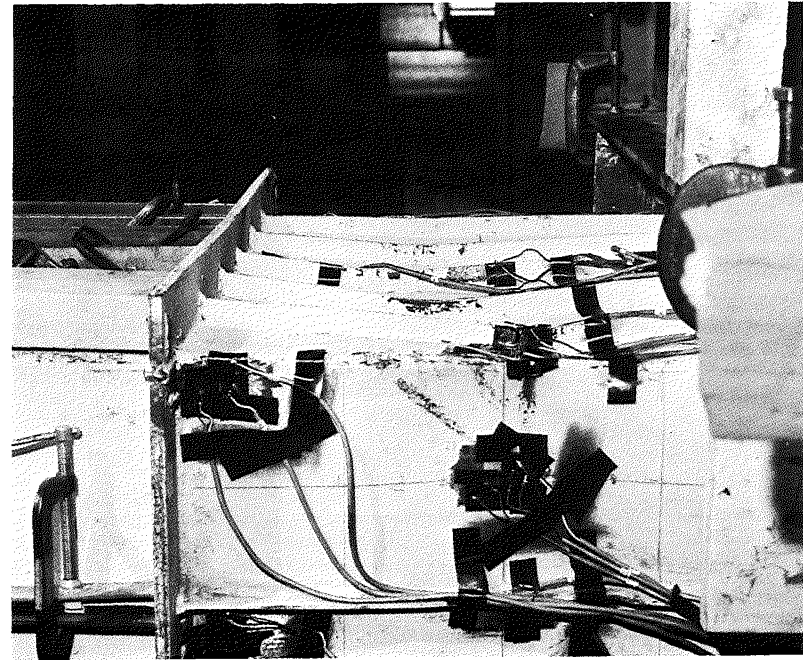
Fig. 46   Deformations of Upper Subpanel of Web 1
           and of Compression Flange (Test 2)
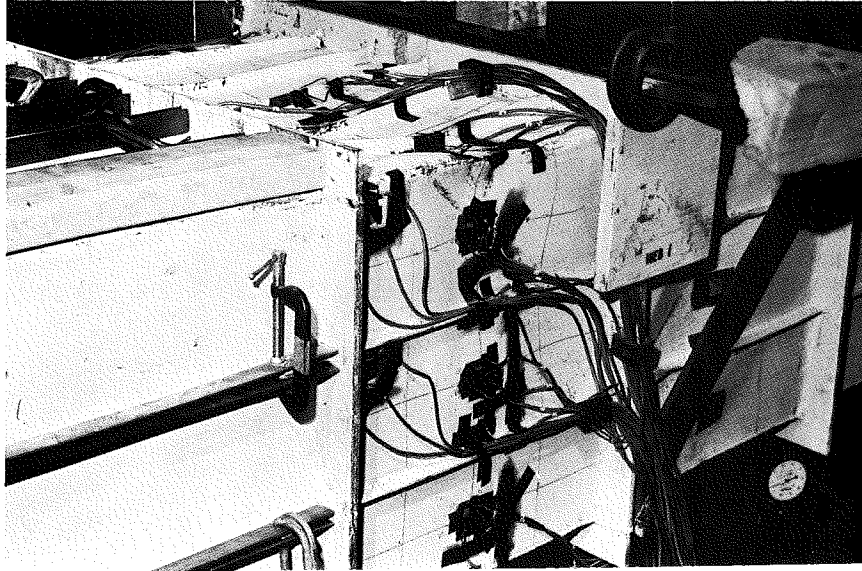
Fig. 47   Lateral Deflections of Web 1 at Ultimate Load
          (Test 2)
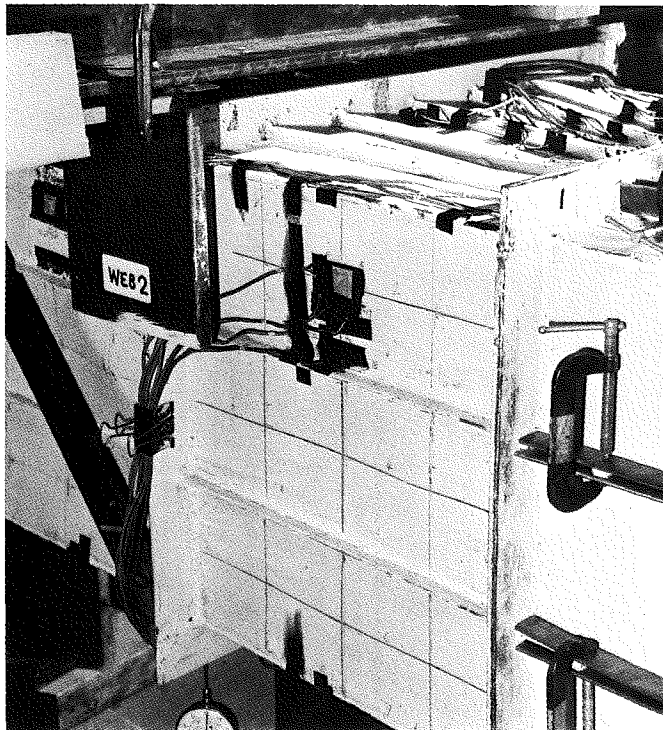
Fig. 48   Deflections of Compression Flange and
          Web 2 at Ultimate Load (Test 2)
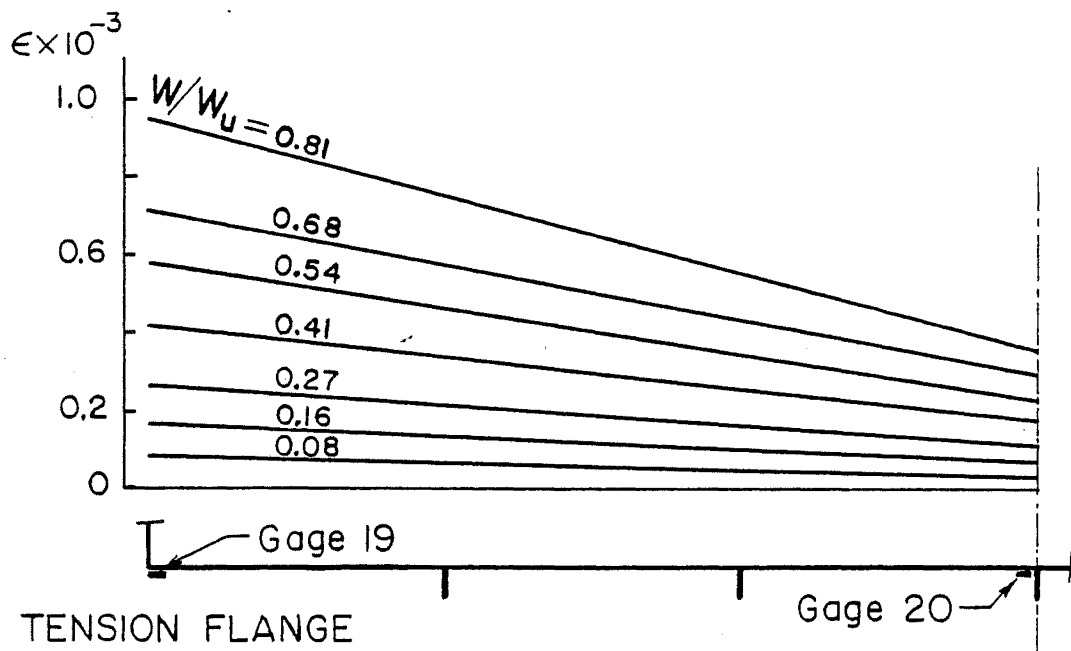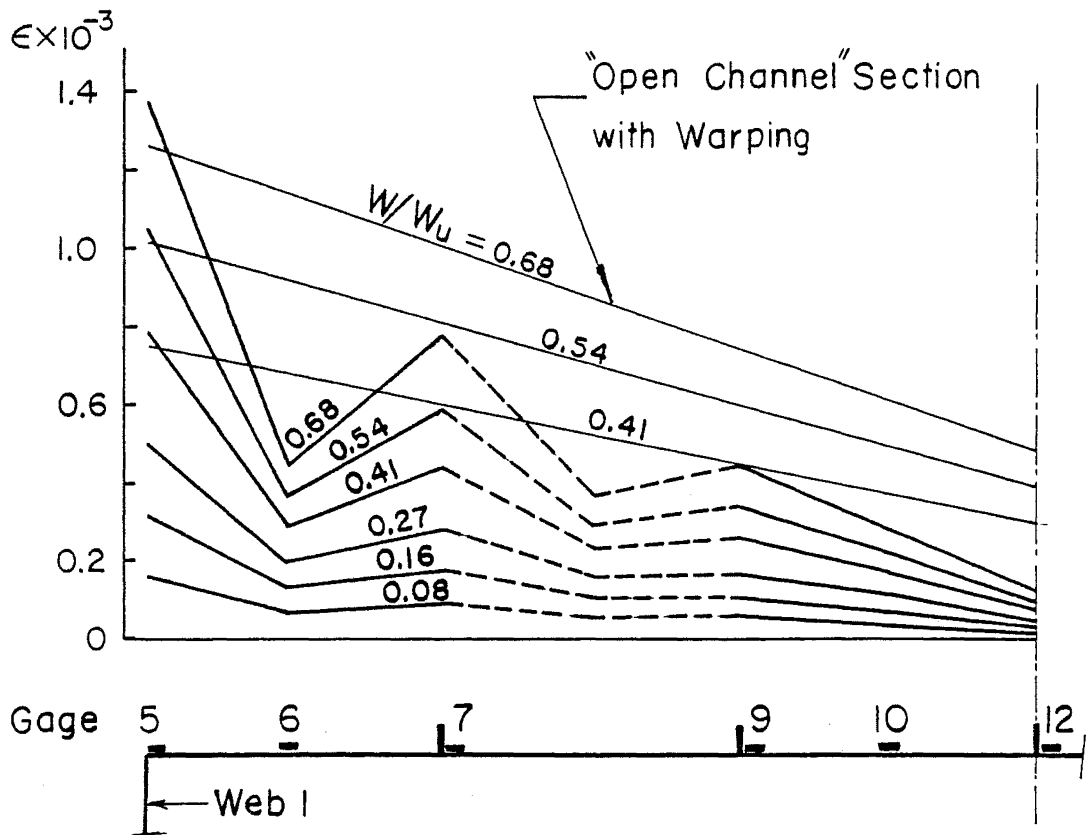
Fig. 49   Strain Distributions in Flanges for Half-Width (Test 2)

133
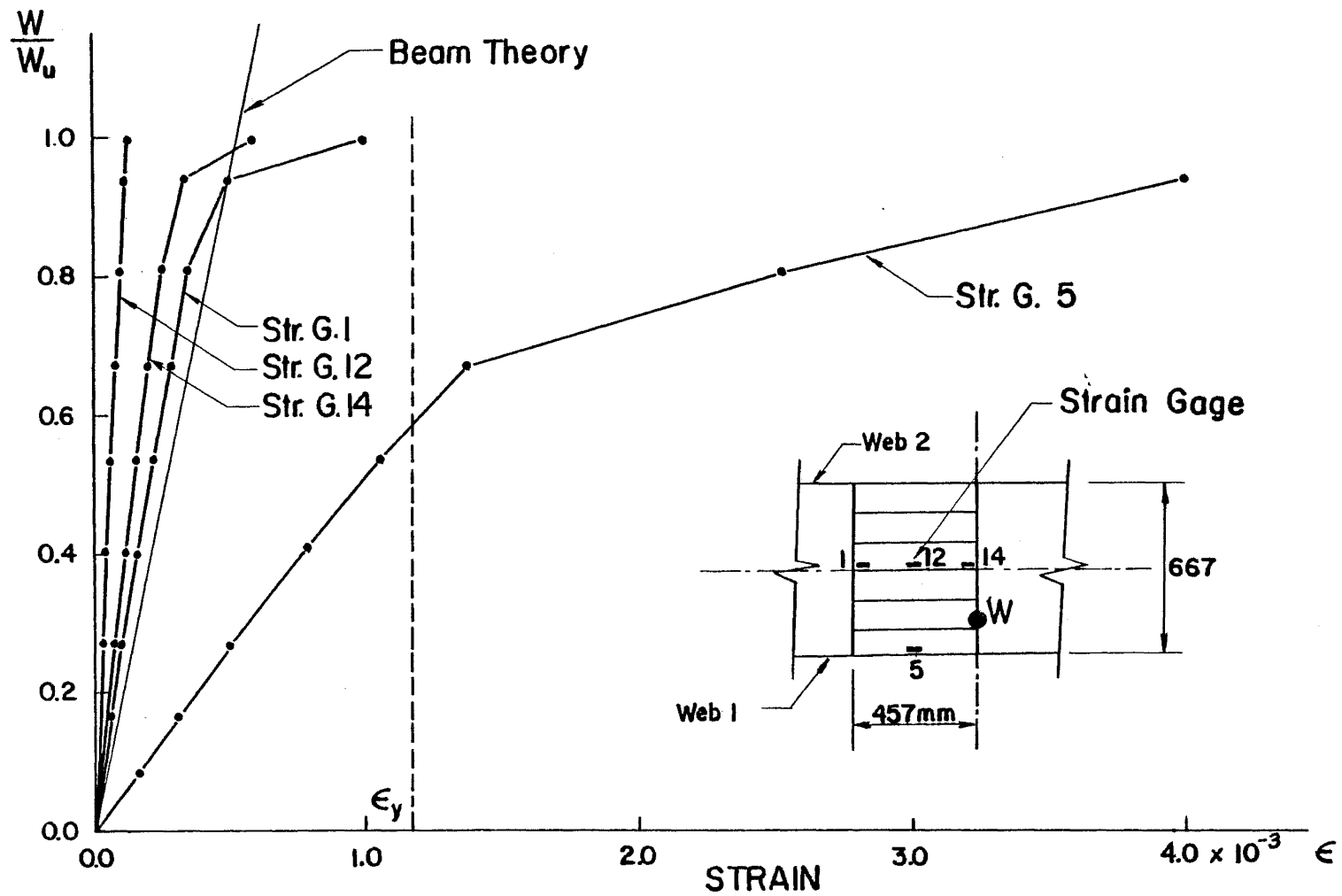
Fig. 50 Load vs. Strain Relationships at Different Points in
Compression Flange (Test 2)

134
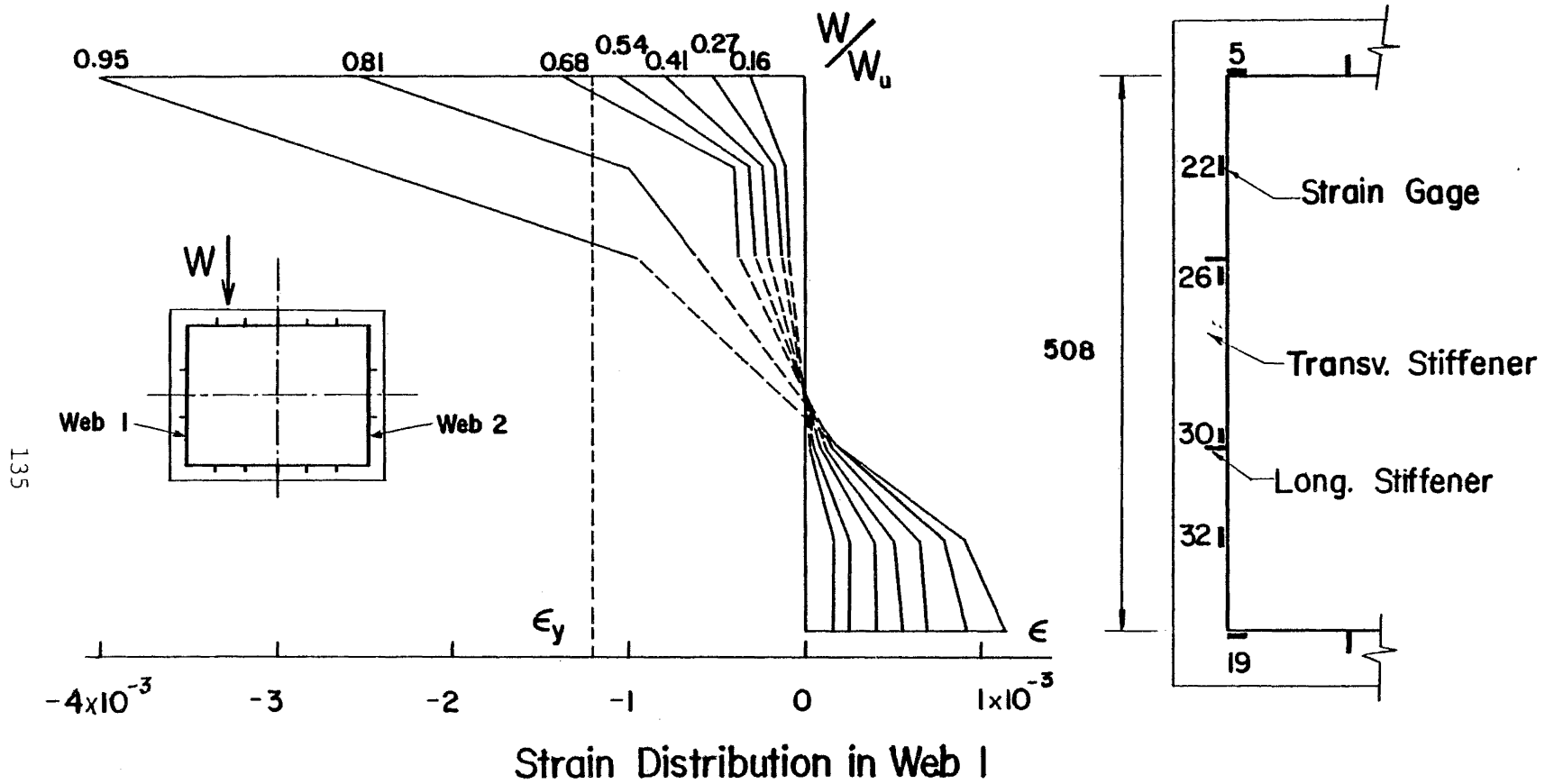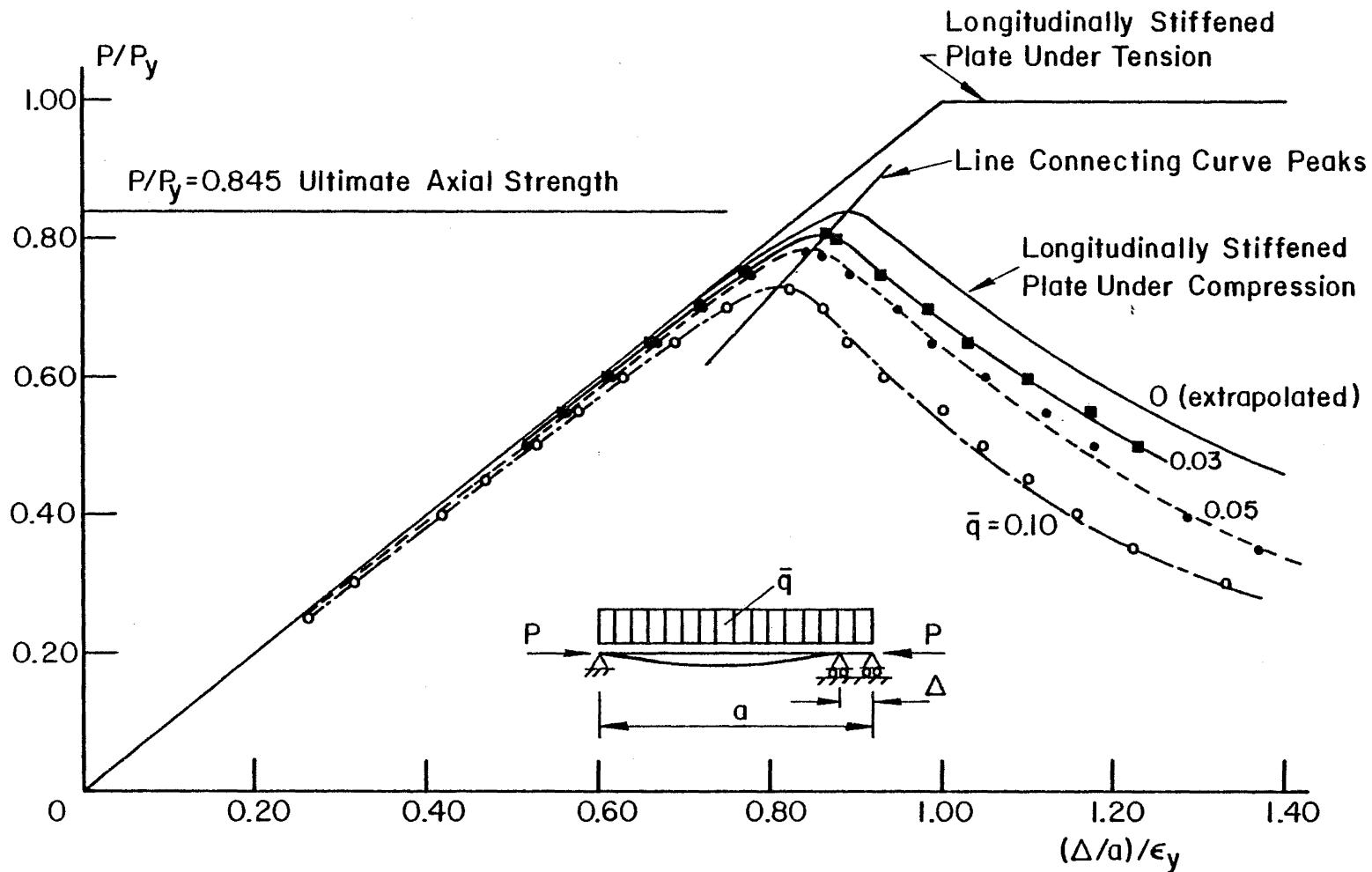
Fig. 51 Strain Distribution in Web 1 (Test 2)

135

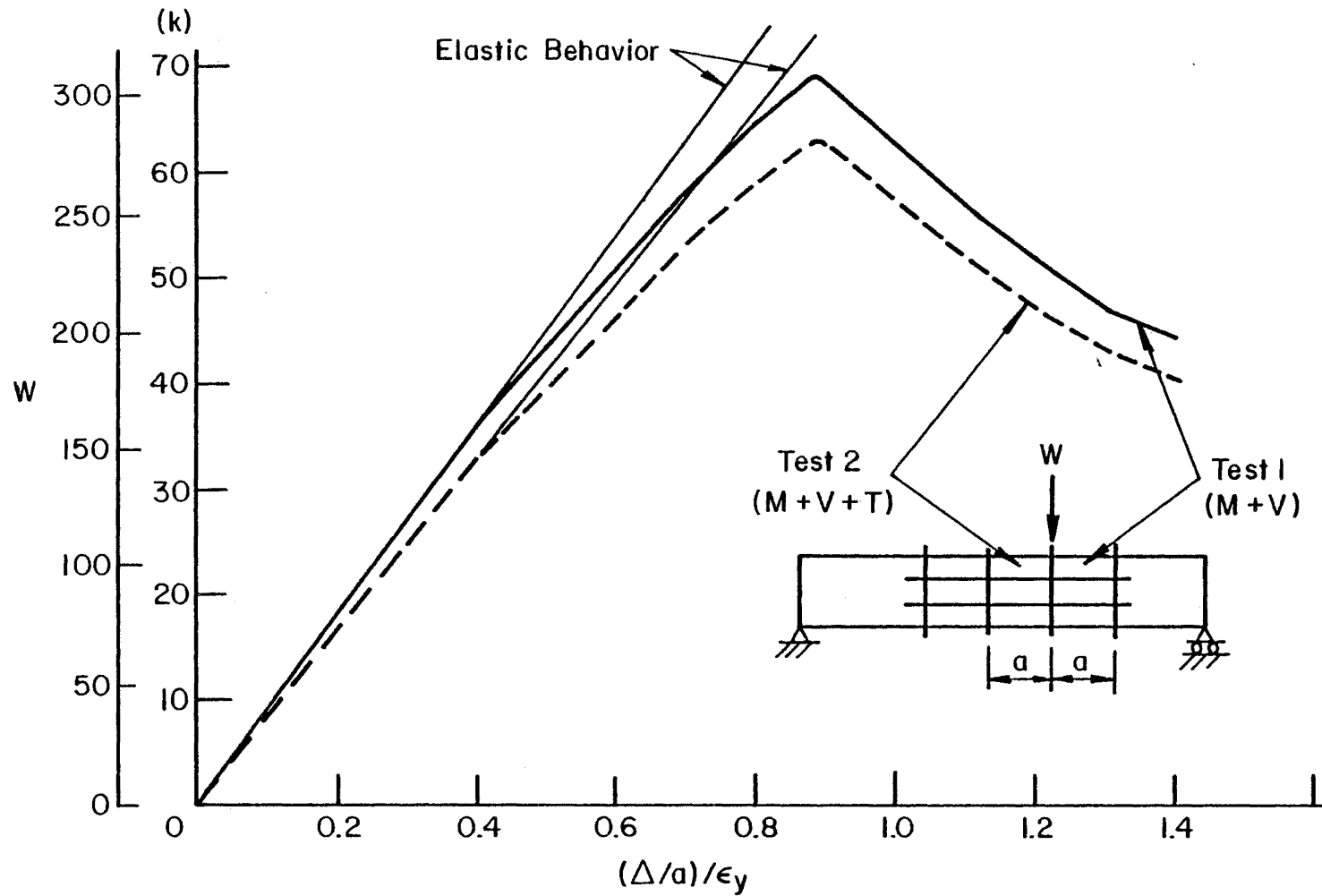Fig. 52   Behavior of Compression Flange under Axial Force in
Test Specimen

Fig. 53 Load vs. Average Strain in Flange-Web Junction for
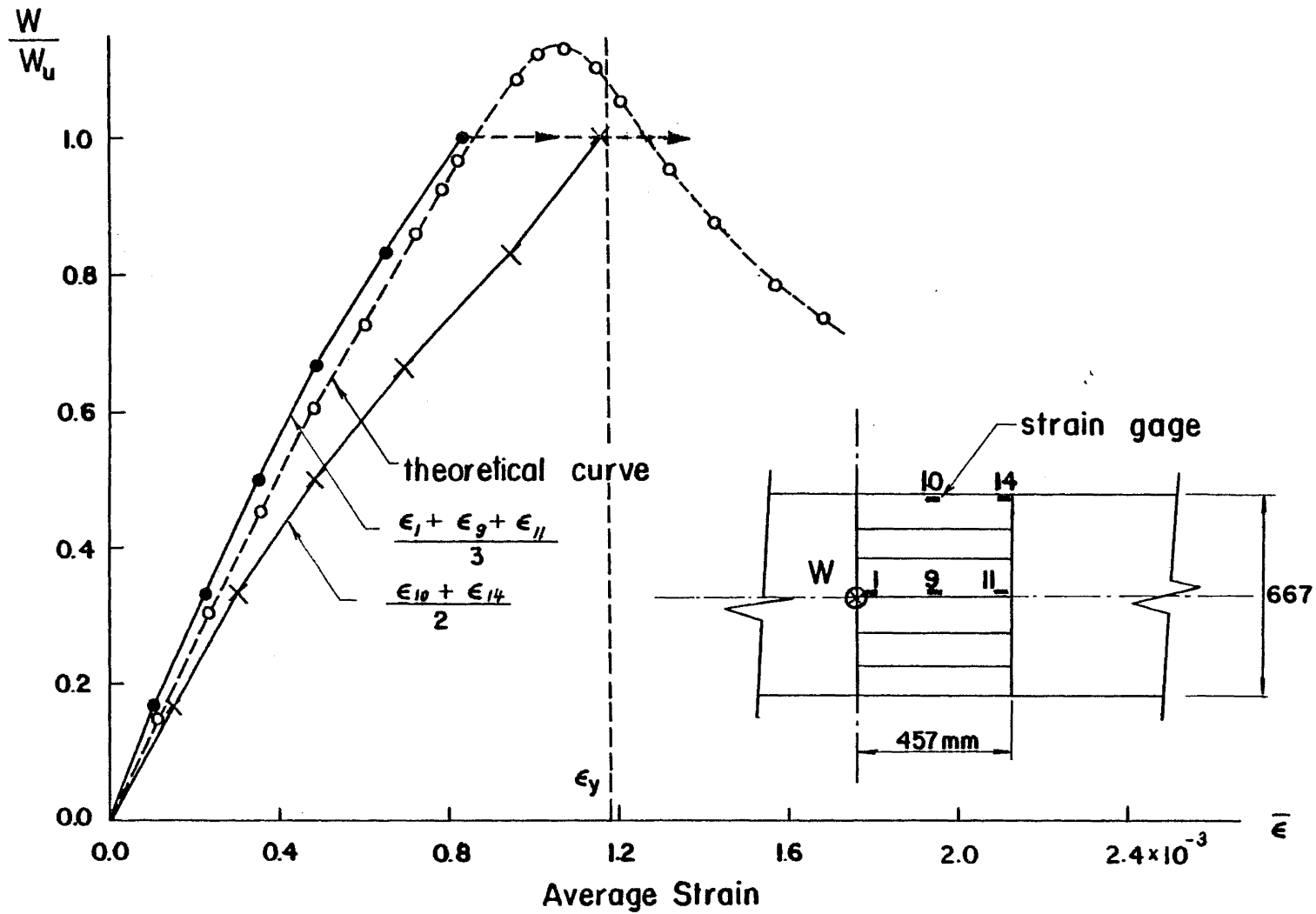Tests 1 and 2

137

Fig. 54   Load vs. Average Strain for Compression Flange (Test 1)